Evaluating the Consistency of Ice Thickness Models Across Regions in Predicting Subglacial Overdeepenings

Ipseeta Nayak

Submitted in accordance with the requirements for the degree of

Master of Science by Research

University of Leeds

School of Geography

Acknowledgements

This Master's by Research thesis was supervised by Dr. Duncan J. Quincey and Dr. Jonathan L. Carrivick of the University of Leeds. I extend my deepest gratitude to them for their mentorship, which went far beyond academic guidance. Their advice, expertise, and unwavering support helped me overcome challenges and successfully complete this work. They are a great combination of supervisors to work with. It would be a pleasure to work with them again sometime in the future.

I am also deeply grateful to Dr. Jenna Sutherland of Leeds Beckett University for providing the ice thickness data for OGGM in the central Himalayas, which was integral to this research.

My heartfelt thanks go to my family and friends for their support and encouragement during difficult times. A big thanks to everyone in Office 10.08, Garstang, for always being there to help with doubts and for brightening up the space with treats.

I am thankful to all the members of the Ice Club and the River Basin Processes and Management Cluster for their constructive feedback, which contributed valuable ideas to this thesis. Further, I would like to thank all the postgraduate researchers and staff of the School of Geography at the University of Leeds for providing a supportive and inspiring academic environment.

Abstract

Glaciers in high mountain regions are retreating rapidly due to climate change, exposing subglacial environments sculpted over millennia. Overdeepenings are a common part of the post-glacial landscape, and their development impacts landscape evolution, proglacial sediment dynamics, glacial lake formation, and associated hazards like Glacial Lake Outburst Floods (GLOFs). While Geographic Information System (GIS)-based approaches integrating Digital Elevation Models (DEMs) and ice thickness models have become critical for estimating overdeepening locations and characteristics, there has been little assessment of the extent to which the results are dependent on the input data that are used. To address this, the study first evaluated the relative influence of DEMs and ice thickness models on overdeepening predictions in the Central Himalayas. It compared results from five ice thickness models: Farinotti's Ensemble, Huss and Farinotti, GlabTop2, OGGM, and Millan; paired with four DEMs: Copernicus, ASTER GDEM, SRTM, and ALOS PALSAR. The analysis revealed that ice thickness models exert a greater influence than DEMs on overdeepening predictions. The combined framework was then applied to other regions, including the Peruvian Andes, Alaska, the European Alps, and New Zealand's Southern Alps, to further assess overdeepening variability and its dependency on the choice of ice thickness dataset. While no consistent trends emerged across regions and models, certain ice thickness models, such as OGGM and GlabTop2, were found to overestimate overdeepening parameters in many instances. Despite some commonalities, the maximum overlap in overdeepening predictions between any two models was 53.6%. To address the uncertainty in using a single ice thickness dataset to predict overdeepening locations, a potential framework that integrates multiple datasets is therefore proposed. In the absence of robust validation data, this approach could be used to provide confidence bounds on the estimation of overdeepening size and volume, helping to communicate uncertainties to stakeholders. More generally, the findings highlighted the variability in overdeepening parameters, emphasizing the need to account for this range when using overdeepenings as a foundation for further analysis. Establishing a clear purpose before estimating overdeepenings is recommended, as it can guide the selection of the most appropriate ice thickness model. This study provides insights into the consistency among ice thickness models and underscores the importance of multi-model approaches for robust and reliable assessments.

Table of Contents

List of Figures

List of Tables

List of Abbreviations

GLOF: Glacial Lake Outburst Flood

DEM: Digital Elevation Model

OGGM: Open Global Glacier Model

RGI: Randolph Glacier Inventory

SRTM: Shuttle Radar Topography Mission

ASTER: Advanced Spaceborne Thermal Emission and Reflection Radiometer

ALOS: Advanced Land Observing Satellite

PALSAR: Phased Array type L-band Synthetic Aperture Radar

GLIMS: Global Land Ice Measurements from Space

HIGTHIM: Himalayan Glacier Thickness Mapper

VOLTA: Volta and Topography Estimation

IDW: Inverse Distance Weighing

GIS: Geographic Information System

1. INTRODUCTION

Changes in both temperature and precipitation over the past four decades (Allen et al. 2018) have led to accelerating glacier retreat (Davaze et al. 2020; Hugonnet et al. 2021) in high mountain regions. This retreat can lead to changes in geomorphology (Prothro et al., 2018) and glacier dynamics (Chandler et al. 2016), as well as revealing the subglacial environment that has been sculpted by processes of erosion and deposition for thousands of years. Overdeepenings are subglacial depressions that are usually formed because of the erosive nature of the glacier (Hooke, 1991; Cook and Swift, 2012). The overdeepenings thus exposed can form glacial lakes, and can also trap sediments that would previously have been delivered to downstream areas (Magrani et al. 2020), influencing the landscape evolution.

Given these overdeepenings cannot be directly observed, GIS based approaches that estimate the subglacial topography are required. There has been a recent surge in studies that have used high-resolution DEMs combined with ice thickness models to understand the morphometry and overdeepening locations (Patton et al. 2016; Haeberli et al. 2016a; Magrani et al. 2020; Schlunegger et al. 2024). The vast majority of such studies rely on a single input DEM and a single ice thickness model to evaluate the subglacial topography. However, the diversity of available terrain datasets and ice thickness models introduces variability in overdeepening predictions (Gharehchahi et al. 2020; Magnin et al. 2020; Otto et al. 2022), and this variability is yet to be fully quantified, or resolved.

Differences in underlying principles, data sources, and times of acquisition between DEMs and ice thickness models complicate direct comparisons. The lack of systematic intercomparison between models and DEMs further limits understanding of any regional variability and precludes a full assessment of the robustness of predictions. Glacier morphology varies significantly across regions (Haeberli et al. 2016), largely because of the combination of spatially variable climatic settings and tectonically controlled topographic characteristics, influencing the accuracy of overdeepening estimates and underscoring the need for context-specific approaches.

To address these gaps, this study aims to evaluate the consistency of different DEMs and ice thickness models in predicting overdeepening characteristics and to assess their applicability across diverse mountain regions. By comparing outputs from multiple datasets and combining model results, this study seeks to develop a more robust framework for overdeepening detection. The thesis is structured as follows: first, a review of the current literature summarises the key studies

that have considered GIS-based approaches for estimating subglacial overdeepenings, and assesses their limitations (Chapter 2) providing the foundation to identify current gaps (Chapter 3); the methods used in the current study are then introduced (Chapter 4); followed by an explanation of the analysis results (Chapter 5); the underlying reasons for the observed patterns and findings are then discussed in detail (Chapter 6) and then the entire study is summarised in the concluding chapter (Chapter 7).

2. LITERATURE REVIEW

2.1. OVERDEEPENINGS: FORMATION, AND RELEVANCE IN DEGLACIATING LANDSCAPE

Overdeepenings are topographic depressions located beneath the ice in a glacier (Penck and Brückner, 1909; Alley et al. 2019). They could be entirely erosional or non-erosional and be present as a part of the bedrock, and they may be of glacial (Figure 2.1) or non-glacial origin. Once exposed at the surface they can often fill with water to form glacial lakes. When located in sensitive and dynamic regions of the glacier (which is usually at the snout of the glaciers) they can affect the glacier

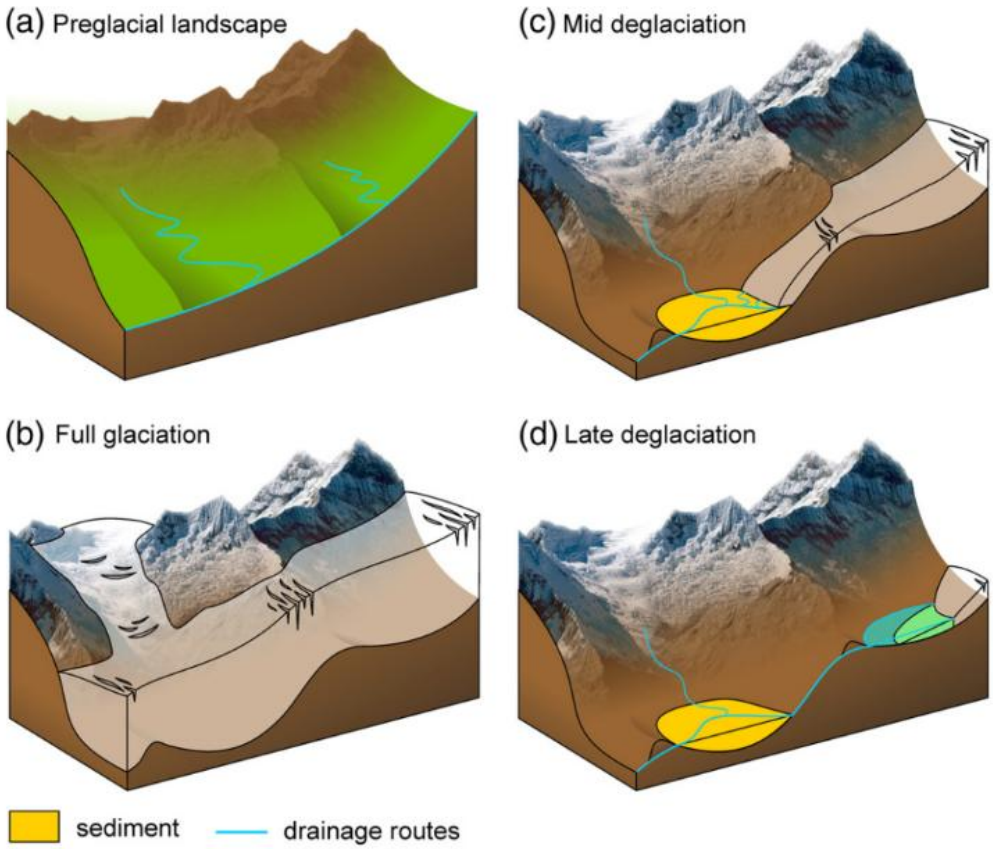

Figure 2.1: Schematic diagram of the subglacial topography (overdeepenings in yellow and green) being exposed at the surface (Cook and Swift 2012)

dynamics and hydrology to a great extent (Cook and Swift, 2012).

Overdeepenings can occur in any part of the glacier, but in a valley, glacier setting they are mostly found along the main tongue (Viani et al. 2020) in areas where there is a sudden change in the bed gradient (Emmer et al. 2015a) and the rate of velocity is high (Lloyd et al. 2023). A possible way of overdeepening formation can be seen in Figure2.1. Large overdeepenings tend to develop where

the rocks are least resistant (Magrani et al. 2020), and they play an important role in storing, releasing and transferring sediments to the downstream areas (Liebl et al. 2021).

A study in the Austrian Alps has shown that 33% of all lakes are present within the terminus area of these glaciers (Emmer et al., 2015b). Although overdeepenings represent a small fraction of total glacier volume - approximately 3% in the Swiss Alps, 3 - 4% in the Himalayan-Karakoram region (Haeberli et al., 2016), and about 0.5 -1% in the Peruvian Andes (Colonia et al., 2017) - their downstream impacts are disproportionately significant. They influence sediment transport, hydrology, and glacial lake formation, highlighting their importance in both glacial and post-glacial environments.

2.2. PREVIOUS WORK TO IDENTIFY SUBGLACIAL OVERDEEPENINGS

The glaciers in the Andes (Colonia et al. 2017; Drenkhan et al. 2018, 2019; Tweed and Carrivick, 2015), High Mountain Asia (Kapitsa et al. 2017; Furian et al. 2021, 2022), the Himalaya-Karakoram (Linsbauer et al. 2012; Allen et al. 2016a; Haeberli et al. 2016; Bhushan et al. 2017; ; ; Sattar et al. 2019; Majeed et al. 2021a; Majeed et al. 2021b; Zhang et al. 2022; Rana et al. 2023; Srinivasalu et al. 2024) and the European Alps (Frey et al. 2010; Haeberli et al. 2016; Magnin et al. 2020; Gharehchahi et al. 2020; Otto et al. 2022 and the New Zealand Southern Alps (Carrivick et al. 2022) have previously been studied for overdeepening locations and characteristics. The third pole and the Himalayas have been studied extensively, and within the Himalayas in particular, the western Himalayas and the Karakoram region have been studied most frequently (Table 2.1).

Paper	Region	Model	DEM	Glacier outlines	Area Threshold	Major Findings
Frey et al. 2010	Swiss Alps	Shallow Ice Approximation	Swiss ALTI		6250 m^2 for glaciers	Introduced the method in which the ice thickness is subtracted from the DEM to produce the overdeepenings. Suggested that SRTM and ASTER can be used for these analysis for other regions of the world.
Haeberli et al. 2016	Swiss Alps	GlabTop	Swiss ALTI	Swiss Glacier Inventory	10000 m^2	The modelled overdeepening in the Swiss Alps were 3% of the total glacier volume. The modelled overdeepening in the Himalayan Karakoram region was 3-4% of the total glacier volume. The overdeepenings in the Himalayas have area more than 50 km^2.
	Himalayan-Karakoram	GlabTop2	SRTM	RGI (Pfeffer et al. 2014)		
Gantayat et. 2017	Indian Himalayas	HIGTHIM	ASTER, SRTM	RGI (Pfeffer et al. 2014)		They suggested that a glacial lake can form on the snout of Drang Drung glacier and the already existing moraine dammed lake near the snout of Samudra Tapu glacier might increase in area and volume.

Table 2.1: Literature Review of studies on overdeepenings

Paper	Region	Model	DEM	Glacier outlines	Area Threshold	Major Findings
Linsbauer et al. 2012	Himalayan-Karakoram	GlabTop2	SRTM	Global Land Ice Measurements from Space(GLIMS) database and Randolph Glacier Inventory (RGI)	10000 m^2	The modelled overdeepenings covered 3.8% of total volume of the glaciers in the Himalayan Karakoram region. These overdeepenings were shallower in Karakoram and Central Himalayas as compared to the deeper overdeepenings in western and eastern Himalayas.
Magnin et al. 2020	Western European Alps	GlabTop	IGN, RGD, ASTER	Glacier outlines drawn within GlaRiskAlps project	10000 m^2	The depth of the overdeepenings varies according to the DEMS, IGN DEM predicted the deepest, largest and most voluminous GBOs whereas ASTER produced shallow GBOs. The GBOs in the region are similar to those present in the Peruvian Andes. Only 2 lakes were likely to form in the region given the retreat rate then.
Srinivasalu et al. 2024	Western Himalayas	Gantayat et al., 2017	ASTER	RGI (Pfeffer et al., 2014), GAMDAM	10000 m^2	A total 132 glaciers were taken to estimate the overdeepenings in the Sutlej and Beas basin, which resulted in 118 potential glacial lakes.
Drenkhan et al. 2018	Andes	GlabTop	SRTM	Landsat 5 and Sentinel-2, NDSI		Total of 219 overdeepenings were identified in the glacier bed, where 49 met the slope threshold and out of which 20 sites were selected as potential future lake formation.

Paper	Region	Model	DEM	Glacier outlines	Area Threshold	Major Findings
Drenkhan et al. 2019	Andes	GlabTop				Future lake formation shows that they can form important water resources though they might not compensate the water loss by the glacier retreat.
Kapitsa et al. 2017	Tien Shan	GlabTop2	SRTM	Serveskiy et al. 2016	11000 m^2	They identified 513 overdeepenings in 2000 glaciers, 67% of which matched with the present glacial lakes. If the area threshold is increased to 20000 m^2, the match increases to 85%. The location of the lakes is quite robust but the morphometry of the lakes is not that robust.
Colonia et al. 2017	Peruvian Andes	GlabTop	SRTM	National Glacier Inventory of Peru	10000 m^2	There are higher chances of lake formation in Cordillera Vilcanota than Cordillera Blanca. They estimated that 201 overdeepenings were formed that consist of 0.5 to 1% of the total glacier volume there. Most of the lakes are likely to form within the next few years.
Viani et al. 2020	Aosta Valley	GlabTop2	Regional DEM by RAVA		10800 m^2	The volume of overdeepenings is 0.8% of the total glacier volume which is like that found in the Peruvian Andes by Colonia et al., 2017. This value is less when compared to the percentage of total volume in Swiss Alps and Himalayan Karakoram.
Furian et al. 2021	High Mountain Asia	Farinotti's Ensemble	ALOS PALSAR		10000 m^2	They predicted 25285 overdeepenings in the region but if the threshold is increased it produces 2700 overdeepenings in the 669 glaciers. The size and location of the overdeepenings is in good agreement with the studies.

Paper	Region	Model	DEM	Glacier outlines	Area Threshold	Major Findings
Furian et al. 2022	High Mountain Asia	Farinotti's Ensemble	ALOS PALSAR		100000 m^2	The future lakes are most likely to develop in the first half of the 21st Century the increase in the volume happens in the second half of the century.
Otto et al. 2022	Austrian Alps	GlabTop2, HF Model	ALOS PALSAR	Glacier outlines were drawn from orthophotos and airborne lasers can data with varying acquisition dates.	Glaciers with area greater than 100000 m^2	The study area has 525 glaciers which were taken and between 86 and 198 overdeepenings were predicted in the region. Both the models performed better for the valley glaciers than for the smaller glaciers.
Gharehchahi et al. 2020	Swiss Alps	VOLTA	SwissALTI and DHM25 L2			The large glaciers which have an area greater than 5 km^2 are better compared to the influence of DEMs on the overdeepenings. They estimated the formation of 125 overdeepenings using Swiss ALTI and 113 using DHM25 L2. The location, area and depth of the overdeepenings were influenced by the choice of the DEM. Out of the 171 overdeepenings that were identified 100 of them were classified as highly likely to form a glacial lake in the future.
Carrivick et al. 2016	South American Glaciers	VOLTA	ASTER			A total of 617 were considered for the study and 282 overdeepenings were identified.

Paper	Region	Model	DEM	Glacier outlines	Area Threshold	Major Findings
Bhushan et al. 2017	Gangotri Glacier	Gantayat et al., 2017	Cartosat -1			They identified 8 possible sites for formation of supraglacial lakes. The overdeepenings present at the snout of the glacier are most likely to form glacial lakes in the future.
Majeed et al. 2021b	Gya Glacier	GlabTop	ALOS PALSAR	Glacier outlines were taken from satellite data		They evaluated the evolution of Gya glacier and how the lake has evolved. The proglacial lake was spreading over ~11 ha, delineated from satellite data.
Rana et al. 2023	Parkachik Glacier	Gantayat et al., 2017	CORONA KH4, Landsat and Sentinel-2A			They found that nearly 74 potential future lakes would form. They examined the expansion of lakes from 1964 to 2017 and found that their total area increased.
Rashid et al. 2022	Pangong Region	GlabTop	ALOS PALSAR			They used this study to show how much lake could expand in the future.

Paper	Region	Model	DEM	Glacier outlines	Area Threshold	Major Findings
Sattar et al. 2019	Dhauliganga Basin	Gantaya t et al., 2017	ASTER	RGI (6.0)	Area of glaciers > 1km^2	They found out that 54 overdeepenings were estimated for the glaciers that have an area of 2.85 km^2.
Carrivick et al. 2022	New Zealand Southern Alps	Farinotti 's Ensembl e	ALOS PALSAR	RGI (6.0)	100000 m²	This paper provides the inventory of the ice-marginal proglacial lakes across the New Zealand Southern Alps and showed a positive relationship between glacier mass balance and lake growth. It was also concluded the number and size of the ice marginal lakes would increase in the future which would affect the drainage.
Zhang et al. 2019	Central Himalayas	GlabTop	TanDEM-X, SRTM	Using LANDSAT images	10000 m²	They found that nearly 74 potential future lakes would form. They examined the expansion of lakes from 1964 to 2017 and found that their total area increased. They compared their findings for the region using the GPR readings and found that the location of the overdeepenings was robust.
Allen et al. 2016b	Himachal Pradesh	GlabTop 2	ASTER		10000 m²	They found out that 279 lakes would form across the entire Himachal Pradesh. This study shows that the potential risk of GLOF hazard would increase in future.

Figure 2.2: Map of the regions that were studied

There have been numerous studies (Figure 2.2) on overdeepenings using the method given by Frey et al., (2010). Studies have relied on a single DEM and ice thickness model to detect overdeepenings and project future scenarios, often without addressing the substantial uncertainties that are inherent in such predictions (Drenkhan et al., 2019; Furian et al., 2022). Most of these are based on High Mountain Asia and Himalayas combined (Bhushan et al. 2017; Majeed et al. 2021a; Furian et al. 2022; Rashid et al. 2022; Rana et al. 2023) as seen in Figure 2.2. This is of some concern where study outputs are classified and then communicated in risk terms, given that communities live within the downstream areas that could be affected (Drenkhan et al. 2019). It also means that broad-scale analyses of potential hydropower that could be available from future overdeepenings are also highly uncertain even on a regional scale (Farinotti et al. 2019b).

The choice of DEM has been shown to have a small influence on determining overdeepening locations, but a greater impact on the morphometric parameters of the overdeepenings (Zhang et al. 2019; Gharehchahi et al. 2020). The most commonly used DEMs are ALOS PALSAR, ASTER and SRTM, given that they are widely available and offer relatively high (~30 m) spatial resolution. Studies like Frey et al. (2010) and Gharehchahi et al. (2020), focussing on the European Alps use Swisstopo, which is a local DEM for the region. Other parameters that vary between studies include the size threshold at which the overdeepenings are considered to be significant – the large majority adopt a threshold of 10,000 m^2 (0.01 km^2) to remove individual pixels and small clusters of pixels that most likely arise from artefacts of the processing the ice thickness datasets (see Table 2.1).

Studies employing multiple DEMs or ice thickness models, such as Magnin et al. (2020) for Peruvian Andes and Gharehchahi et al. (2020) for the Swiss Alps, have highlighted that there is uncertainty of ±10 m in determining the depth of the overdeepening, and of ±24% in determining the ice thickness of the glaciers, respectively, both within ice thickness models, considering their absolute accuracy with reference to measured bedrock elevations. This emphasises on the fact that irrespective of region, DEM and ice thickness model used, the uncertainties remain an inherent part of the analysis.

Otto et al. (2022) combined two ice thickness models (Huss and Farinotti and GlabTop2) with three glacier outline datasets, enhancing confidence in their estimates through a multi-model approach, which seems to show promising application for a more robust evaluation of overdeepening locations and characteristics where a number of independent evaluations are available. Out of all the overdeepenings, 70% overlapped with the already present lakes in the glaciers. However, none of these studies have sufficiently explored any regional variability among models or the choice of DEM.

The accuracy of the glacier outlines used in GIS-based workflows has also been regarded as important because many valley glaciers, especially the ones in the Himalayas, have proglacial lakes that develop at the terminus of the glaciers and hence the dimensions of the lake, and any identified overdeepenings, change every time the outline changes (Paul et al. 2019). Further, several approaches for estimating ice thickness (such as VOLTA; James and Carrivick, 2016, HIGTHIM; Gantayat et al. 2017), use the algorithm to reach an ice thickness of zero at the terminus, which can be erroneous where glaciers terminate with a steep ice face into a proglacial lake (James and Carrivick, 2016; Gantayat et al. 2017). The most widely used glacier outlines have been from the RGI version 6.0 (https://www.glims.org/RGI/randolph60.html; Pfeffer et al. 2014); these are easy to access, generally considered to be one of the most accurate assessments of glacier extent, and can also readily integrate with existing GIS-based workflows. Some studies (Yang et al. 2016; Freudiger et al. 2018) have used satellite images to construct their own glacier outlines, but this is not common.

Studies present overdeepening estimates in terms of specific volume, and area percentages, without adequately addressing how to manoeuvre around the uncertainties inherent in these predictions (James and Carrivick, 2016; Drenkhan et al. 2019; Gharehchahi et al. 2020). An intercomparison of different ice thickness models and the DEMs could help address a major gap and improve the reliability of future hazard assessments

2.3. ICE THICKNESS MODELS

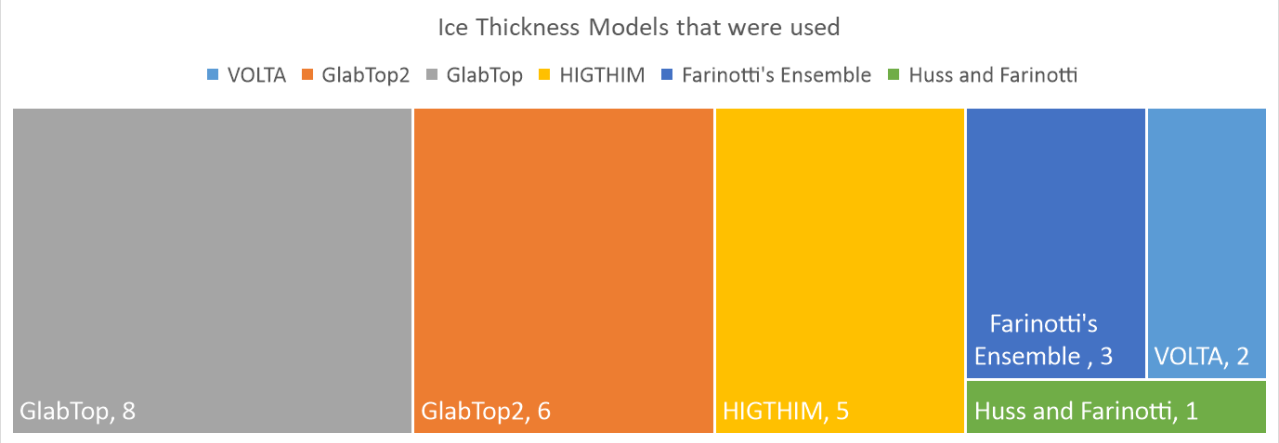

Figure 2.3: Ice thickness models being used in different studies from Table 2.1 with the number of studies they have been used in

Most previous studies have used GlabTop (Paul and Linsbauer, 2012) for ice thickness estimation as seen in Figure 2.3; this was one of the first methods available and the also the programming code for the model is readily accessible. It was therefore integrated into many early analyses of glacier volume estimation, and then subsequently, studies seeking to characterise glacier bed topography. Recent studies have used ice thickness from Farinotti's ensemble (Carrivick et al. 2022; Furian et al., 2021, 2022) because the data are readily available and they are now considered to be the most robust, comprising the best estimations across a range of input models. Unlike global ice thickness models such as GlabTop and Farinotti's ensemble, which are designed for broad applicability, the approach developing by Gantayat et al. (2017), known as HIGTHIM, is specifically tailored to Himalayan glaciers that are valley type (Gopika et al. 2021). This method was employed to estimate ice thickness exclusively within the Himalayas, reflecting its region-specific focus and utility (Bhushan et al. 2017; Majeed, et al. 2021a; Sattar et al. 2019; Srinivasalu et al. 2024).

A small number of studies have shown that different ice thickness models show regional variability. For instance, the GlabTop model underestimated the volume of overdeepenings in the Argentiere glacier of the Swiss Alps (Magnin et al. 2020), by 2.8 to 3.7 Mm^3 when compared to the measured bed topography by Vincent et al. (2019). Whereas, it overestimated bed topography by ~14% of volume in the Andes (Drenkhan et al. 2018). When compared with the Ground Penetrating Radar (GPR) readings or existing glacial lakes most of the ice thickness models accurately predict the location of known overdeepenings but the size and morphometry of the overdeepenings are not accurate (Zhang et al. 2019; Gharehchahi et al. 2020; Furian et al. 2021; Otto et al. 2022). More

generally, individual ice thickness estimates have been shown to vary considerably (10±24% from mean ice thickness), with the range among 17 different models being comparable to the magnitude of the ice thickness itself (Farinotti et al., 2017). Understanding different approaches for the models used in this study is therefore likely to be important for understanding any differences in their outputs.

In summarising each of the approaches below, the following symbols are used for the parameters within each of the models, with any deviation from this notation mentioned in the text.

ρ *:* density of ice (kg m^{-3})

g : acceleration due to gravity (ms^{-2})

f : shape factor

τ : basal shear stress (Nm^{-2})

n : Glen's flow law exponent (considered as 3 by default)

2.3.1. GlabTop (Linsbauer et al. 2012)

GlabTop follows the principle as given by Cuffey and Patterson, (2010); given the ice is assumed to be perfectly plastic, basal sliding is not considered, and the ice body is assumed to have almost 10 times greater extent than the vertical depth of the ice body. Then the ice thickness can be calculated assuming it depends on the slope and the basal shear stress using the following equation:

$$d = \frac{\tau}{(\rho g f sin\alpha)} \qquad \text{Equ(1)}$$

Where d is the ice thickness, ρ is set to 900 kgm^{-3}, g is taken as 9.81 ms^{-2} and f is set at 0.8 (Patterson, 1998). The value of τ is calculated using Haeberli et al., (1989) quadratic regression to all data points:

$$\tau = 0.005 + 1.598 \triangle h - 0.435 \triangle h^2 \qquad \text{Equ (2)}$$

τ is calculated for each grid cell of a glacier and smoothed using an appropriate kernel size of 25m. The values of τ are stored in a separate grid which is later used for calculating ice thickness. $\triangle h$ is the elevation range. The model requires three inputs: a DEM, glacier outlines and centrelines that are manually digitized. The digitised branch lines are then converted to 100 m raster cells, and divided into sectors of 50 m elevation range. The slope is calculated and averaged for these sectors and this mean value is assigned to the centroid cell of the sector. The values of τ for the glacier and

the mean slope value thus calculated are used for estimating the ice thickness for the centroid cell. The centroid cell is then converted into a vector (a point feature) that forms the base point for the calculation of ice thickness. Inverse Distance Weighting (IDW) is used to calculate the ice thickness for the cells between the base points on the branch lines of different sectors. These values are then interpolated using the topogrid to estimate the ice thickness for the continuous grid of the glacier.

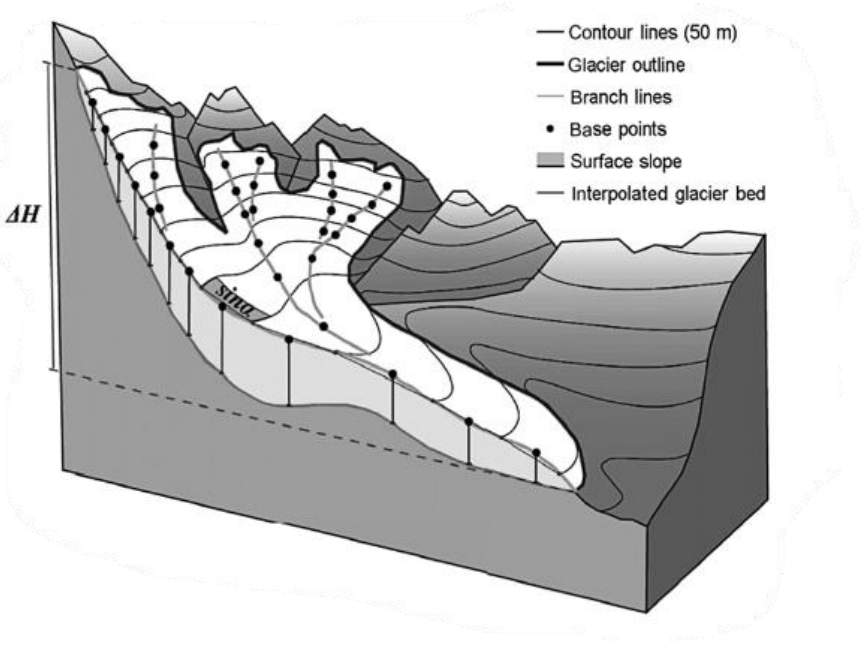

Figure 2.4: Parameters used for ice thickness estimation (Paul and Linsbauer, 2012)

2.3.2. Huss and Farinotti's (HF) Model (Huss and Farinotti, 2012)

The Huss and Farinotti approach require glacier outlines and a DEM as the primary inputs. First, the glacier outline is used to mask the DEM and derive mean slope $\tilde{\alpha}_i$ and area S_i for a given elevation band (i) of 10 m vertical spacing (dz = 10 m) for a given glacier. The width (w_i) of the elevation band is calculated using $w_i = S_i/l_i$ = Si. tan ($\tilde{\alpha}_i$)/dz, where l_i is the elevation band's horizontally projected length. This way the 3-dimensional glacier as seen in Figure 2.4, is converted into a 2-dimensional (2D) shape and the calculations from hereon make use of the values from the 2D shape.

The apparent mass balance $\underline{b}$ of the glacier is calculated using the ice flux divergence, surface mass balance $\dot{b}$ and elevation change $\partial h/\partial t$ using the following equation:

$$\underline{b} = \dot{b} - \rho . \partial h/\partial t \qquad \text{Equ (3)}$$

The apparent mass balance is determined using accumulation and ablation area altitudinal gradients $d\underline{b}/dz_{acc}$ and $d\underline{b}/dz_{abl}$, respectively. These gradients are linearly related to each other by a constant factor $f_{db/dz}$ = 0.55. Since maritime and continental glaciers have different gradients, the model defines a continentality index (C):

$$C = \left(\frac{ELA_{lat} - ELA_g}{f_{cont}}\right) + 1 \quad \text{Equ(4)}$$

Where f_{cont} = 2400 m is a constant parameter, ELAlat is latitude-dependent reference ELA and ELA_g is median altitude. After this C is used to adjust the apparent mass balance gradient to $d\underline{b}/dz_0$ local conditions:

$$d\underline{b}/dz = d\underline{b}/dz_o \,.\, C \quad \text{Equ(5)}$$

Once the apparent mass balance is estimated using the gradients and balanced mass budget, the ice volume flux for elevation band i of the glacier is obtained by integrating the apparent mass balance along the glacier. After this, Glen's flow law is used to obtain the ice thickness. It is assumed that some of the deformation in ice can be due to basal sliding and it is taken into consideration using the equation:

$$f_{sl} = c_1 + c_2 \,.\, (S - 10) + c3.\,(C - 1) \quad \text{Equ(6)}$$

Where c1= 0.2, c2 = 0.1 and c3 = 4 are constants, S is the glacier area (km^2) and C is the continentality index from equation 4. The ice thickness for each band elevation band is calculated using the Glen's flow law (Glen, 1955):

$$h_i = \sqrt[n+2]{\frac{(1 - f_{sl}) \,.\, q_i}{2A_f\,(T)} \cdot \frac{n+2}{(F_{s,i}\rho g \sin\tilde{\alpha}_i)^n}} \quad \text{Equ(7)}$$

Where f_{sl} is a basal sliding factor, q_i is the normalised ice flux, $F_{s,i} = w_i/(2h_i + w_i)$ is a valley shape factor (Nye, 1965). A_f is the flow law's rate factor that depends on the temperature of the glacier.

For temperate glaciers, A_f is assumed to be 0.075 bar^{-3} yr^{-1}. For non-temperate glaciers, A_f is reduced with constant factor $f_{A(T)}$ = 7°C as:

$$A_f(T) = A_f(T = 0). \frac{f_{A(T)}}{f_{A(T)} - T} \qquad \text{Equ(8)}$$

In the final step, the elevation band's ice thickness is extrapolated from the simplified 2-D shape of the glacier to a regular grid by using IDW.

2.3.3. GlabTop2 (Frey et al. 2014):

This model works on the same principles as GlabTop but is automated and does not require manual input of flowlines.

DEM and glacier masks are inputs to estimate the glacier's ice thickness. Parameters from volume area scaling and slope-dependent thickness estimation are used to calculate the ice thickness for a glacier complex and are pixel-based. The glacier is divided into different cells (pixels) for ice thickness estimation. First, the glaciers that share a margin are assigned a combined ID. The process is implemented for cells in one ID, setting aside the glacier cells of different IDs. Cells within the glacier boundary are termed glacier cells, whereas those outside the boundary are called non-glacier cells. Non-glacier cells adjacent to glacier cells are referred to as glacier-adjacent cells. Glacier cells at the boundary edge are identified as glacier marginal cells. The glacier cells inside the glaciers and next to the glacier marginal cells are called the inner cells.

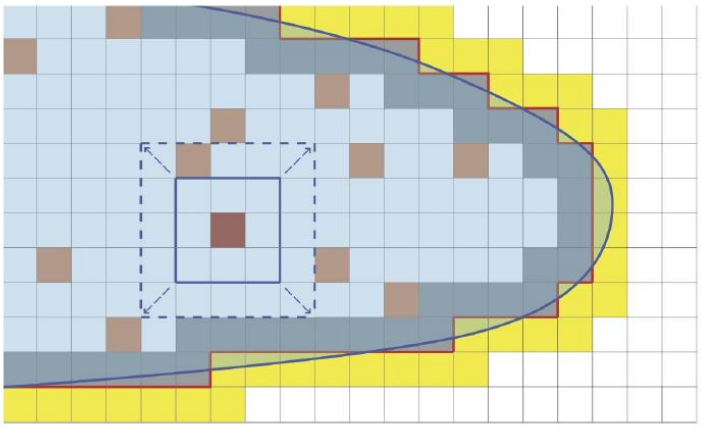

Figure 2.5 : GlapTop2 Workflow: Blue outline: the outline for glacier polygon; Red outline: the outline for glacier cells; Light blue cells: inner glacier cells; Powder blue cells: glacier marginal cells; Yellow: Glacier adjacent cells; White cells: non–glacier cells. Dashed blue square: randomly selected inner cells (Frey et al., 2014)

It is essential to set some parameters for GlabTop2 (t, f, h_{min}, r, h_{ga} and n) for the calculation of the ice thickness. τ is calculated using the following equation from Haeberli and Hoelzle, (1995) using the vertical extent ΔH :

$$\tau[\mathrm{kPa}] = \begin{cases} 0.5 + 159.8\,\Delta H - 43.5\,(\Delta H)^2 & : \Delta H \leq 1.6\ km \\ 150 & : \Delta H \geq 1.6\ km \end{cases} \qquad \text{Equ(9)}$$

Where $\Delta H\ (\mathrm{km})$ is the elevation range of the glaciers. f is taken as 0.8 for all the glaciers. h_{min} is the minimum elevation, till which the buffer should extend. h_{ga} is the minimum ice thickness for the marginal cells of very narrow glaciers. The parameters n, r and h_{ga} are calculated by considering an idealised valley cross-section in a previously glaciated terrain. The values for n are the number of model runs and r is the percentage of inner cells that are set to fit best for all the glaciers. While n does not have much influence over the total ice thickness of glaciers, the value of r is important for the ice thickness's interpolation from marginal cells and random cells to all grid cells of the glaciers.

Random cells are selected from inner glacier cells and a buffer of 3x3 is laid around each cell, this buffer is then extended until the cell that has a difference in DEM equal to or greater than h_{min}, as seen in Figure 2.5. The mean surface slope α of the selected cells is then used in the following formula to calculate the ice thickness h_f:

$$h_f = \frac{\tau}{f\,\rho\,\sin(\alpha)} \qquad \text{Equ(10)}$$

The IDW method is used to interpolate the ice thickness generated for the random cells to all the cells in the glacier. This method is repeated n times. The ice thickness for each cell is then calculated n times and the mean of these calculations is used as the final ice thickness estimate.

2.3.4. HIGTHIM (Himalayan Glacier Thickness Mapper; Gantayat et al. 2017)

HIGTHIM is a semi-automated tool that can be used to calculate the ice thickness. It requires 6 inputs; glacier outline, glacier flowlines, surface velocity of glaciers, moraines outline, DEM and contour polygons. The glacier outlines can be either delineated manually or can be downloaded from open sources. The flowlines are constructed such that the difference between two adjacent flowlines is ~300 m and ~150 m distance of the flowline from the glacier's boundary. Surface velocity is calculated using LANDSAT images with minimal snow cover and the panchromatic band of 15m resolution. The moraines can be delineated using the LANDSAT imagery and False Colour Composite. The contour polygons are made at an interval of 100 m using the DEM.

The tool uses the laminar flow equation keeping Cuffey and Paterson's (2010) method as the base for ice thickness estimation:

$$H = \sqrt[4]{\frac{1.5\ U_s}{Af^3(\rho g sin\alpha)^3}} \qquad \text{Equ(11)}$$

Where the parameters are set for ρ as 900 kg/m^3, acceleration due to gravity g as 9.8 ms^{-2}, creep parameter A as 3.24 x 10^{-24} Pa^{-3} s^{-1} (Cuffey and Paterson, 2010) shape factor f as 0.8 which is the standard value for valley glaciers (Haeberli and Holzle, 1995; Cuffey and Paterson, 2010; Linsbauer et al. 2012), and the surface slope angle a is determined across 100 m elevation contours.

The glacier polygon is split into different zones of 100 m each. The length of the flowline is determined for each of these zones. The slope of the contours is calculated using the length of the flowline for the individual zone. The surface velocity of the glaciers is used to extract the velocity for the flowline of the glaciers. This velocity is then used to calculate the ice thickness of pixels along the flowline using the laminar flow equation. The ice thickness for the rest of the glacier is calculated by interpolating the thickness from the flowline using thin plate spline interpolation.

2.3.5. Volume and Topography Estimation (VOLTA; James and Carrivick, 2016)

This model requires only a DEM and a glacier outline as input for ice thickness estimation. First, VOLTA uses a minimum bounding geometry (MBG) which creates a polygon around the glacier.

Following this, a glacier axis is created by joining the two farthest points of the glacier, within the polygon (Figure 2.6(a)). Perpendicular traverses are created on the glacier axis at the DEM's resolution (Figure 2.6(b)). These lines are then clipped to the glacier outline. After this, midpoints are placed on the clipped perpendicular traverses. These midpoints are then joined to construct a centreline, which is smoothed using the Polynomial Approximation with Exponential Kernel (PAEK) algorithm (Fig 3(c)). Glacier area controls the amount of smoothing, as per Kienholz et al., (2014):

$$l = \begin{cases} 2.10^{-6}.A + 200 & : l \leq l\,max \\ l\,max & : l > l\,max \end{cases} \qquad \text{Equ(12)}$$

Where A is the glacier area (m^2) and *l max* is 1000 m.

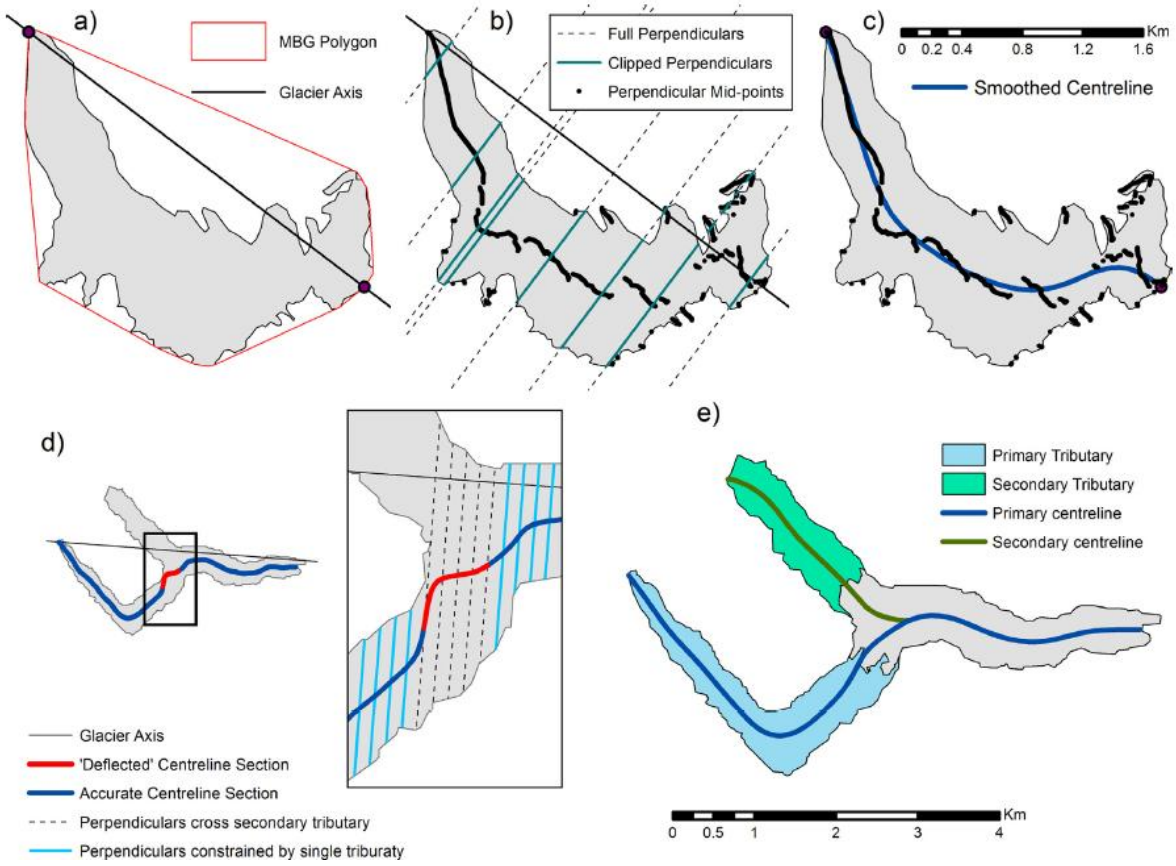

Figure 2.6: Method of centreline production in VOLTA (James and Carrivick, 2016)

For more complex glaciers, which have multiple tributaries and therefore more than one centreline, VOLTA follows the calculation of the upstream area at an interval of 1% of the total length of the centreline. The total upstream area increases down the centreline. If the increase in area between two successive points of the centreline is greater than 30%, a new tributary is identified there. Also, the newly identified tributary should have an area of greater than 20% of the total area. Once, the new tributary is identified, the centrelines are created in the same way as above (Figure 2.6(d) and

2.6(e)). Any perpendicular traverses of the previous tributary are not considered for midpoints. The initial centreline is considered as the primary, following the branch order by Kienholz et al. (2014).

VOLTA uses the following equation to calculate the ice thickness along the centrelines:

$$h = \frac{\tau_b}{f \rho g \tan \alpha} \qquad \text{Equ(13)}$$

A shape factor f is required for valley glaciers. VOLTA uses the approach given by Li et al. (2012) to set the shape factor dynamically. The only difference is VOLTA estimates the vertical ice thickness perpendicular to the horizontal x-axis,

$$h = \frac{0.9\, w\ (\frac{\tau_b}{\rho g \tan \alpha})}{0.9\, w\ - (\frac{\tau_b}{\rho g \tan \alpha})} \qquad \text{Equ(14)}$$

VOLTA has conditions for checking for any inaccurate values of f. Once these conditions are met, the ice thickness for those points is calculated using Equ(14). If the conditions are not met then the ice thickness is calculated using the average shape factor for the centreline and Eq(13). Then VOLTA interpolates the ice thickness using the ANUDEM 5.3 (Hutchinson et al. 2011) through the Topo to Raster tool, using ice thickness and glacier outlines as input. Basal shear stress is found using the formula:

$$\tau_b = 2.7 \,.\, 10^4 \sum_{i=1}^{n} \left(\frac{A_i}{\cos \alpha_i}\right)^{0.106} \qquad \text{Equ(15)}$$

Where A_i is the elevation band area and $\cos \alpha_i$ is calculated over 200 m elevation bands.

Slope averaging distance α_d is the distance through which the centreline gradient is analysed. It is set to 10 times the average thickness $\hat{h}$, which is calculated using the volume area scaling method where A is the glacier area:

$$\hat{h} = \frac{0.2055 A^{1.375}}{A} \qquad \text{Equ(16)}$$

A threshold is defined for minimum slope α_o as otherwise the ice thickness may be overestimated for flatter regions of the glacier. It is set to 4˚ for VOLTA.

2.3.6. Open Global Glacier Model (OGGM; Maussion et al. 2019):

OGGM is a relatively recent ice thickness model. It works on a mass conservation approach. Firstly, gridded climate data for monthly precipitation and temperature are used to calculate the mass balance of the glacier using the formula:

$$m_i(z) = p_f P_i^{Solid}(z) - \mu^* \max(T_i(z) - T_{Melt}, 0) + \varepsilon \quad \text{Equ(17)}$$

where m_i is the monthly mass balance at an elevation z, p_f is a global precipitation correction factor, P_i^{Solid} is the monthly solid precipitation and is calculated as a fraction of the global precipitation ranging from 100% to 0%, T_i is the monthly air temperature, T_{Melt} is the monthly air temperature above which ice melt is assumed to occur, and ε is a bias correction term. T_{Melt} is set to -1°C and p_f is set to 2.5. μ^* is the glacier's temperature sensitivity, and it is calibrated using the approach by Marzeion et al. (2012). μ is calibrated across several years and it is assumed that the mass balance across these years sums to zero. Hence, the mass balance is taken as zero for 31 years and μ(t) is calculated. This μ(t) is then used to calculate the bias ε(t). This calculation is done for more than one given year. The time with the least bias value is taken as the time for calculation and the value of μ(t) for this time is taken as μ^*. This value of t* is then interpolated for different glaciers which do not have observations using the inverse distance interpolation.

The flowlines for the model are constructed using the algorithm provided by Kienholz et al., (2014) (Figure 2.7(b)). Initially, centrelines are created which are then converted into flowlines. There is a main branch line and the rest of the centrelines are tributaries, the tails of the tributaries are cut before they join their respective descendants (Figure 2.7(b) and 2.7(c)). These flowlines are ordered using the Strahler, (1957) ranking system. This order helps in mass flow routing.

The catchment area for the centrelines is defined using the algorithm used to define the centrelines. Intersecting the normals to the flowlines with the catchments or the glacier's boundary provides estimates for the geometrical width (Figure 2.7(c)). These geometrical widths are then corrected by a factor to preserve the altitudinal distribution of the glacier (Figure 2.7(d)). To keep the total area of the glacier the same, these widths are then multiplied by another factor, specific to the altitudinal unit, which ensures that the area of the glacier remains the same as provided in the RGI dataset.

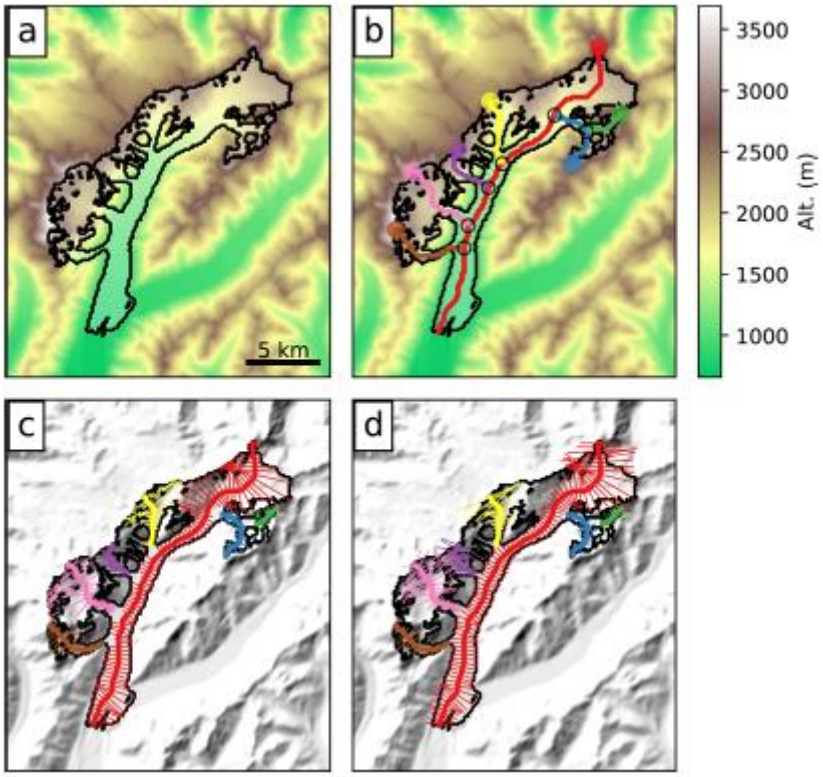

Figure 2.7 : Workflow of OGGM Model for New Zealand's Tasman Glacier; a) preprocessing of topographical data b) centrelines *c) geometric width determination for the glaciers d) geometric width correction for the glaciers (Maussion et al., 2019)*

The mass balance obtained from the above equation, the flowlines computed from the centrelines using an algorithm developed by Kienholz et al. (2014) and the geometrical widths along them, calculated from the catchment areas are used in the ice thickness inversion method. The method uses the following formula for ice flux:

$$q = uS \qquad \text{Equ(18)}$$

Where q is the ice flux (m^3s^{-1}), u is the average ice velocity (ms^{-1}), and S is the cross-section of the area. S varies according to the shape of the glacier bed; for a parabolic bed, it is approximately 2/3 of the area of a rectangular bed. Shallow ice approximation is used to calculate the average ice velocity:

$$u = \frac{2A}{n+2} h\tau^n \qquad \text{Equ (19)}$$

Where h is the ice thickness, A is the ice creep parameter ($s^{-1}Pa^{-3}$), τ^n is the basal shear stress and is calculated using the equation:

$$\tau = \rho g h \alpha \qquad \text{Equ(20)}$$

Where ρ is set to 900 kg m^{-3}, g is set to 9.81 ms^{-2} and α is the slope calculated along the flow line. Sliding velocity can be added to the equation using the following formula:

$$u_s = \frac{f_s \tau^n}{h} \qquad \text{Equ(21)}$$

Mass balance is then used in the equation of mass conservation where the glaciers are assumed to be in a steady state:

$$q = \int_{\Omega}^{n} \left(\dot{m} - \rho \frac{\partial h}{\partial t} \right) dA = \int_{\Omega}^{m} \acute{m} dA \qquad \text{Equ(22)}$$

$\dot{m}$ is the mass balance and $\acute{m}$ is the apparent mass balance at a point in the glacier. For this model, it is assumed that the glacier is in a steady state and $\dot{m} = \acute{m}$. This mass balance is then used with the bed topography, flowline, slope and width:

$$\frac{\partial s}{\partial t} = w\,\dot{m} - \nabla . u \qquad \text{Equ(23)}$$

This equation is solved using a formula that ensures numerical stability and does not include h ($\Delta t = \gamma \frac{\Delta x}{\max(u)}$), where γ is a dimensionless courant number chosen between 0 and 1. This formula is governed by the shape of the glacier bed, unlike other diffusivity formulas which depend on the value of h and overlook the geometry of the bed. *S* at $t + \Delta t$ is used to calculate h ($t + \Delta t$) for local bed geometry. This way h can be calculated for points along the flowline, which is later interpolated for the entire glacier.

2.3.7. Farinotti's Ensemble (Farinotti et al. 2019)

Farinotti's ensemble used five models to estimate the ice thickness of the glaciers. RGI version 6 was used for the outlines of the glaciers. Different DEMs were used for ice thickness models, based on the location of the glaciers. To estimate the final thickness, the ice thickness models were weighted according to inverse variance and bias. A composite solution û for the ice thickness h_i is computed assuming that the ice thickness models are independent. û is calculated as:

$$\hat{u} = \frac{\sum h_i w_i^{-1}}{\sum w_i^{-1}} \qquad \text{Equ(24)}$$

Where w_i is a weighting that represents both the variance σ_i^2 and the bias b_i. b_i is taken as an absolute value penalising both overestimation and underestimation. One-third of the data for ice thickness was used for cross-validation, to estimate the bias and the variance. The remaining two-

thirds of the data was used for model validation. The cross-validation experiment was performed thrice, and the deviations between modelled and measured ice thicknesses were stated relative to the mean ice thickness. The mean and interquartile range of the pooled deviations (from the three experiments) were estimated for b_i / h_i and 1.5 σ/h_i, respectively. The variance û is given by:

$$\sigma_{\hat{u}}^2 = \frac{1}{\sum \sigma_i^{-2}} \qquad \text{Equ(25)}$$

The sensitivity of the weighting strategy was calculated by combining the results of the cross-validation experiment for separate RGI regions. The results are not sensitive to this scheme.

2.3.8. Millan's ice thickness (Millan et al. 2022)

Millan et al. (2022) have mapped 98% of the world's glaciers for ice thickness. Satellite images were orthorectified and used to map the glacier velocity using the method described in Millan et al. (2019). This velocity was calculated for each mosaicked glacier of each sub-region. The outliers from the calculated velocity are removed and a Gaussian smoothing is performed for spatial adaptive filtering. This velocity is used in Shallow Ice approximation, where basal sliding is taken into consideration to calculate the ice thickness using the following equation:

$$v_s = v_b - 2(\rho g)^n \| \nabla s \|^{n-1} A \frac{H^{n+1}}{n+1} \nabla s \qquad \text{Equ(26)}$$

Where v_s is surface velocity, v_b is basal velocity, ρ is set to 917 kg m^{-3}, g is set to 9.81 ms^{-2}, n is taken as 3, s is the ice surface elevation (∇ s being the surface slope) and A is the creep parameter. The slope map of the entire region and the velocity were used to calculate the ice thickness:

$$H = \left(\frac{(v_s - v_b)(n+1)}{2A(\rho g)^n \|\nabla s\|^n} \right)^{\frac{1}{n+1}} \qquad \text{Equ(27)}$$

Since, the basal velocity is not known, a ratio between basal and surface velocity B is used where $v_b = \beta v_s$. This changes the above equation into the following equation:

$$H = \left(\frac{v_s(1-\beta)(n+1)}{2A(\rho g)^n \|\nabla s\|^n} \right)^{\frac{1}{n+1}} \qquad \text{Equ(28)}$$

A and β from the above equation needs to be calibrated. A is calibrated using the following equation:

$$A = \left(\frac{v_s\,(1-\beta)\,(n+1)}{2(\rho g)^n \,\|\nabla s\|^n H^{n+1}}\right) \qquad \text{Equ(29)}$$

2.3.9. Section Summary

Most of the models used in previous studies were included in the ITMIX calculation by (Farinotti et al., 2017) and can be broadly grouped into 4 categories based on their approach to estimating the ice thickness. These are:

1. Mass conservation approaches: HF, OGGM, VOLTA
2. Shear stress-based approaches: GlabTop, GlabTop2
3. Velocity-based approaches: Millan's ice thickness, HIGTHIM
4. Minimization approaches: Ensemble

Nb. Ensemble can fall into all the categories because it uses at least one model from the categories but it has been classified as a minimization approach here which is the main principle behind it

Though these approaches might seem different, several of them follow similar principles. For example, the shear stress-based approach does use velocity in its calculation even though it is not classified as a velocity-based approach. Parameterization becomes important for defining the differences in the ice thickness models. Setting parameters is one of the initial steps for ice thickness calculation. The most common parameters used are the basal shear stress, slope of the glaciers, shape factor, acceleration due to gravity, Glen's flow law constant and density of ice. Among these, definitions of basal shear stress and slope of the glaciers vary for different models. The shape factor is set as 0.8 for GlabTop, GlabTop2 and HIGTHIM, whereas for OGGM, VOLTA and HF model, it is calculated. These parameters are then applied with the required equation for further calculations.

The primary inputs required by all the models include a DEM and glacier outlines, though the specific sources might be different for each model. Apart from that, velocity is also a frequently required input for the models. Some models like HIGTHIM and Millan's ice thickness model calculate the velocity from satellite images by incorporating them in mathematical formulae whereas OGGM does not calculate the velocity though it uses mathematical formulae to estimate the ice thickness.

Over time the complexity of ice thickness models has increased leading to a greater variety of required inputs. Earlier models like the HF- model required only DEM and a glacier outline. In contrast, recent models like the OGGM use climate data, catchment area width and flowlines along with DEM and outline. While flowlines are not a required input for all the models, they still play an important role in determining the ice thickness. All models follow Kienholz et al. (2014) for the construction of flowlines though the method used for constructing them can be different. Models like GlabTop and HIGTHIM require manual construction of the flowlines, whereas VOLTA and OGGM can generate them based on DEM and the glacier outline provided.

The glacier flowline is also used as a base unit for ice thickness estimation. The base unit can be considered the smallest part of the glacier for which the ice thickness is calculated and later interpolated to generate the ice thickness for the entire glacier. HF Model has an elevation band as a unique base unit when compared to other models that use cells (pixels) as their base unit. These cells are along the flowlines for most of the models. The interpolation technique that is commonly used is IDW. VOLTA and HIGTHIM use spline for interpolation and Millan's ice thickness model has used kriging specifically for Antarctica.

Millan's model, OGGM and Farinotti's Ensemble have estimated the ice thickness of all the glaciers worldwide. HF model has estimated the ice thickness of 300 glaciers worldwide. These ice thickness outputs can be further used as foundational data for various glaciological studies. The parameters, methods, equations, and inputs differ not only between models but also within the same model across various environmental settings. As a result, analyses based on these ice thicknesses are likely to vary.

2.4. IMPORTANCE OF PREDICTING FUTURE OVERDEEPENING POSITIONS

While glacial lakes play a crucial role in glacier dynamics, they also pose hazards. In regions like the Himalayas and Peruvian Andes, where glacial hazards are common, early detection and monitoring of overdeepenings can enhance preparedness and mitigation efforts, particularly for hazards such as GLOFs (Sattar et al. 2019). Globally, the number and size of glacial lakes have been increasing (Carrivick et al. 2022; King et al. 2020; Majeed et al. 2021a), which is a trend that is expected to continue in future years (Furian et al. 2025).

There have been many glacial lake outburst floods in recent years. The recent GLOF in August 2024, due to a break in the dam of Thynabo Lake in Nepal, swept away the major infrastructure of Thame

village and displaced at least 135 people (Khatri, 2025). Such events underscore the importance of identifying and assessing hazard potential in downstream locations. Given that glacial lakes are often unstable during their early formation stages (Emmer et al. 2015b), it is crucial to predict and monitor the evolution of overdeepenings to anticipate future hazards.

Overdeepenings play a central role in predicting the formation of future lakes, though not all overdeepenings transform into lakes (Fountain and Walder, 1998; Evans, 2008). Nevertheless, they remain important because they influence sedimentation patterns and contribute to landscape evolution. Advanced detection techniques, particularly remote sensing, have proven invaluable in identifying overdeepenings in inaccessible regions (Haeberli et al. 2016; Magnin et al. 2020). This technological progress enhances our ability to manage GLOF risks and contributes to long-term hazard reduction strategies (Drenkhan et al. 2018, 2019; Sattar et al. 2019).

2.5. SUMMARY

Current and future overdeepenings have become a popular focus in the glaciological literature, mostly on a regional basis in the valley glacier setting, and in mountain regions where communities live within the downstream areas (Drenkhan et al. 2019). While overdeepenings in the ice sheet environment is crucial for understanding broader glaciological processes and the delivery of sediments to the oceans (Carrivick et al. 2022), those in valley glacier settings demand particular attention due to their direct implications for human safety and hazard management. Frey et al., (2010) first explained how ice thickness, glacier outline and DEM can be used for estimating overdeepenings. This method has since been used very broadly.

Despite the easy availability of DEMs and ice thickness data, most studies use either one ice thickness model and one DEM or at most two ice thickness models or two DEMs. The overdeepenings produced from just one combination of a DEM and ice thickness model are then used as a base to gain future perspectives on a hazard assessment (Drenkhan et al., 2019; Furian et al., 2025). Given that existing datasets often lack precision in determining the morphometry of overdeepenings, relying on them without accounting for their inherent uncertainties can amplify errors in future predictions. Accurate morphometry is crucial for assessing the potential downstream impacts of overdeepenings, particularly if they evolve into glacial lakes capable of triggering GLOFs. Therefore, addressing these uncertainties is essential for reliable hazard assessment and management.

The wide variety of datasets available for glaciological studies has led to inconsistencies in the data used across individual studies. This lack of standardization makes it challenging to compare results between different regions, even when the glaciers are of similar type. Studies that use multiple datasets often yield varying results, highlighting the inconsistencies from using different data sources. Given these variations and the availability of various DEMs and ice thickness models, a comparative study incorporating multiple datasets could offer valuable insights. Such an analysis would help clarify how different models and DEMs perform relative to each other, ultimately improving our understanding of their reliability and the potential biases they introduce. This is the primary motivation for the current study.

3. AIMS AND OBJECTIVES

Based on the literature review, it can be seen that only a few studies have used more than one DEM or one ice thickness model to detect subglacial overdeepenings. Those studies that do use more than a single approach are still limited by the fact they only implement their process within a single region. To date, there has not been an intercomparison between the models and the DEMs to assess whether there is regional variability among the models.

Considering the findings from the previous studies, the aims of this study are, therefore, to:

1. Determine the consistency of different DEM and ice thickness model combinations in predicting the depth, volume and area of subglacial overdeepenings.
2. Determine the extent to which the outputs from different ice thickness models vary across different regional settings.
3. Propose a method that can account for the uncertainties produced by different ice thickness models.

These aims will be met by addressing the following objectives:

1. Generate quantitative estimations of overdeepening location, depth, area and volume using different combinations of DEM and ice thickness products for a single test area (Central Himalayas).
2. Investigate how variations in overdeepening predictions manifest across different mountain regions (in different climatic and topographic settings) to explore regional trends and inconsistencies.
3. Explore the effectiveness of combining outputs from multiple ice thickness models to improve the robustness of overdeepening assessments and reduce uncertainties.

4. METHODS

4.1. STUDY AREAS

Globally glaciers from five regions were chosen as study area, see Figure 4.1 and Figure 4.2 for reference. These regions were the Himalayas, Peruvian Andes, Alaska, New Zealand Southern Alps and the European Alps.

4.1.1. Himalayas

The Himalayas range from Namche Barwa in the east to Arkan Yoma in the West spanning over 2400 kilometres across five countries: India, China, Nepal, Pakistan and Bhutan. They are a major water source for Asian perennial rivers like Indus, Ganges and Brahmaputra. A recent glacier inventory for the Himalayan Karakoram glaciers shows that there are around 21,000 glaciers (Cogley, 2016). In the Himalayas, these glaciers cover an area of around 23,000 km^2, which has a volume of 1,071 km^3 (Bolch et al. 2012). Although the rate of glacial retreat varies across different parts of the Himalayas, studies have shown that approximately 13% of a mapped 11,000 km^2 of the glaciated area has been lost due to glacier retreat (Kulkarni and Karyakarte, 2014). As these glaciers retreat, they expose new areas of the landscape leading to the formation of a large number of glacial lakes and increasing the risk of natural disasters such as GLOFs. This threat to mountain communities is additional to that posed by an increasingly uncertain water supply as glaciers reach and pass peak water (Huss and Hock, 2018), where temperature and precipitation patterns become more erratic and more extreme (Regmi and Bookhagen, 2022).

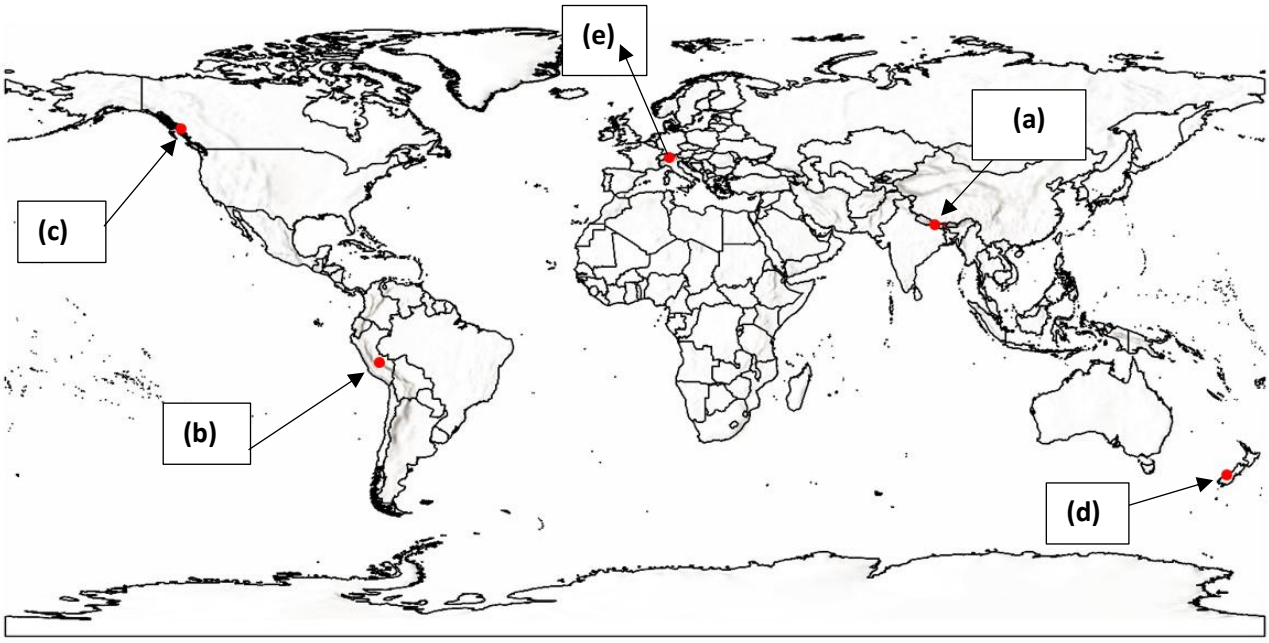

Figure 4.1: Study regions in the world map. Note the red dots represent the study region, and the letters refer to panels in Figure 4.2

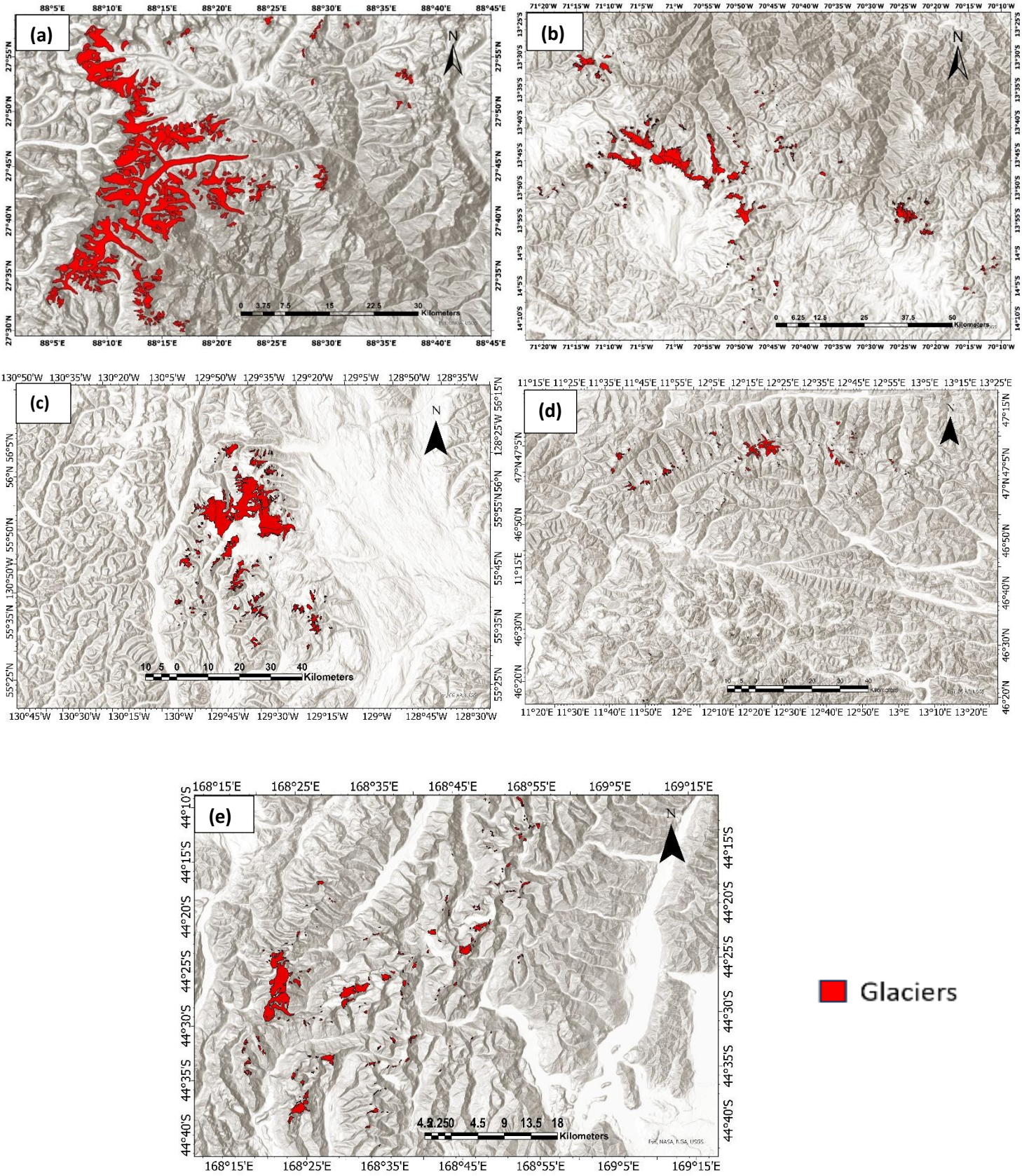

Figure 4.2: Selected glaciers in the (a): Himalayas (b) Peruvian Andes (c) Alaska (d) European Alps (e) New Zealand Southern Alps

4.1.2. Andes

The Andes are home to over 99% of the world's tropical glaciers (Kaser, 1999). These glaciers are distributed across several countries including Bolivia, Peru, Ecuador and Colombia-Venezuela and are found at elevation ranges from 4,000 m and, to 6,500 m in altitude. Collectively, they cover a total area of 2,560 km^2 (Rabatel et al. 2013). These tropical glaciers are particularly sensitive to changes in moisture and precipitation and act as early indicators of climate change (Jomelli et al. 2009). Glaciers in the inner tropics will be more sensitive to warming in the future (Vuille et al. 2018). Similar to the glaciers present worldwide, at present they are also undergoing retreat since the Little Ice Age. Glaciers in the Cordillera Blanca region have decreased in area by 46% from 1930 to 2016 (Torres and Jaquet, 2017) and in the Cordillera Vilcanota they have decreased in area by 54% from 1975 to 2020 (Taylor et al. 2022). This ongoing retreat poses risks, as it can increase the likelihood of various glacial hazards, including avalanches, rockfalls, and GLOFs (Chevallier et al. 2011).

4.1.3. Alaska

There were around 100,000 glaciers in Alaska that covered 74,705 km^2 (equal to 4.33% total area of present-day Alaska) in 1980 (Meier et al. 1985). Recently the glacier retreat has increased in Alaska, with it projected to contribute the highest amount to sea level rise from 2015 to 2100 (Rounce et al. 2023). An example can be seen in glaciers like Barry Glacier where glacier thinning has accelerated in recent years, from 2010 to 2017 (Dai et al. 2020). It has resulted in a horizontal slope displacement of 120m for the glacier.

The mass balance of glaciers here is complicated as there are glaciers that show retreat and there are few glaciers that show advance (Alifu et al. 2016; Johnson et al. 2013), like the Hubbard Glacier. Glaciers in Alaska, and the West Fork Glacier, have experienced surging in the past. Between 1987 and 1988, the West Fork Glacier displaced approximately 4 km of ice by surging (Harrison et al. 2003).

The rising temperatures and changes in precipitation patterns govern the glacial dynamics here. Alaska's glaciers, in particular, have played a substantial role in this process, accounting for a significant portion (0.4m of sea level rise equivalent) of the overall sea level increase during this period (Zemp et al. 2019). Previous work focussing on Alaskan glaciers has focussed on the formation of glacial lakes, an increase in risk due to glacial lake outburst flood and also changes in the nutrient content that can affect the aquatic life downstream (Dorava and Milner, 2000; Moore et al. 2009).

4.1.4. European Alps

The European Alps extend around 1,000 km across Germany, France, Austria, Italy, Slovenia, Switzerland and Liechtenstein. Rather than forming a continuous expanse of ice, the glaciers in the Alps are scattered throughout. The range has a few high summits, with Mont Blanc standing as the tallest peak, reaching an elevation of about 4,800 m (Deline et al. 2012).

These glaciers have lost roughly 0.5 a^{-1} volume of ice thickness ranging in a span around 12 decades starting from 1850, this loss accelerated sharply after 1975 till 2000 with a change of 25% and further with a change of 10-15% in the early 2000s (Haeberli et al. 2007). As a result, the total glacier surface area fell to just over 2,000 km² by the early 2000s (Sommer et al. 2020).

This rapid decline in the glacier area (Zemp et al. 2006) has far-reaching consequences for the region including disruptions to the water cycle, increased risk of natural hazards and alterations to the landscape like landslides and formation of glacial lakes (Haeberli, 2013; Haeberli et al. 2017).

4.1.5. New Zealand Southern Alps

The New Zealand Southern Alps stretch over approximately 500 kilometres along New Zealand's South Island. In the mid-1970s, the region contained 3,132 glaciers, covering a total area of 1,139 km². Of these, only 702 glaciers were larger than 0.2 km², and they accounted for about 86% of the entire glaciated area according to Hoelzle et al., (2007). There has been a loss of 41% to 62% (of the Little Ice Age (LIA) volume) in the volume of the glaciers since LIA till 2019 (Carrivick et al. 2020). These glaciers are located in a cool temperate climate, characterized by significant variations in precipitation, ranging from about 1.5 meters per year to nearly 12 meters per year (Henderson and Thompson, 1999) across the topographic divide. Among these glaciers, only a small number terminate in lakes (Chinn, 1999). Despite their limited number, these lake-terminating glaciers play an important role in the region’s tourism (Purdie, 2013).

The New Zealand Southern Alps experienced a positive mass balance for many glaciers in the 1990s, indicating a period of relative stability and growth. However, recent studies (Anderson et al. 2021; Carrivick et al. 2022) have highlighted a marked shift, with glaciers in the region now experiencing a more pronounced retreat. Along with the retreat, the expansion of ice-marginal lakes can cause changes in the glacial dynamics in the New Zealand Southern Alps (Carrivick et al., 2022).

4.2. DATA SOURCES

4.2.1. Glacier Outlines:

Most previous studies have used Randolph Glacier Inventory version 6 (RGI 6.0, Pfeffer et al., 2014) for estimating overdeepenings and ice thicknesses for valley glaciers worldwide. This study also used RGI 6.0 for estimating the overdeepenings to ensure uniform data processing. RGI is a global inventory of glaciers worldwide (excluding the Greenland and Antarctica ice sheets). It is a subset of the Global Land Ice Measurement from Space (GLIMS) initiative (Raup et al. 2007), which has more attributes than the RGI. RGI glacier outlines were first released in 2012 and have been continuously updated since then.

4.2.2. Ice Thickness Models:

Five ice thickness models were used in this investigation. Three of them (GlabTop2, OGGM and Huss and Farinotti) were selected from those included in Farinotti's Ensemble, with Farinotti's Ensemble itself being chosen for the analysis (Farinotti et al. 2019a). The fifth ice thickness was that of Millan et al. (2022). All ice thickness models require glacier outlines and DEMs as basic inputs to estimate ice thickness. Additional inputs may vary depending on the model. OGGM requires climate data, while the Millan model incorporates glacier velocity data. The ice thickness of OGGM for the Himalayas was estimated manually. The parameters were set to default for the estimation. The resulting ice thickness estimates are available in raster formats, with a resolution of 49.99 m for the Millan model and 30 m for other ice thickness models. Data were downloaded using the following links:

Millan's ice thickness: SEDOO/2022 https://doi.org/10.6096/1007

HF, GlabTop2, OGGM and Farinotti's Ensemble: ETH Zurich/2019 https://doi.org/10.3929/ethz-b-000315707

4.2.3. Digital Elevation Models (DEMs):

Four DEMs were used in the study (Copernicus, ASTER GDEM, SRTM and ALOS PALSAR), to assess the extent to which the choice of DEM impacted overdeepening location and characterisation. Among these DEMs, Copernicus and ALOS-PALSAR have a global coverage whereas the SRTM and ASTER GDEM have a *nearly* global coverage. SRTM and ASTER GDEM have been used most widely to

estimate the ice thickness. Recent studies (Furian et al. 2023) have acknowledged ALOS-PALSAR for being high resolution and it has been used for validation of the overdeepenings estimate. These particular DEMs were chosen to represent sources that were easily available (i.e. open source), have been widely used in other studies (so provide potential comparison with this study), have published accuracies that demonstrate their quality, and do not contain voids that would complicate and/or compromise the validity of the processing chain. Previous studies have indicated that the choice of surface DEM can be important for the identification of overdeepenings (Linsbauer et al. 2012; Magnin et al. 2020), but without assessment across a broad area.

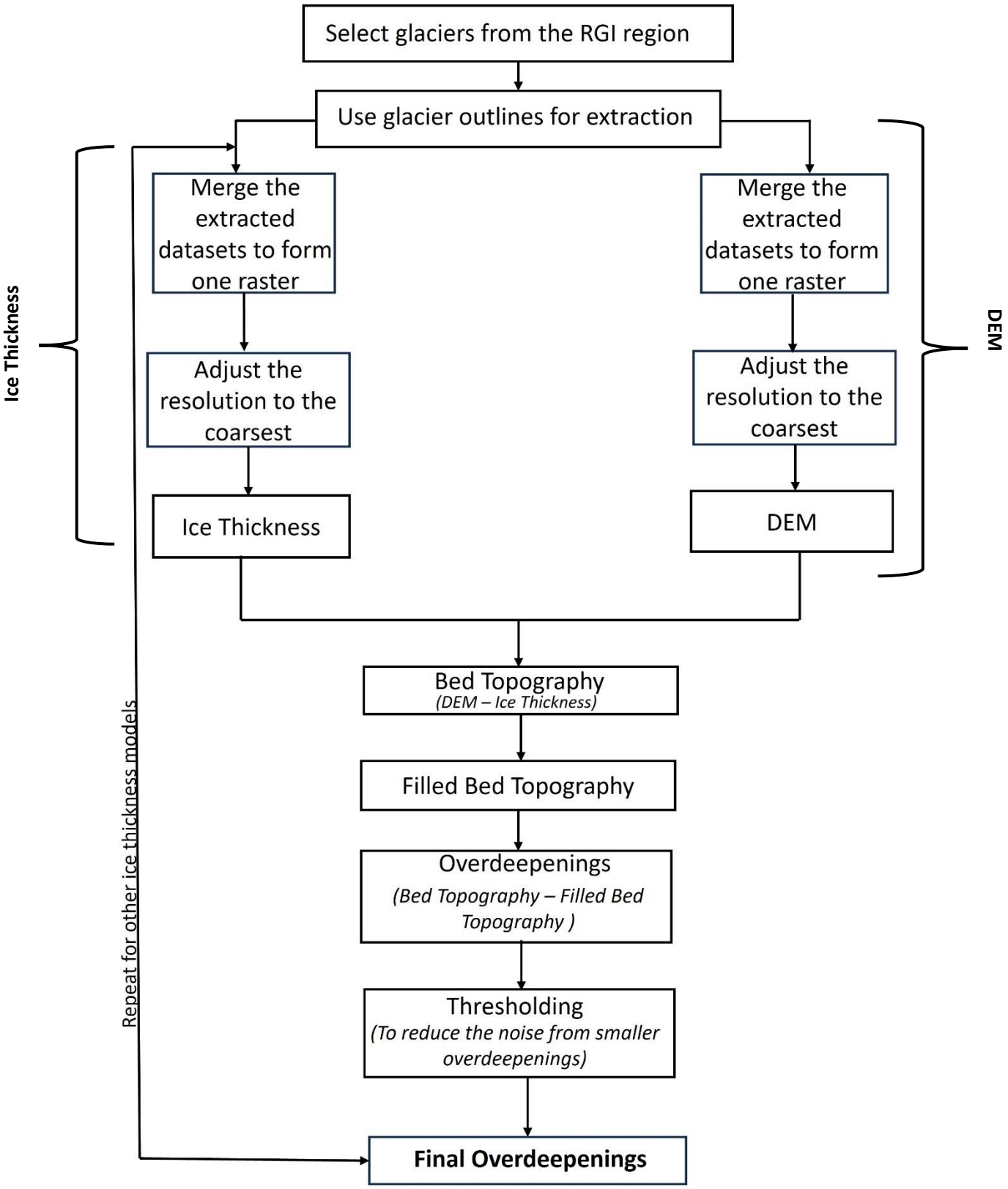

Figure 4.3: Flowchart of the methodology followed

4.3. DATA PREPROCESSING

Figure 4.3 represents the data processing followed in this study.

4.3.1. Selecting glaciers in one RGI region

There are 19 RGI regions for all glaciers worldwide in the inventory. Five regions containing valley glaciers were chosen for analysis in the current study. These regions are heavily populated (and therefore knowledge of overdeepening locations is of practical benefit to society) as well as representing a range of climatic conditions (monsoon, westerlies, tropical), geologies, and topographies.

The Central Himalayas were selected as the initial region for method development before extending the approach to other areas, given its stored water potential (Shruti et al. 2025) . The region near the Zemu Glacier (27°45'51.19"N, 88°22'32.57"E) was chosen, as it recently garnered attention due to a major GLOF that occurred in October 2023 (Sattar et al. 2025). This event was triggered by intense rainfall in Sikkim, where the region experienced double its usual precipitation. The excessive rainfall caused the moraine dam of South Lhonak Lake to breach, resulting in a catastrophic GLOF. The flood had devastating downstream effects, claiming at least 93 lives and severely damaging infrastructure, including the Chungthang hydroelectric dam on the Teesta River. The other regions (as described above) were Alaska, New Zealand's Southern Alps, the Peruvian Andes, and the European Alps. In all the regions except for the Himalayas, area breaks were defined using the histograms observed in ArcGIS Pro. For the Himalayas, the subset was chosen randomly with glaciers including and around the Zemu Glacier. In each of these other four regions, area breaks were established, and 200 representative glaciers were chosen from these defined area ranges from the RGI region. These area breaks were determined by the histograms observed in ArcGIS Pro. Area was chosen as the basis to select the representative glaciers, to maintain the heterogeneity in terms of parameters like slope, debris cover, aspect without introducing a bias to any other factor, while also ensuring the sample size of 200 was representative of the entire RGI region (in terms of area breaks). The distribution of glaciers in the entire RGI region and the subset are given in Table 4.1 and Figure 4.5. The distribution of the glaciers in the subset is representative of the distribution in the RGI region (Table 4.1 and Figure 4.4, Figure 4.5), based on the defined area breaks. The median glacier area of the entire RGI region was then compared to that of the subset. As seen in Table 4.2, the median

value for the entire region and the subset is similar for all the regions, indicating that the findings from the analysis could be broadly applicable to all glaciers within that region.

Table 4.1: Area breaks and distribution of glaciers in the subset and the RGI region

		Number of glaciers	
Region	**Area Breaks (km^2)**	**RGI region**	**Subset**
Alaska	0 – 0.1	5070	38
	0.1 –1	16357	120
	1 –10	4924	36
	>10	757	6
European Alps	0 – 0.1	2181	112
	0.1 – 1	1339	68
	1 – 3	271	14
	>3	136	6
Andes	0 - 0.5	1921	116
	0.5 – 0.9	292	20
	0.9 – 1.4	218	13
	>1.4	460	51
New Zealand Southern Alps	0 – 0.1	2120	120
	0.1 – 0.5	1053	60
	0.5 – 0.9	185	10
	>0.9	179	10

Subsequently, a Wilcoxon test was conducted to more robustly assess the similarity of the distributions. A Wilcoxon test is a non-parametric test to check if two datasets are significantly different.

The p-value for all regions is greater than 0.05 except the Andes, indicating there is a significant similarity in distribution among the subset and the entire region (see Table 4.2). The p-value for Andean glaciers is 0.0266 but excluding the largest glacier from the Andean subset increases the p-value to 0.07, and it still does not affect the median as much (it changes from 0.2765 to 0.2760). Suggesting the distribution is resistant to extreme values even with presence of some bias. Hence, it can be assumed that the inclusion or exclusion of this glacier does not meaningfully alter the central tendency. Therefore, the glacier was retained in the subset, as its presence does not significantly impact the overall analysis.

Table 4.2: Median values for the RGI glaciers and the subset with p-value of the Wilcoxon test

	Median Values		**Wilcoxon Test**
Region	**RGI glaciers**	**Subset glaciers**	**p-value**
Alaska	0.313	0.311	0.5975
European Alps	0.077	0.078	0.9782
Andes	0.218	0.276	0.0266
New Zealand Southern Alps	0.077	0.066	0.7207

Study Area	Histograms for Subsets	Histograms for the Entire Region
Andes	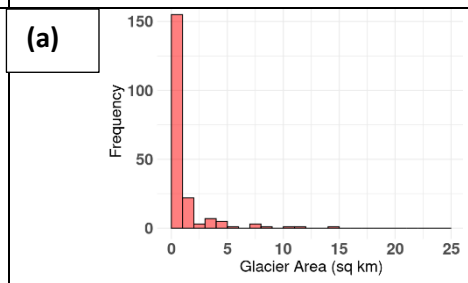	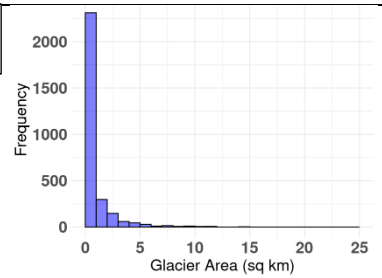
Himalayas	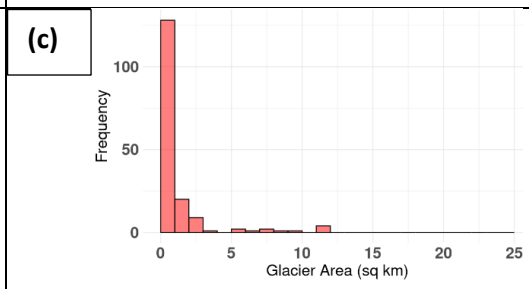	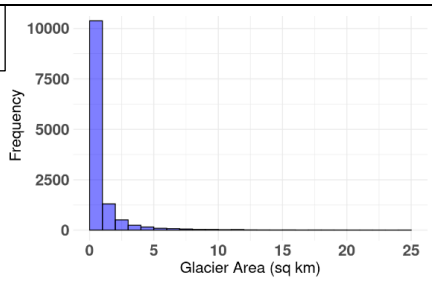
New Zealand Southern Alps	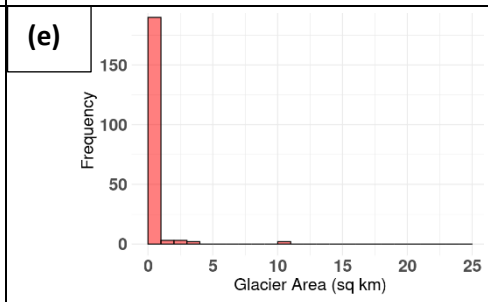	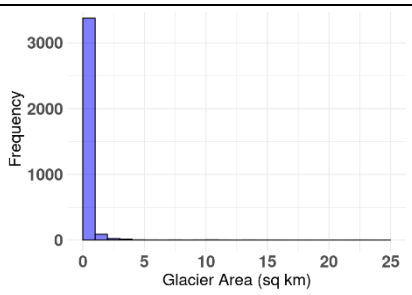
Alaska	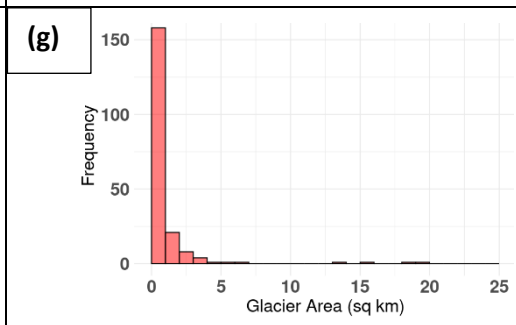	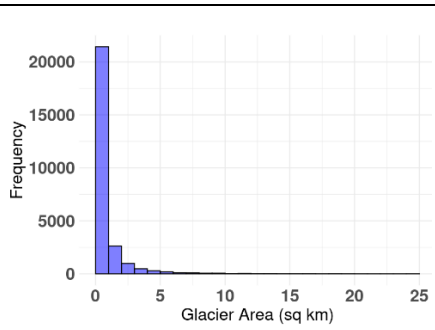
European Alps	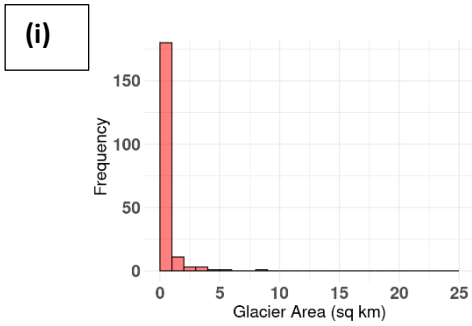	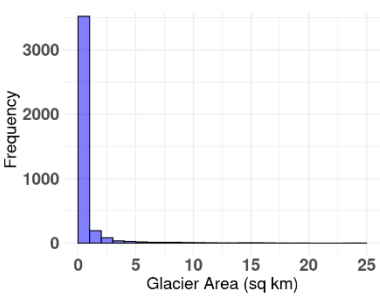

Figure 4.4: Histograms of area distribution of the RGI region glaciers and the selected subsets

Study Area	Histograms for Subsets	Histograms for the Entire Region
Andes	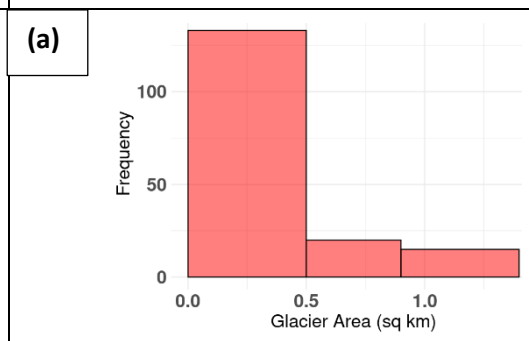	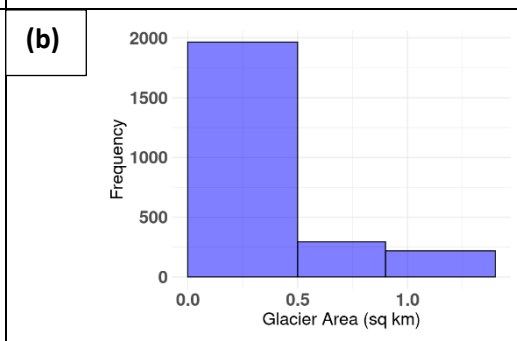
New Zealand Southern Alps	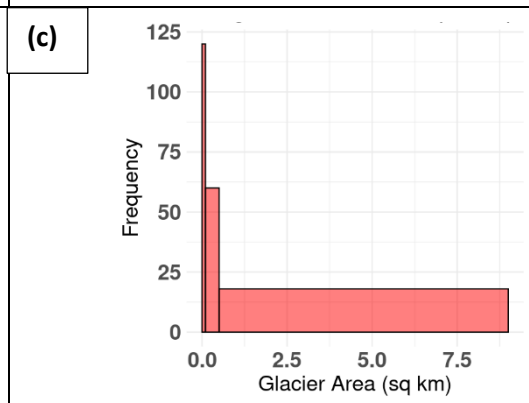	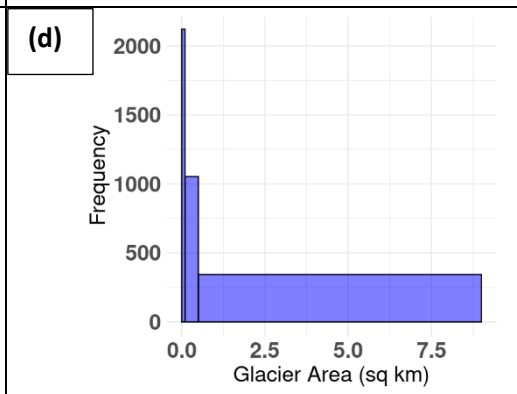
Alaska	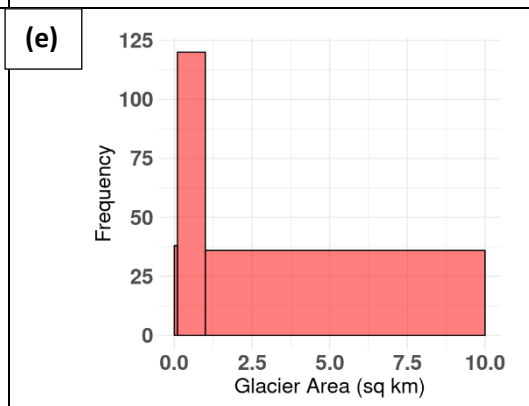	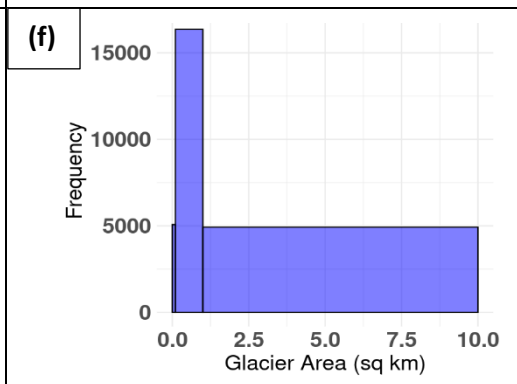
European Alps	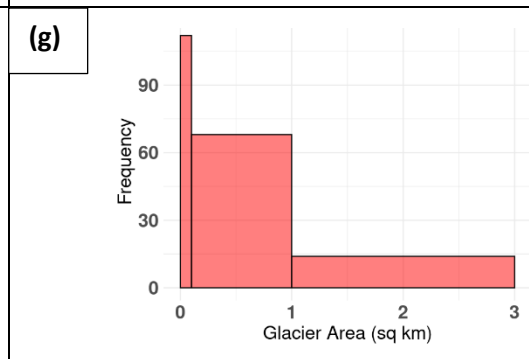	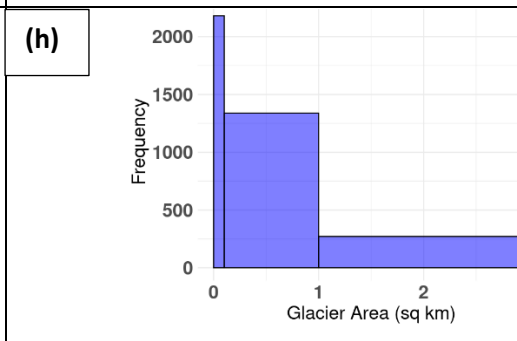

Figure 4.5: Histograms of area distribution of the RGI region glaciers and the selected subsets with defined area breaks

4.3.2. Selecting the ice thickness models

Five ice thickness models were chosen for the analysis. These were:

i) *Farinotti's Ensemble (Farinotti et al. 2019a)*: This is one of the latest ice thickness datasets available. It has an input of 5 ice thickness models as an ensemble, suggesting it may be more robust than using any single model in isolation.

ii) *Huss and Farinotti (Huss and Farinotti, 2012):* This is one of the oldest models and has been used in estimation of ice thickness for various studies. The ice thickness for this model is also available for all glaciated regions.

iii) *GlabTop2 (Frey et al., 2010):* This is one of the widely used models for estimating overdeepenings in glaciated regions, as seen in Chapter 2, and has been frequently applied to estimate the ice thicknesses of valley glaciers.

iv) *Open Global Glacier Model (OGGM; Maussion et al. 2019)*: This is one of the recent ice thickness models, developed to simulate glacier evolution rather than ice thickness *per se*. OGGM requires inputs (like the precipitation and temperature data) and the data for this model are also available for all the glaciated regions.

v) *Millan* (*Millan et al. 2022*): This is the latest ice-thickness product available for the glaciated regions.

4.3.3. Ice thickness grids were available on an individual glacier basis, except for the Millan dataset where the grid comprised the entire RGI region. In this particular case the thickness estimates for selected glaciers were clipped and merged before inserting into the workflow. Areas of no-data exist in several of the models, in particular around the glacier margins. Where necessary these pixels were removed by masking the rasters with the glacier outlines. The cleaned rasters were then merged to create an ice thickness dataset for the subset of the region.Selecting the DEM

The following DEMs were used in the initial analysis for the Central Himalayas:

i) *Advanced Space Borne Thermal Emission and Reflection Radiometer (ASTER) DEM*: It is obtained from the ASTER instrument (Fujisada et al. 1998) onboard the National Aeronautics and Space Administration's (NASA) Terra satellite, launched in 1999. It has a spatial resolution of 30 m and covers most of the Earth from latitudes 82˚North to 82˚ South. This is one of the recommended DEMs for studying the Himalayan glaciers (Bhambri and Bolch 2009; Bolch et al. 2012; Ragettli et al. 2016).

ii) *Shuttle Radar Topography Mission (SRTM) DEM*: This mission was launched in 2000 as a joint venture of NASA, the National Geospatial-Intelligence Agency (NGA), and the German and Italian Space Agencies. It covers latitudes ranging from 60˚North and 56˚ South (Rabus et al., 2003). The DEM has two resolutions one of 30 m and the other of 90 m. This study has used the resolution of 30 m. Also, it is one of the most widely used DEMs for the Himalayas (Fujita and Nuimura, 2011; Pandey and Venkataraman, 2013; Yao et al. 2012).

iii) *Copernicus DEM*: This was programmed and launched by the European Union Earth Observation. This covers data from pole to pole. It is derived from the German Aerospace Center's (DLR) TanDEM-X mission data. This radar interferometry mission used twin satellites (TerraSAR-X and TanDEM-X) to generate a global digital elevation model of Earth's surface from 2010 to 2014. The 30m resolution was used for this study.

iv) *Advanced Land Observing Satellite Phased Array L-band Synthetic Aperture Radar (ALOS PALSAR) DEM*: This DEM is generated by the PALSAR instrument onboard the ALOS satellite that covers the global region from 80˚North to 80˚South. The DEM is available in two main resolutions 12.5m and 30 m. This study has used the resolution of 30 m. This product has been used in several recent studies in the Himalayas (Furian et al. 2021, 2022).

4.3.4. Standardizing the resolution of all the datasets

Given that the DEMs and ice thickness models had differing spatial resolutions (Table 4.3), keeping them at their native resolution may have introduced some uncertainty in the comparisons between the model outputs. ALOS-PALSAR DEM was selected for the second part of the analysis because of its high resolution and worldwide void-free coverage. It was downsampled to 49.99 m for all of the analysis. This also ensured that the method this study follows, can be adapted easily. Therefore, all datasets were resampled to the lowest resolution using the 'Resample Tool' in ArcGIS Pro to minimize such errors. The resampling technique used was cubic convolution, producing a geometrically less distorted raster than that obtained by the nearest neighbour technique. Also, it uses values based on the smooth curve on the 16 nearest input cells. Since Millan's ice thickness model had the coarsest resolution of 49.99m, all other datasets were adjusted to match it. The rationale behind taking Millan et al. (2022) ice thickness data as one of the five datasets was to introduce at least one ice thickness model that is recent and is not a part of Farinotti's Ensemble

(Farinotti et al. 2019). This was done to check Millan's ice thickness performance (whether it produces any anomalies) in estimating overdeepenings in comparison with other ice thickness models across regions.

It is acknowledged as the data becomes coarser it might lead to change in size of the estimated overdeepenings. At the same time, it ensures that the overdeepenings thus generated might have less error in data as the predicted depth values become smoother with the use of cubic convolution while down sampling. Overdeepenings with at least 4 pixels were taken into consideration to ensure that area and volume generated by these would be high enough for inter-model and inter-regional comparison.

Table 4.3: Datasets and their resolution

Dataset	**Resolution**
Farinotti's Ensemble Ice Thickness	25m
GlabTop2 Ice Thickness	25m
Millan's Ice Thickness	49.99m
OGGM's Ice Thickness	25m
HF's Ice Thickness	25m
ALOS-PALSAR DEM	30 m

4.4. ESTIMATING THE OVERDEEPENINGS

Frey et al. (2010) explained a multi-level strategy to investigate the formation of future glacial lakes in which they identified four levels. This study implements the first three levels of this strategy to determine the overdeepenings using the DEM and the ice thickness. The first two levels of identifying the study area with glaciers and selecting the appropriate datasets for analysis are explained in the section 4.4.1. and the third level of performing the analysis for estimating the overdeepenings is explained in 4.4.2. The aim of this study was to find consistency among the datasets, the fourth level of validating the datasets with ground data was avoided, as measuring the accuracy of the datasets was not in the scope of this study.

4.4.1. Estimating the Bed Topography

Understanding the bed topography beneath the glacier aids in a better understanding of the landscape evolution in the glaciated region (Linsbauer et al. 2012). This serves as the key to predicting overdeepening locations and characteristics. Since the bed topography beneath the glacier is covered by ice, and the DEM gives information about the elevation of the ice thickness and the bed topography, the bed topography was calculated by subtracting the ice thickness from the DEM.

4.4.2. Predicting the Overdeepenings

With a simulated bed topography, it was possible to automatically identify overdeepening locations by using hydrological tools to identify surface (glacier subsurface) depressions (Figure 4.6). These depressions were filled using the Fill Tool in ArcGIS to level the bed topography. The filled bed topography was then subtracted from the original bed topography (with sinks) to yield the overdeepenings.

(a)

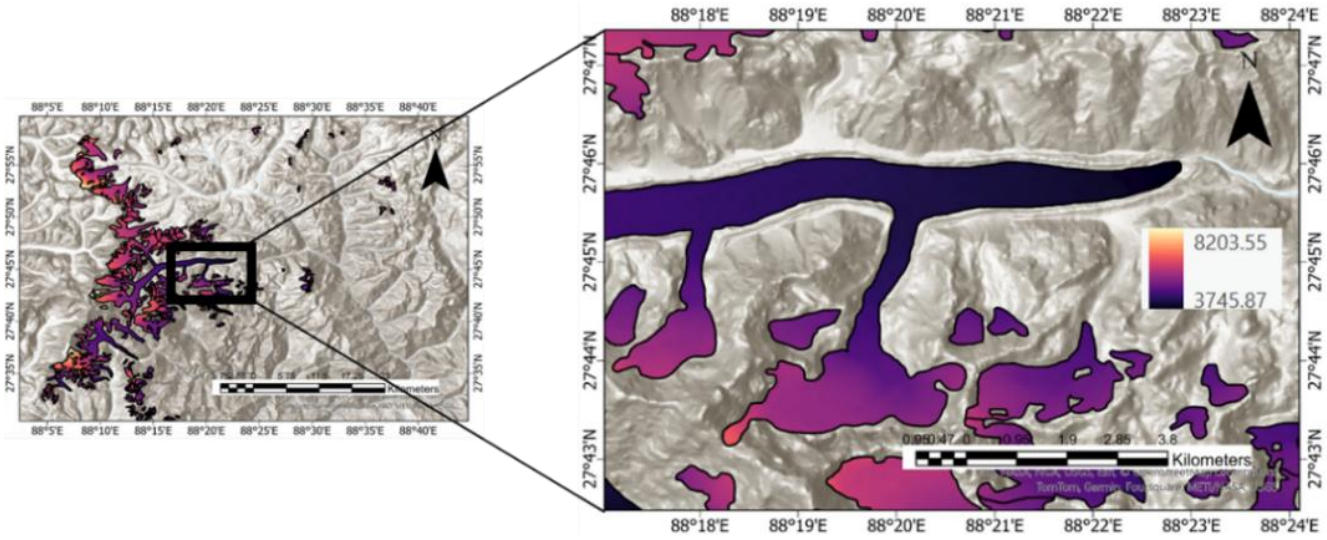
88°18'E
88°19'E
88°20'E
88°21'E
88°22'E
88°23'E
88°24'E
27°47'N
27°46'N
27°45'N
27°44'N
27°43'N
N
8203.55
3745.87
Kilometers

(b)

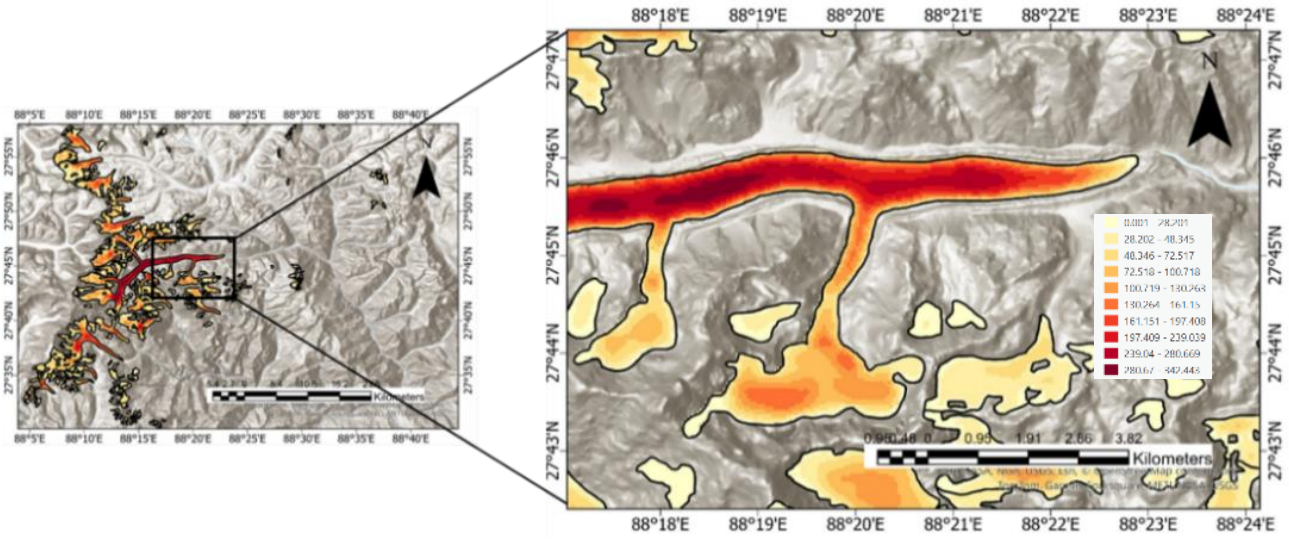
88°18'E
88°19'E
88°20'E
88°21'E
88°22'E
88°23'E
88°24'E
27°47'N
27°46'N
27°45'N
27°44'N
27°43'N
N
28.202 - 48.345
40.346 - 72.517
72.518 - 100.718
100.719 - 130.268
130.264 - 161.15
161.151 - 197.408
197.409 - 239.039
239.04 - 280.669
Kilometers

(c)

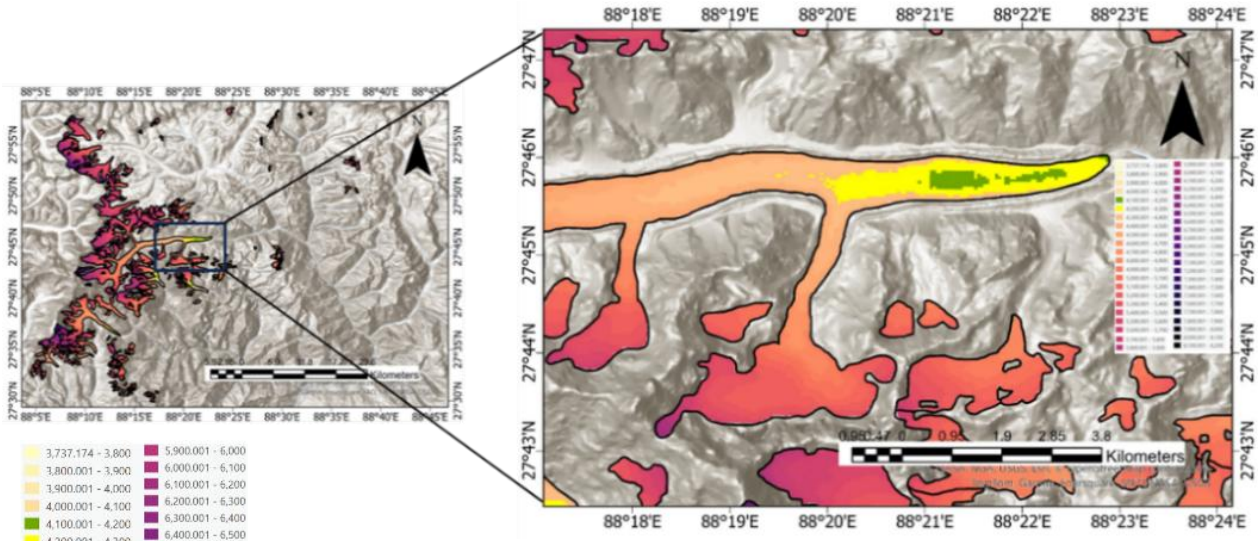
88°18'E
88°19'E
88°20'E
88°21'E
88°22'E
88°23'E
88°24'E
27°47'N
27°46'N
27°45'N
27°44'N
27°43'N
N
Kilometers

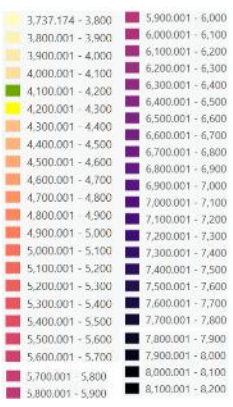
3,737,174 - 3,800
3,800,001 - 3,900
3,900,001 - 4,000
4,000,001 - 4,100
4,100,001 - 4,200
4,200,001 - 4,300
4,300,001 - 4,400
4,400,001 - 4,500
4,500,001 - 4,600
4,600,001 - 4,700
4,700,001 - 4,800
4,800,001 - 4,900
4,900,001 - 5,000
5,000,001 - 5,100
5,100,001 - 5,200
5,200,001 - 5,300
5,300,001 - 5,400
5,400,001 - 5,500
5,500,001 - 5,600
5,600,001 - 5,700
5,700,001 - 5,800
5,800,001 - 5,900
5,900,001 - 6,000
6,000,001 - 6,100
6,100,001 - 6,200
6,200,001 - 6,300
6,300,001 - 6,400
6,400,001 - 6,500
6,500,001 - 6,600
6,600,001 - 6,700
6,700,001 - 6,800
6,800,001 - 6,900
6,900,001 - 7,000
7,000,001 - 7,100
7,100,001 - 7,200
7,200,001 - 7,300
7,300,001 - 7,400
7,400,001 - 7,500
7,500,001 - 7,600
7,600,001 - 7,700
7,700,001 - 7,800
7,800,001 - 7,900
7,900,001 - 8,000
8,000,001 - 8,100
8,100,001 - 8,200

(d)

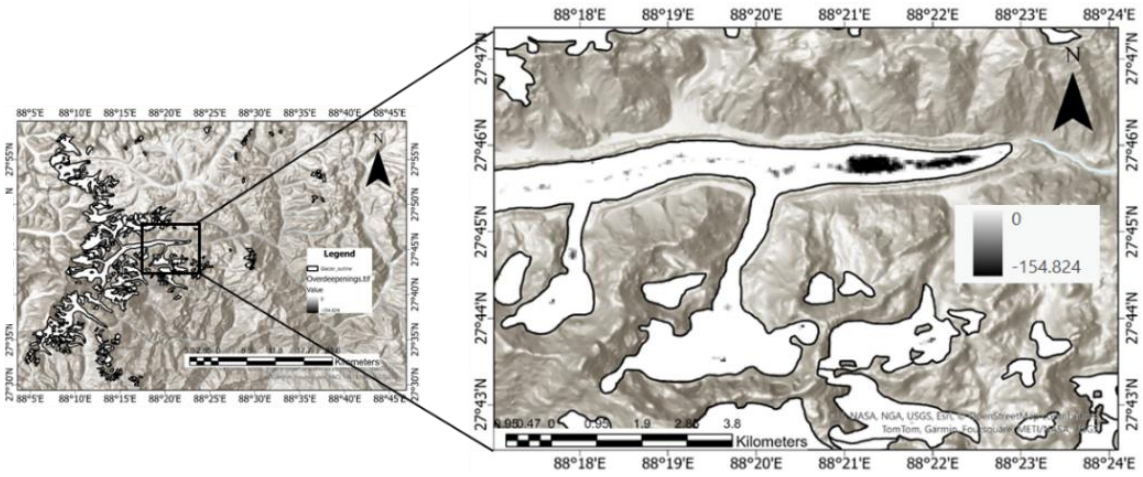

Figure 4.6 : (a) Elevation of the profile (m) (b) Ice Thickness of the region (m) (c) Bed Topography (m) (d) Overdeepenings (m)

4.5. THRESHOLDING

The overdeepenings obtained are large in number, and the smaller overdeepenings (with area less than 0.01 km^2) can create noise and give false positives (Viani et al. 2020). Filtering out this noise, and improving the confidence in the locations of the overdeepenings that remain, is therefore important. Here, a thresholding approach was used to remove the smallest of the identified overdeepenings (with area less than 0.01km^2).

Two thresholds commonly used in previous studies were applied to the overdeepenings, and the resulting changes in their total area and the number of overdeepenings were analysed. Previous studies have typically used thresholds of 0.01 km^2 (Colonia et al. 2017; Linsbauer et al. 2012; Magnin et al. 2020; Srinivasalu et al. 2024) and 0.05 km^2 (Kapitsa et al. 2017; Viani et al. 2020). In the current study, thresholds of 4 pixels and 20 pixels were selected, as they closely approximate 0.01 km^2 and 0.05 km^2, respectively. The equation below shows the area of one pixel of the overdeepenings.

$$\boldsymbol{Area\ of\ one\ pixel\ =\ 49.999\ m\ *\ 49.999\ m\ \cong\ 2499.901\ m^2}$$

Since this study has five regions and five ice thickness models, it is important to assess the sensitivity of all different regions and models. Figures 4.7 to 4.11 (below) show the result of applying different thresholds to each of the studied regions. In each case, the y1-axis denotes the number of overdeepenings and the y2-axis denotes the total area of the overdeepenings in square kilometres. It can be seen that although the number of overdeepenings changes markedly once the 4-pixel threshold is applied, the change in the total area of the overdeepenings is relatively less. For 20 pixels the change in the number of overdeepenings reduces to as low as 4 overdeepenings for Farinotti's Ensemble and HF in the European Alps. This suggests that the number of overdeepenings

is highly sensitive to the 20-pixel threshold, leaving limited scope for further in-depth analysis. This can be noted from Appendix I, which shows that changing the threshold from no threshold to 4 pixels yields a maximum percentage decrease in number of overdeepenings of 78.33% (for New Zealand Southern Alps and Farinotti's Ensemble as model), whereas the decrease in area of overdeepenings is 8.94%. When the threshold changes from no threshold to 20 pixels, the percentage decrease of number of overdeepenings is 90%, whereas the percentage decrease in area is 15.08%.

A 0.01 km^2 threshold has been commonly used in studies of the Andes (Colonia et al. 2017; Drenkhan et al. 2018), Himalayas (Allen et al. 2016; Srinivasalu et al. 2024; Zhang et al. 2019), and European Alps (Magnin et al. 2020; Otto et al. 2022). Sensitivity analysis (Figure 4.7, 4.8, 4.9, 4.10, 4.11) also shows that a 4-pixel threshold works well to retain a substantial number of overdeepenings, ensuring good representation across all regions. Therefore, a 4 pixel-threshold was chosen for further analysis.

Alaska

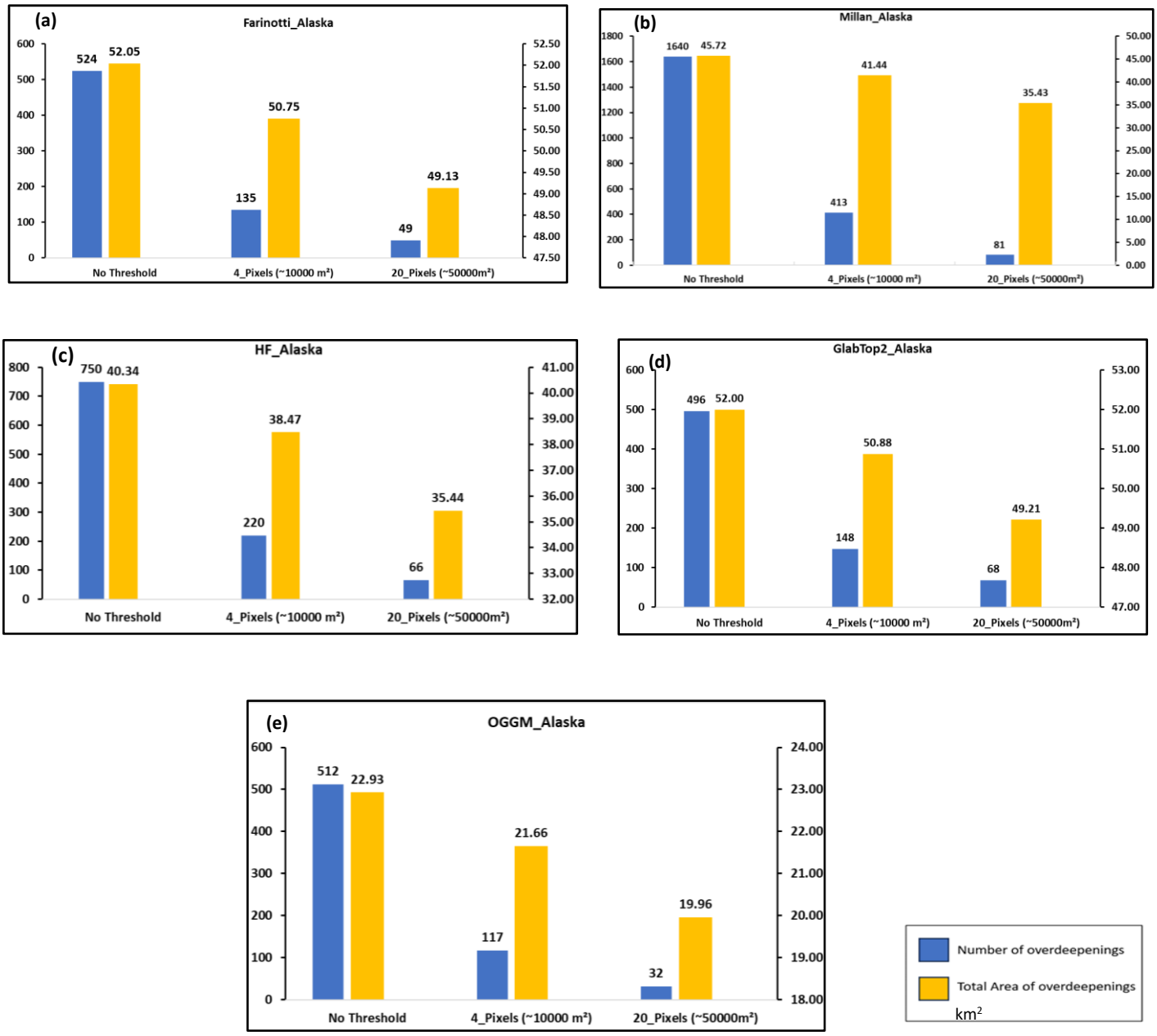

Figure 4.7: Sensitivity analysis for the threshold for selected glaciers in Alaska

European Alps

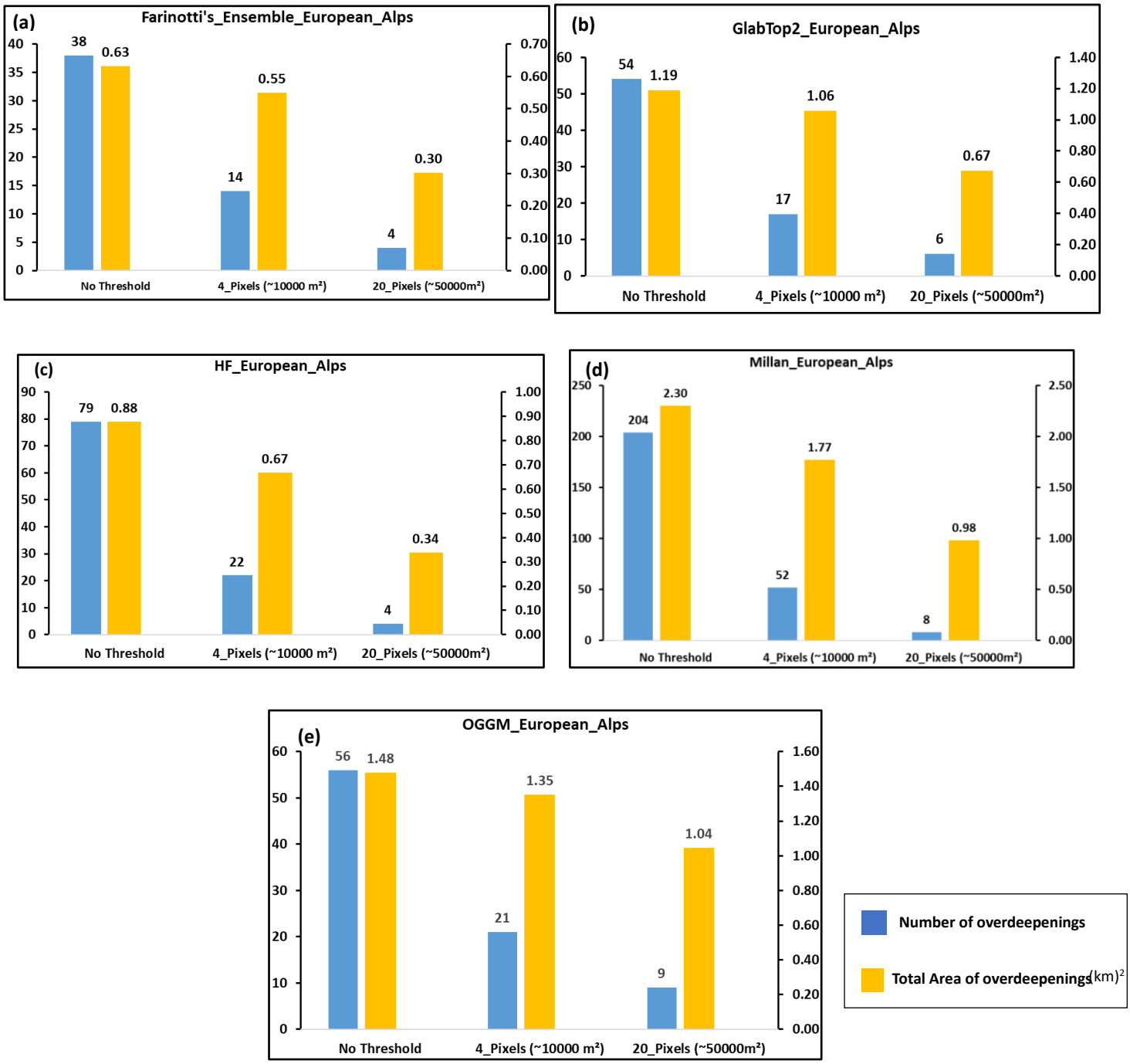

Figure 4.8: Sensitivity analysis for the threshold for selected glaciers in the European Alps

New Zealand Southern Alps

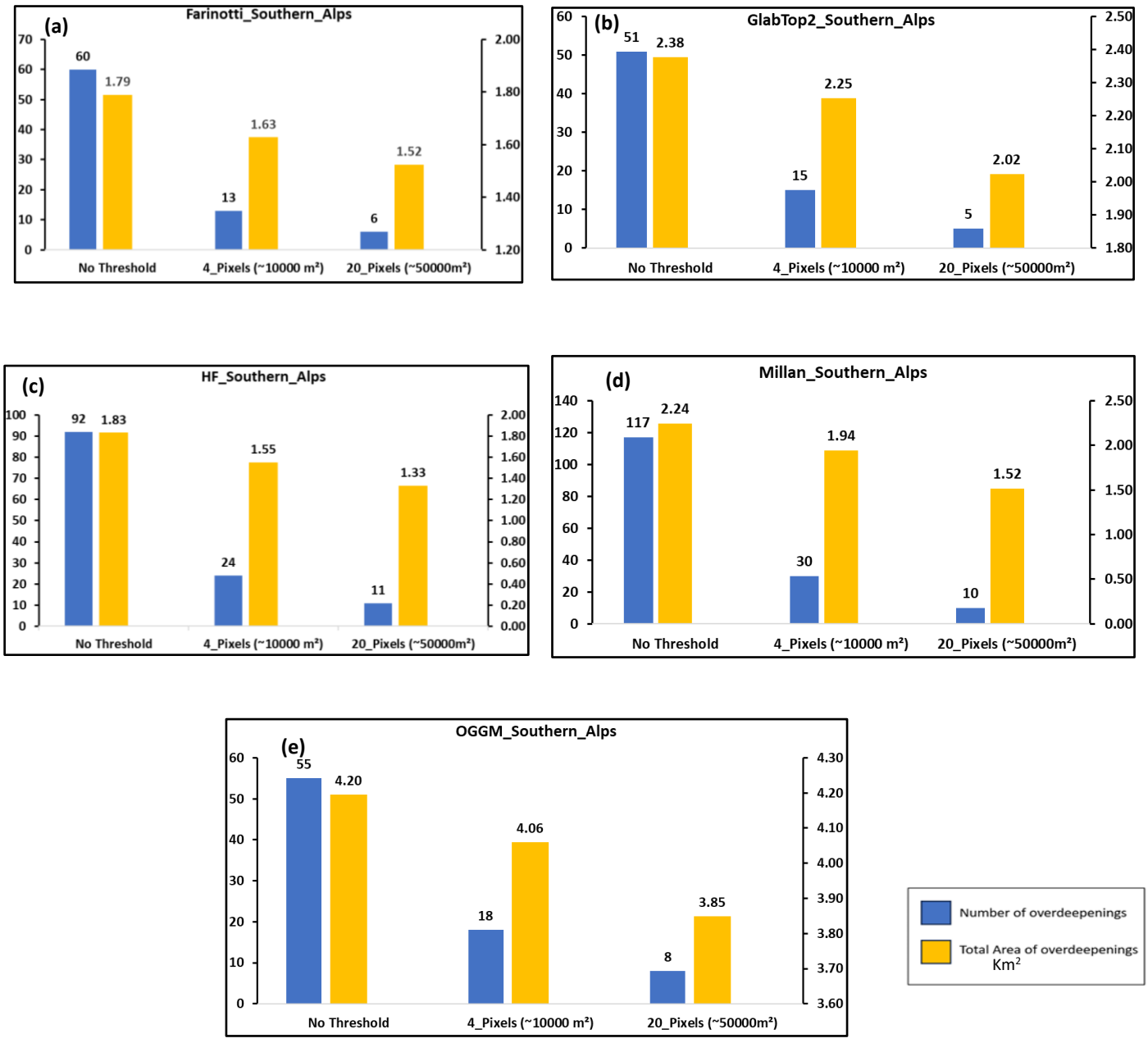

Figure 4.9: Sensitivity analysis for the threshold for selected glaciers in the New Zealand Southern Alps

Andes

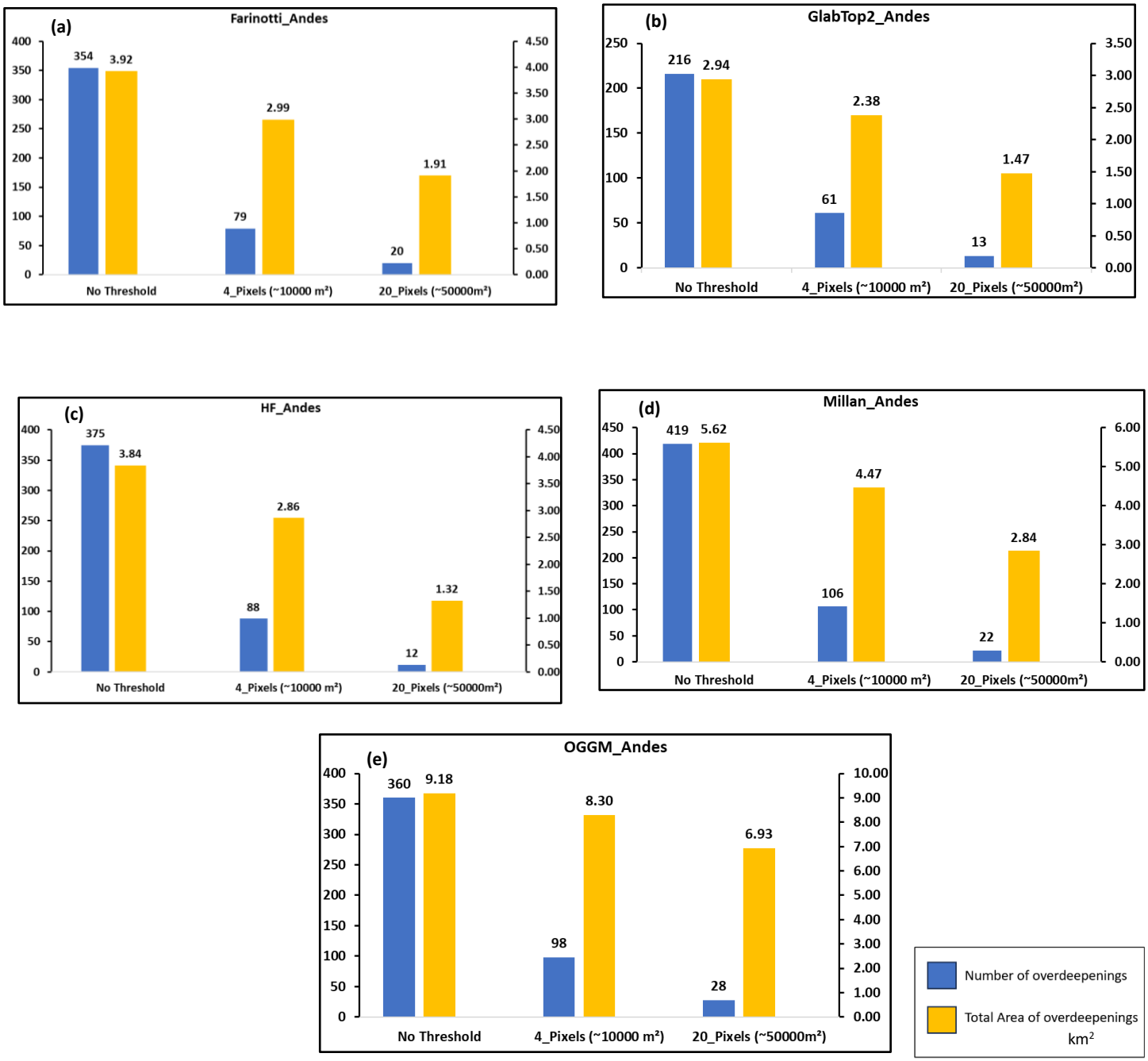

Figure 4.10: Sensitivity analysis for the threshold for selected glaciers in Andes

Himalayas

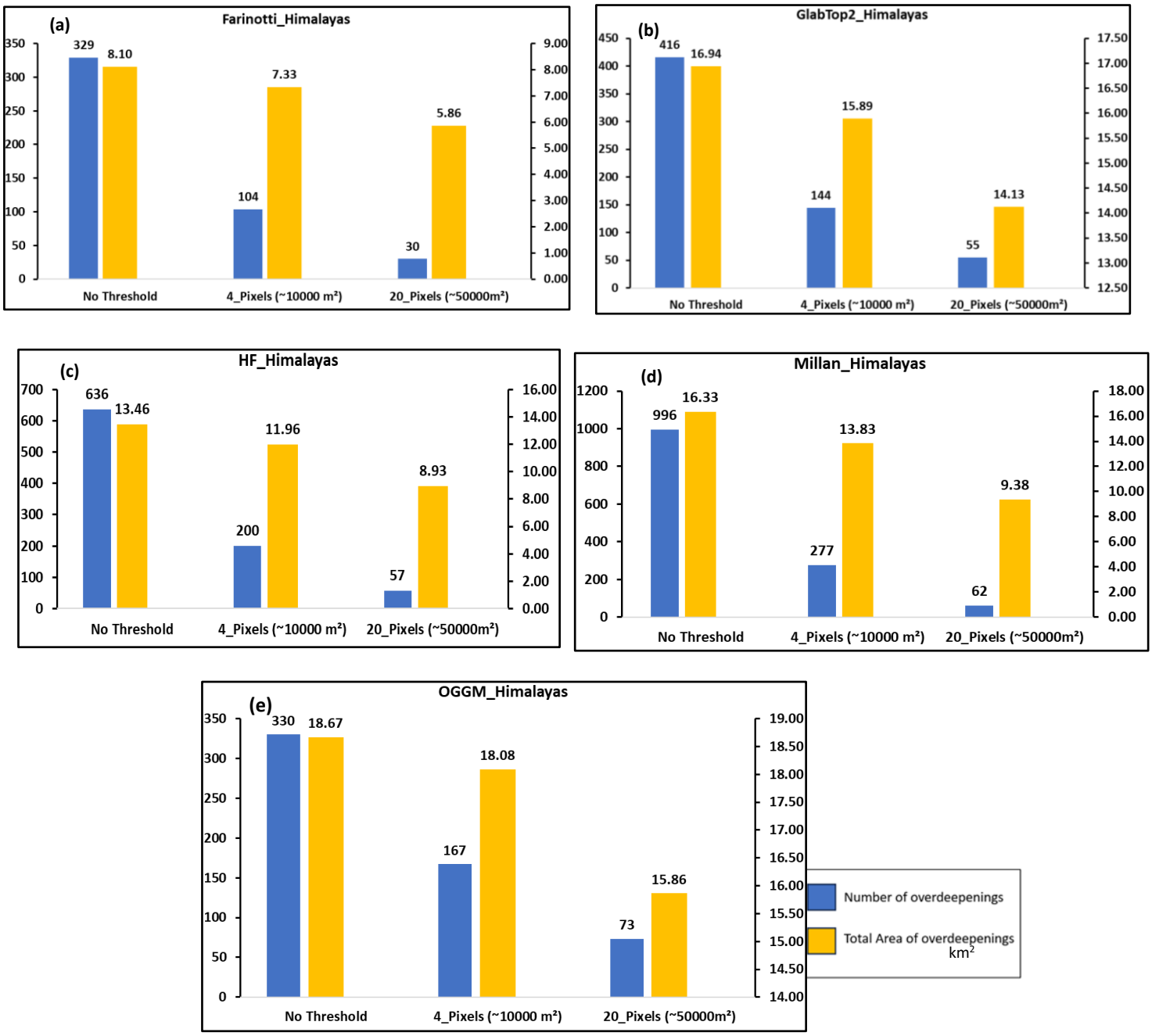

Figure 4.11: Sensitivity analysis for the threshold for selected glaciers in the Himalayas

4.6. ANALYSIS

4.6.1. Zonal Statistics

The overdeepenings were initially in raster format, with depth values assigned to individual pixels. For the analysis of each overdeepening, the pixels were first converted into polygons. Each pixel became an individual polygon. Adjacent polygons (until there was no adjacent polygon) were then merged using dissolve tool in QGIS to generate entire overdeepenings. These overdeepening polygons were used as zones in the Zonal statistics as a Table tool in ArcGIS, allowing for the calculation of various statistics including the mean, median, maximum, count, sum and minimum depth values. These statistics were then used to determine the area and volume of each overdeepening, as well as the total area and volume of all overdeepenings. The following equations state how area and volume of overdeepenings are calculated.

$$\boldsymbol{Area\ of\ an\ overdeepening} = \boldsymbol{Count}\ (\boldsymbol{the\ total\ number\ of\ pixels\ in\ an\ overdeepening})\ \boldsymbol{x\ Area\ of\ one\ pixel}$$

$$\boldsymbol{Volume\ of\ an\ overdeepening} = \boldsymbol{Sum}\ (\boldsymbol{sum\ of\ the\ depth\ of\ the\ pixels\ in\ the\ overdeepening})\ \boldsymbol{x\ Area\ of\ one\ pixel}$$

This was done for all the models and all the regions to estimate the area and volume of the overdeepenings and their distribution.

4.6.2. Combinations of ice thickness datasets

Since ice thickness models vary in their behaviour, they produce overdeepenings with differing depths, locations, and areas. To evaluate the relationship and performance of individual models with each other, the overdeepening rasters from each model were combined, with pixels assigned values based on their presence across models. This approach allows for further analysis of model comparisons, accounting for differences in the modelling approach and ice thickness estimates across models.

Overdeepening pixels were assigned values using the Con tool in ArcGIS: pixels with depth values less than 0, indicating depressions, were set to 1, while those with depth values of 0 or more were set to 0. This procedure was applied across all ice thickness models.

The overdeepenings from different ice thickness models were then combined using the raster calculator. Pixels were then analysed for their presence (and absence) within different model

combinations. Pixels were assigned a ranking number based on how many models they appeared in; for example, for a two-model combination a pixel that fell in both ice thickness models was given a rank of 2, whereas a pixel that occurred in just one of the models was given a rank of 1. If the ice thickness models are combined with each other in three different ways then it will give 25 model. In the first case, two different models are combined (${}^5C_2 = 10$), in the second case three different models are combined (${}^5C_3 = 10$) and in the third case four different models are combined (${}^5C_4 = 5$). Adding all the possible model combinations, there was a total of 25 model combinations assessed for all given regions.

5. RESULTS

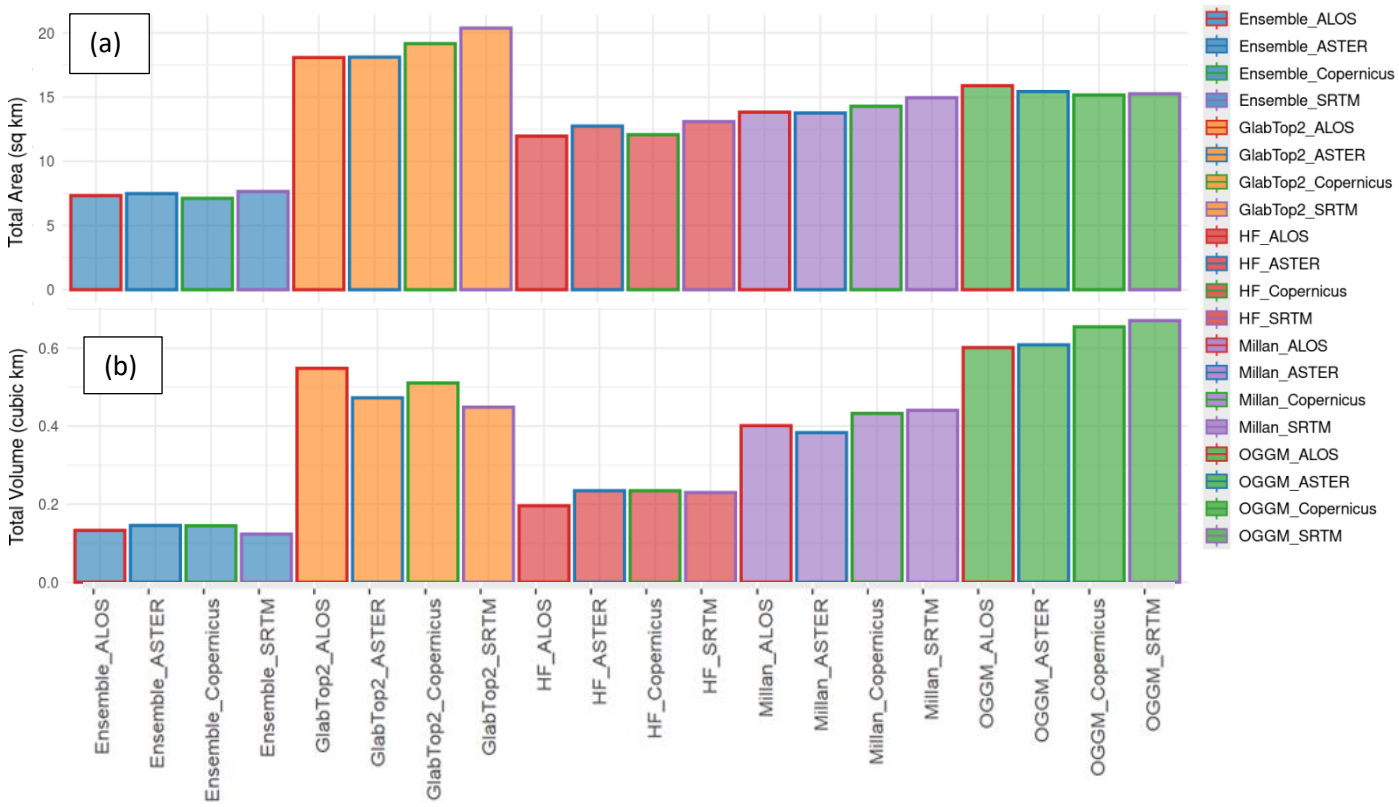

Figure 5.1: Total (a) area and volume (b) for all the model-DEM combinations for Himalayas

The results are structured in two main sections; the first section presents an analysis of the effects of using both different ice thickness models and different DEM combinations for the Central Himalayan region, as a proof-of-concept and to determine the focus of subsequent steps. Based on these findings, the second section presents a regional intercomparison of overdeepening characteristics using different ice thickness models but with a consistent DEM to isolate the ice thickness model effects.

5.1. MODEL AND DEM COMBINATIONS FOR GLACIERS IN THE CENTRAL HIMALAYAS

Four DEMs (ALOS, ASTER, Copernicus and SRTM) and five ice thickness models (Farinotti ensemble, GlabTop2, Huss and Farinotti, Millan and OGGM) were chosen to make an initial assessment of the extent to which the choice of input dataset is a determinant of the resulting overdeepening characteristics. Figure 5.1 shows the total area and volume of overdeepenings for the test region of the Central Himalayas.

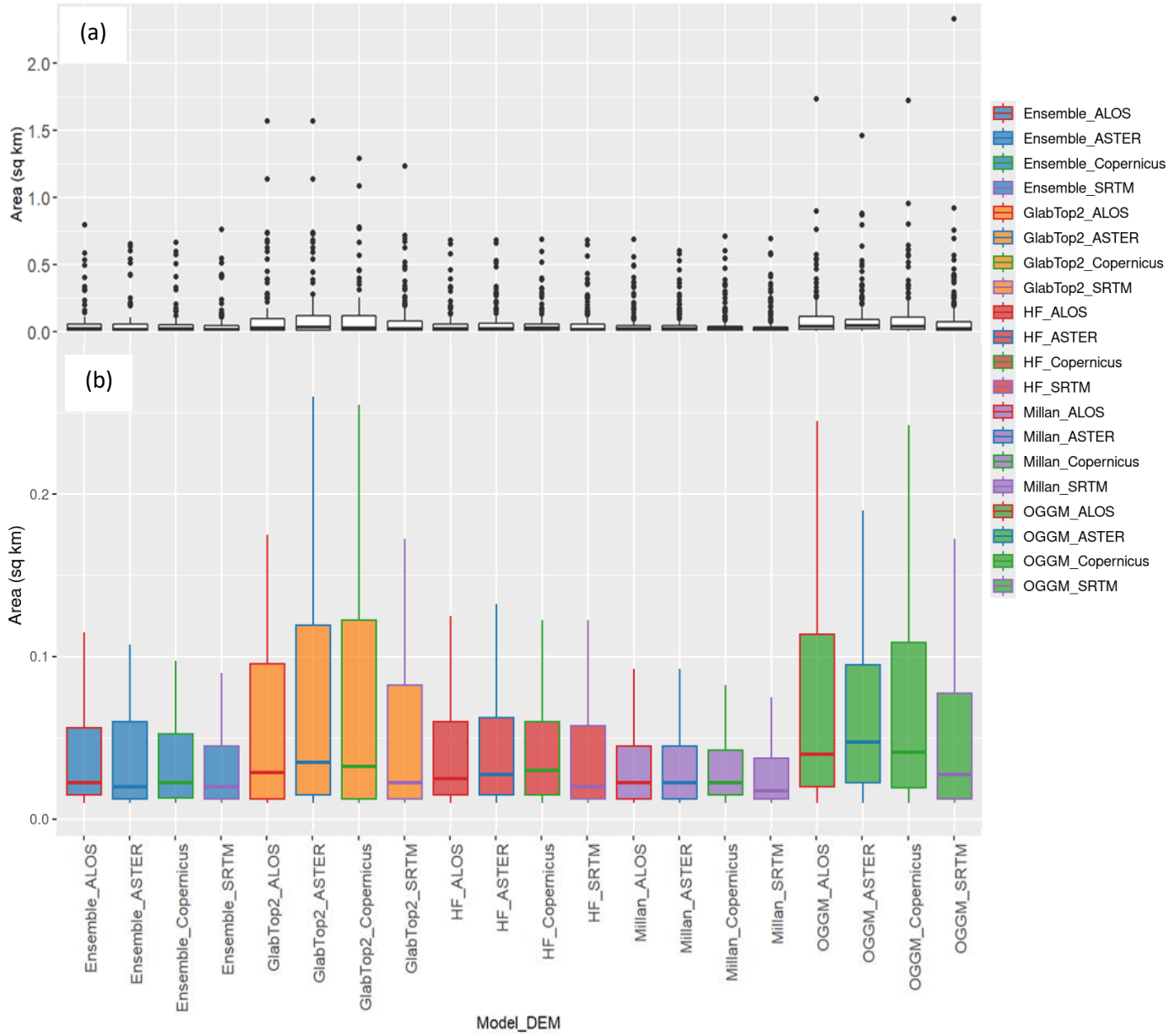

Figure 5.2: (a) Overdeepening areas for all the Model-DEM combinations (b) As a) but with outliers removed to improve visualisation. Note the box midpoint bars represent the median value and the whiskers represent the range.

5.1.1. Overdeepening Area

The total overdeepening area ranges from 7.12 km² (Farinotti's Ensemble-Copernicus model-DEM combination) to 20.37 km² (GlabTop2- SRTM; Figure 5.1). DEM choice seems to make more of a difference for some models than it does for others. For example, Farinotti's Ensemble shows a range of 0.53 km² depending on DEM choice, whereas for OGGM the range is much larger at 2.29 km². Among all the DEMs, SRTM gives the highest total area (highest total area as 20.37 km² for GlabTop2-

SRTM for all the models (see Appendix G for reference) except for OGGM, where ALOS gives the highest total area (15.88 km^2).

Given this range, the GlabTop2 model paired with any DEM consistently results in the highest total area of overdeepenings, while Farinotti's Ensemble paired with any DEM produces the lowest total area.

Similarly, the range, distribution and median of the area of individual overdeepenings remain consistent irrespective of DEM choice, although there is again considerable variation between ice thickness models (Figure 5.1 and Figure 5.2). Here, GlabTop2 (gives an overdeepening with the highest area of 1.56 km^2 when combined with ALOS-PALSAR) and OGGM (with SRTM gives 2.32 km^2 as the highest area for an overdeepening) consistently produce the largest overdeepenings, Figure 5.1(a) and Figure 5.2 (b).

5.1.2. Overdeepening Volume

The total volume of the overdeepenings ranges from 0.123 km^3 (Farinotti's Ensemble- SRTM) to 0.670 km^3 (OGGM-SRTM; Figure 5.1 (b), Appendix G). OGGM follows the trend of predicting the highest volume across (0.670 km^3) all the DEM combinations whereas Farinotti's Ensemble predicts the lowest volume. Again, DEM choice appears to affect some models more than others, for example, Farinotti's ensemble has a range of 0.022 km^3 depending on the DEM, whereas GlabTop2 ranges by 0.099 km^3.

Combined, Figures 5.1 and 5.2 show very clearly that the choice of DEM has little influence over the area and volume estimated by each combination, but there is large variability in the results depending on the ice thickness model that is chosen. Assessing the impact of ice thickness model choice across other glacierized regions therefore became the primary focus for the study.

5.2. INTER-REGIONAL COMPARISON USING FIVE ICE THICKNESS MODELS

The five regions considered for subsequent analysis were Alaska, the Peruvian Andes, the New Zealand Southern Alps, the Central Himalaya and the European Alps. ALOS-PALSAR DEM has been chosen for the analysis here.

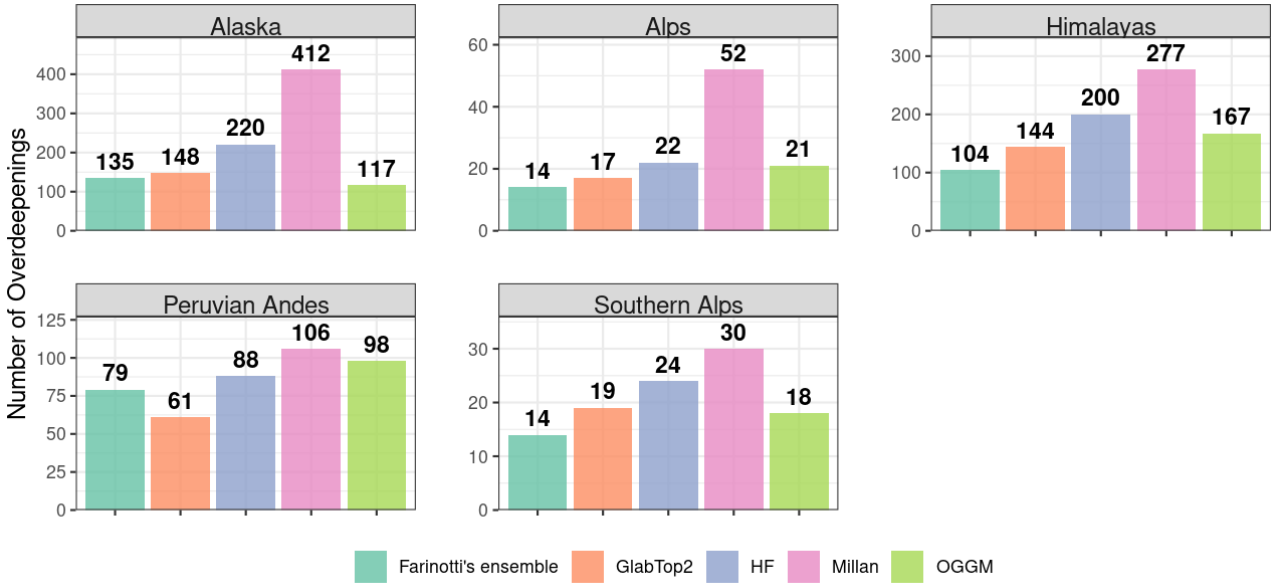

Figure 5.3: Number of overdeepenings across all regions

5.2.1. Number of Overdeepenings

Among all the regions Alaska has the highest number of overdeepenings and also has the widest range, with Millan predicting 412 overdeepenings versus OGGM predicting 117 (Figure 5.3). The

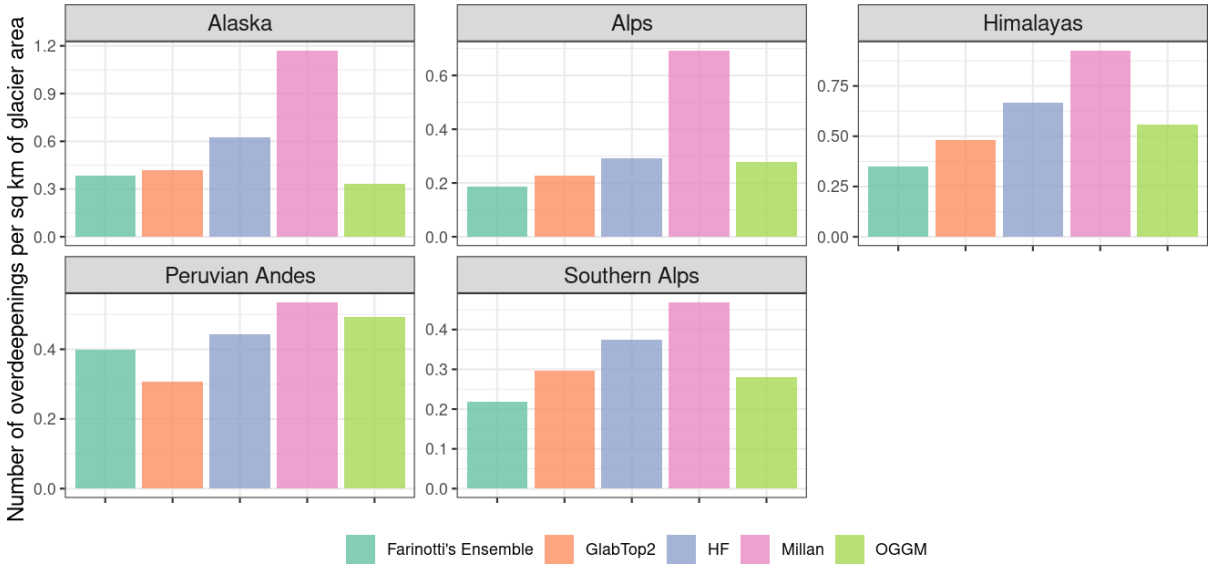

Figure 5.4: Number of overdeepenings per glacier area across all regions and all models. Note the y-axis varies between regions.

New Zealand Southern Alps contain the fewest overdeepenings and also the least variation among the model predictions, taking the difference between the highest and lowest number of overdeepenings as the basis for calculation. Millan consistently has the highest number of overdeepenings for all the regions and Farinotti's Ensemble has the least overdeepenings for the Himalayas, European Alps and New Zealand Southern Alps. For the Peruvian Andes, GlabTop2 predicts the lowest number of overdeepenings.

Alaska and the Himalayas have a higher number of overdeepenings per glacier area compared to the other regions. Among all the models Millan predicts the highest number of overdeepenings per glacier area for all the regions with the highest for Alaska, which is 1.17 overdeepenings per km^2 of glacier area (Figure 5.4).

5.2.2. Area of overdeepenings

As well as having the highest number of predicted overdeepenings, Alaska also has the highest total area among all the regions (Figure 5.5). In Alaska, GlabTop2 has the highest total predicted area (50.87 km^2). In contrast, OGGM has the highest total predicted area for the Central Himalayas (18.08 km^2), Peruvian Andes (8.29 km^2) and New Zealand Southern Alps (4.06 km^2). For the European Alps, Millan predicts the highest total area of 1.77 km^2.

Except for Alaska, Farinotti's Ensemble and Huss and Farinotti consistently show the lowest total area of overdeepenings

Figure 5.5: Total area of the overdeepenings across all the regions in m^2, note the values of y-axis differs based on the region taken into account

Alaska

All models predict the majority of overdeepenings to be smaller than 0.1km², while a small number of exceptionally large overdeepenings exceed 10 km² (Figure 5.6). Farinotti's Ensemble (0.0099 km^2 to 12.11 km^2) and GlabTop2 (0.0099 km^2 to 8.8 km^2) show the widest range of overdeepening areas. It is worth noting that several particularly large overdeepenings substantially increase the mean of both of these models.

More generally, the overdeepening area is highly consistent between three of the models, (HF, OGGM and Farinotti's Ensemble) with the median value ranging between 0.0225 km² and 0.0295 km²; GlabTop2 predicts larger overdeepenings compared to other models (median of 0.0412 km²), and Millan predicts smaller overdeepenings (0.017 km²).

European Alps

GlabTop2 and OGGM predict larger overdeepenings and a more varied range compared to the other models (Figure 5.6). As compared to OGGM, GlabTop2 has a higher number of large overdeepenings. Millan has the smallest range, as well as predicting generally smaller overdeepenings (median of 0.015 km²), albeit with several large (> 0.1 km^2) overdeepenings.

Himalayas

There is reasonable consistency between the results of the five models, with four of the median values ranging from 0.02 km² to 0.03 km² (Figure 5.6). The exception is OGGM, which estimates larger overdeepenings with a median of 0.040 km². GlabTop2 (0.0099 km^2 to 1.567 km^2) and OGGM (0.0099km^2 to 1.732 km^2) show the most varied range.

Peruvian Andes

There is marked consistency in the area of the overdeepenings predicted by all five models (median range of 0.022 km² to 0.024 km²) (Figure 5.6). The models also show a similar range, except for OGGM which has several very large overdeepenings with sizes greater than 1 km².

New Zealand Southern Alps

Farinotti's Ensemble, Huss and Farinotti and OGGM are consistent in their prediction of the largest overdeepenings (median values of 0.036 km^2, 0.034 km^2 and 0.033 km^2, respectively) (Figure 5.6), whereas GlabTop2 and Millan predict smaller overdeepenings (median values of 0.017 km^2 to 0.023 km^2). OGGM shows the broadest range, as a consequence of having several very large predicted overdeepenings.

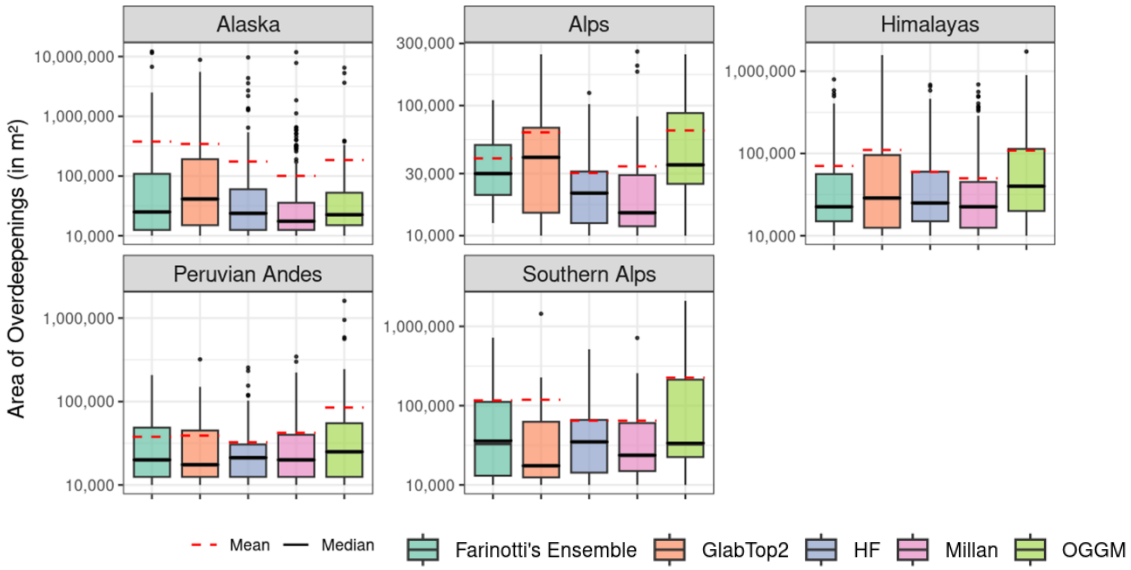

Figure 5.6: Area of individual overdeepenings with the outliers for all five regions. The black solid line represents the median and the red dotted line represents the mean. The black dots represent the outliers. The y-axis are logarithmic to fit the results and inconsistent to fit the variability between the regions and the overdeepenings.

Summary

The range of the predicted overdeepening areas changes from one region to another, with Alaska showing the largest individual overdeepenings as large as 12.11 km². The largest overdeepening for all other models is around 1 km^2 whereas for the Alps it is just 0.3 km^2. Across all regions and models, a few exceptionally large overdeepenings heavily influence the mean. The mean size of overdeepenings varies by region, ranging from 0.015 km² (Alps) to 0.37 km² (Alaska), with Alaska also showing the highest mean values across all models, from 0.010 km² to 0.376 km². This suggests that the very few large overdeepenings that exist are also highly variable in size.

While the mean shows a wide range across regions, the median values, ranging between 0.014 km² and 0.041 km², suggest that the majority of overdeepenings across all regions and models are relatively similar in size. OGGM displays a wide range of overdeepening sizes in all regions, except in

Alaska, where it has the narrowest range. In Alaska, GlabTop2 and Farinotti's Ensemble show the widest range of overdeepening sizes. Millan consistently estimates smaller overdeepenings for all of the regions. The Millan data also show a relatively narrow range for overdeepenings across all regions, yet in each region, it also identifies several exceptionally large overdeepenings that fall outside this typical range. Appendix B, C, D, and E represent the distribution of depth of all the pixels of the overdeepenings for comparison. Appendix F has the values of area and volume of the overdeepenings.

5.2.3. Volume of Overdeepenings

Table 5.1: Total volume of overdeepenings for all the ice thickness models across all the regions (in km^3)

	Farinotti's Ensemble	GlabTop2	HF	Millan	OGGM
Alaska	3.700	6.86	1.957	2.740	0.585
Himalayas	1.427	0.553	2.020	0.413	0.589
Peruvian Andes	0.037	0.439	0.294	0.096	0.330
European Alps	0.0347	0.079	0.256	0.474	0.246
New Zealand Southern Alps	0.00319	0.017	0.0058	0.043	0.025

Among all the regions, in Alaska, the total volume of overdeepenings estimated by all the models is notably high (Table 5.1). Among all the models, GlabTop2 estimates a volume of 6.86 km^3 for Alaska, accounting for 10.9% of the total glacier volume estimated by the model - the highest total volume across all regions and models. In contrast, the New Zealand Southern Alps have a lower total volume of overdeepenings across all models compared to other regions. The Farinotti Ensemble produces the smallest estimate, with a volume of 0.00319 km^3, representing only 0.1% of the total glacier volume estimated by this model. This is represented pictorally in Appendix A.

The total estimated volume is not only inconsistent between regions but also between the models of a given region.

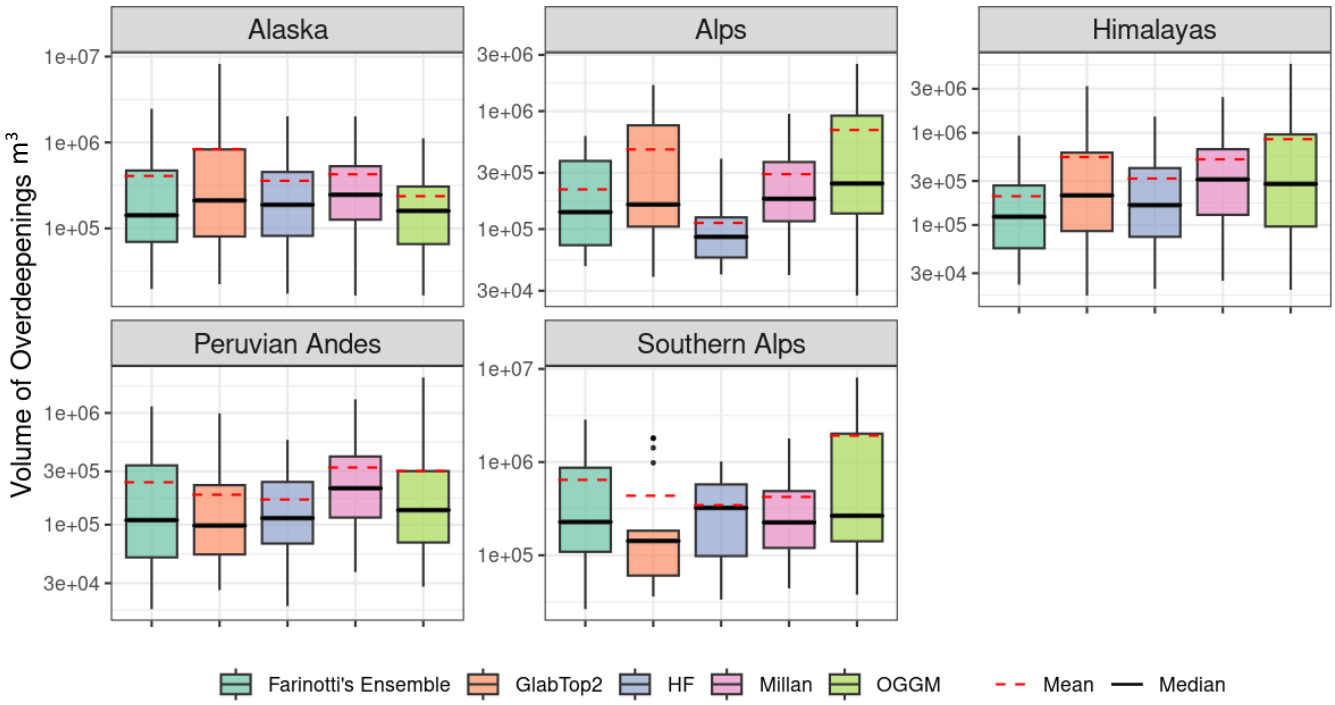

Figure 5.7: Volume of overdeepenings in m^3 across regions and models. Note the inconsistent logarithmic scales across regions.

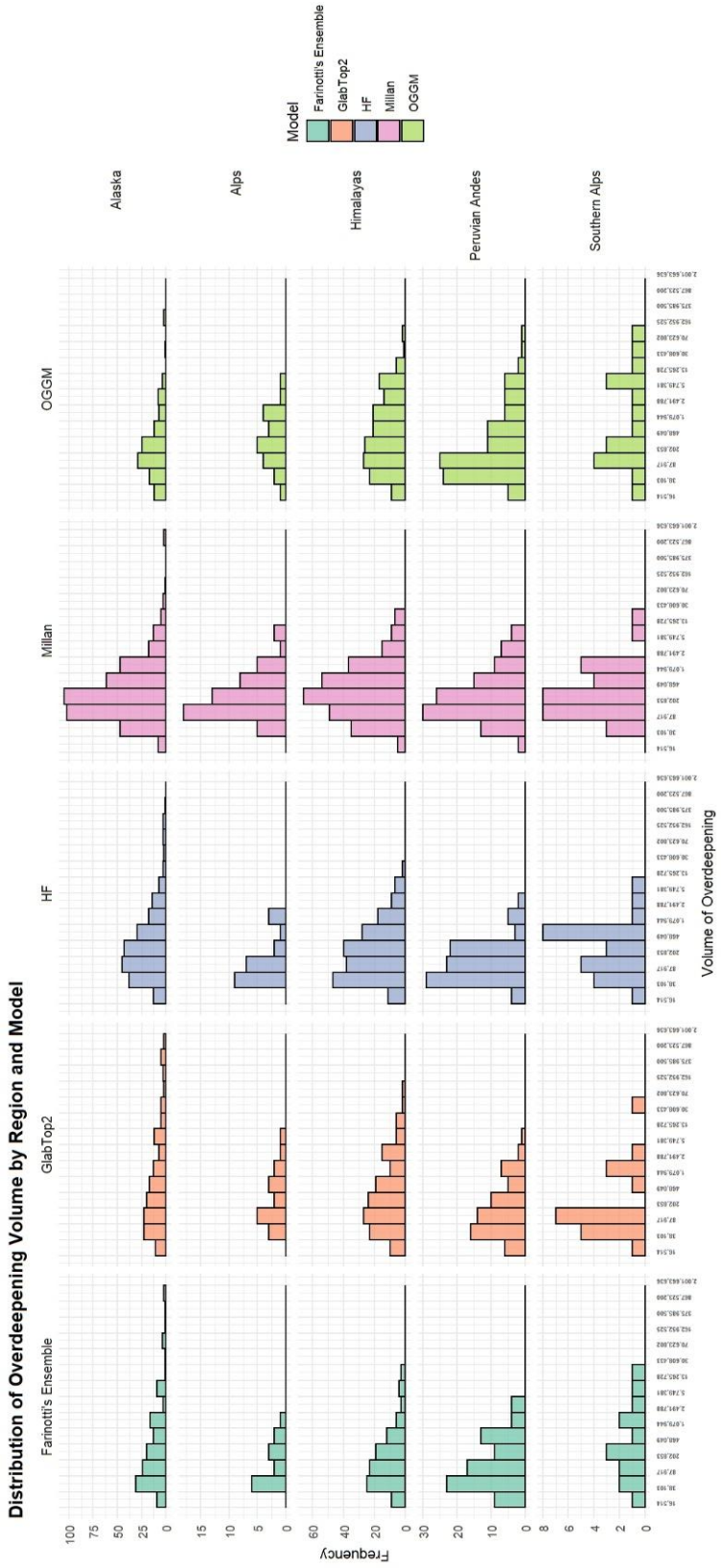

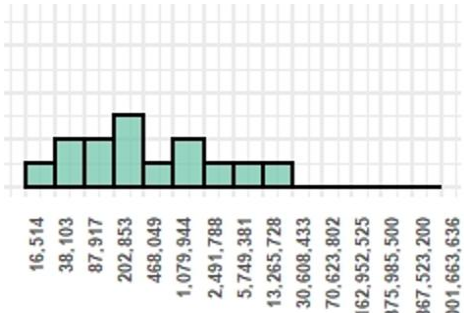

Figure 5.8 (a) : Zoomed version of Farinotti's ensemble volume distribution for Southern Alps

Range of volume in m^3
16,514
38,103
87,917
202,853
468,049
1,079,944
2,491,788
5,749,381
13,265,728
30,608,433
30,608,433
70,623,802
162,952,525
375,985,500
867,523,200
2,001.663.636

Figure 5.8:(b) Distribution of volume of the overdeepenings. The y-axis denotes the frequency, and the x-axis denotes the volume of the overdeepenings in m^3 . Each column represents a model, and each row represents a region.

Alaska

Huss and Farinotti and GlabTop2 both predict most of their overdeepenings to range from around 38 x 10^{-6} km^3 to 470 x 10^{-6} km^3 (Figure 5.7) but they also have a long tail (reaching around 0.163 km^3) of overdeepenings that have higher volumes (Figure 5.8). Farinotti's Ensemble, Millan and OGGM also suggest most of the overdeepenings will be less than 5 x 10^{-4} km^3 in volume (Figure 5.7) but have very few overdeepenings with volumes greater than $10^{-3}km^3$ (Figure 5.8).

Alps

All the models except for OGGM, show a majority of the overdeepenings to be within 5 x 10^{-5} km^3 (Figure 5.7). For OGGM the volume of estimated overdeepenings is more distributed (Figure 5.8), with fewer small features, and a greater number of larger features, compared to the other model results.

Himalayas

All the models except OGGM are left skewed suggesting that most of the overdeepenings have a low volume (Figure 5.8). OGGM again has a uniform spread throughout suggesting that there are overdeepenings with both high and low volume. The Himalayas show a slightly more balanced distribution of overdeepening volumes compared to other regions, indicating a relatively higher prevalence of larger overdeepenings.

Peruvian Andes

All the models except OGGM estimate that most of the overdeepenings will be small in volume (Figure 5.7). For OGGM, although the majority of overdeepenings are also predicted to be small, there is a high number of larger overdeepenings, reaching as large as around 0.163 km^3.

New Zealand Southern Alps

Farinotti's Ensemble and OGGM show a normal distribution suggesting that both of these models predict overdeepenings that incorporate that there are more overdeepenings in the middle and fewer overdeepenings at the extreme ends (Figure 5.8).

GlabTop2 estimates that most of the overdeepenings will be small in volume (up to 2.02 x 10^{-4} km^3) but three overdeepenings have a very high volume that increases the mean of the distribution. For Huss and Farinotti most of the overdeepenings are within 5 x 10^{-4} km^3 and very few overdeepenings

exceed 10^{-3} km^3. As with other regions, OGGM shows considerable variation in predicted overdeepening volumes.

Summary

Figure 5.7 and 5.8 show that most of the overdeepenings across all models and regions are predicted to have a volume of less than 5 x 10^{-4} km^3. As compared to other regions, all the models predict the volume of overdeepenings to be widely varying for Alaska. In contrast, for all other regions, the overdeepenings are consistently within a range of 1.6 x 10^{-5} km^3 to 3.1 x 10^{-2} km^3; the results from Huss and Farinotti and Millan are particularly consistent in this regard. Millan predicts mid-volumed overdeepenings with most of them within the range of 1.5 x 10^{-5} km^3 to 50 x 10^{-5} km^3. Among all the regions except for Alaska (where GlabTop2 produces the widest range), OGGM consistently has the widest range for all the regions where it predicts overdeepenings with both small and large volumes. For all the models the vast majority of the overdeepenings are relatively small, with only a few that are exceptionally large. In Alaska, the Himalayas and the New Zealand Southern Alps, there are overdeepenings with predicted higher volumes, irrespective of the model choice, as compared to the other regions.

5.3. PERCENTAGE OF COMMON PIXELS

Each model was compared with another and the percentage of common pixels was plotted using pie charts (Figure 5.9). The size of each pie reflects the total number of pixels for each combination of models, applied across all regions, to visualise the level of agreement when combining 2 models (Figure 5.9a), 3 models (Figure 5.9b), and 4 models (Figure 5.9c). In a combination of two models : the pixel score of 1 means there are that pixel falls in only one model and the a score of 2 means it falls in two models. The pixel score of 3 means that the pixel falls in 3 models and the pixel score of 4 means it is present in 4 models. The size of the pie chart represents the total number of pixels for the model combination; for instance, in Figure 5.9 (a) for Alaska the model combination of GlabTop2 and Huss and Farinotti has the highest number of pixels compared to other two-model combinations, hence the pie chart for this model has the largest diameter with a total of 122381 pixels while Millan and OGGM having a total of 21872 pixels has the smallest diameter (see Appendix H for reference and Figure 5.9(a)).

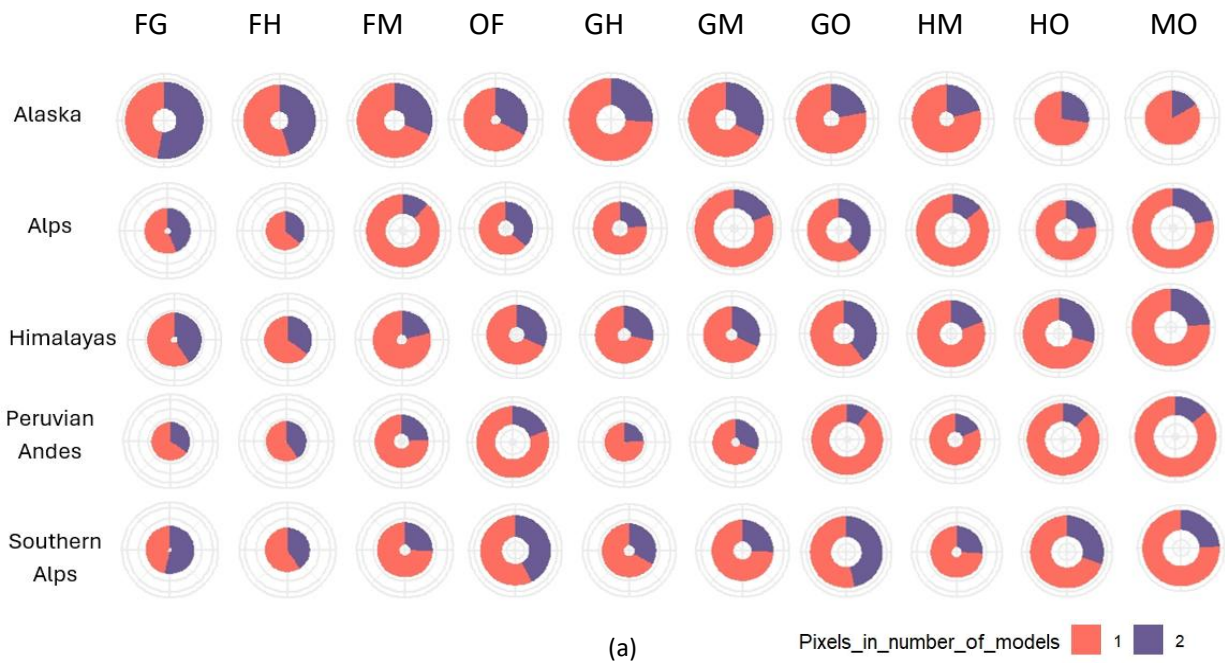
FG
FH
FM
OF
GH
GM
GO
HM
HO
MO
Alaska
Alps
Himalayas
Peruvian Andes
Southern Alps
Pixels_in_number_of_models
1
2

(a)

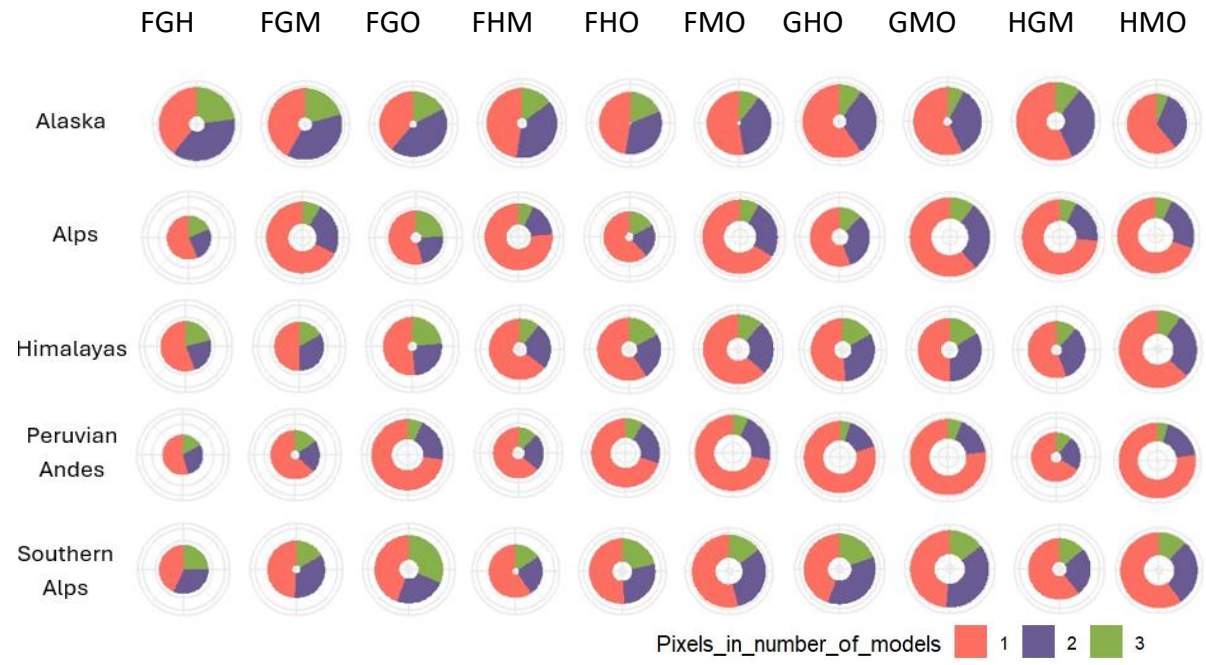
FGH
FGM
FGO
FHM
FHO
FMO
GHO
GMO
HGM
HMO
Alaska
Alps
Himalayas
Peruvian Andes
Southern Alps
Pixels_in_number_of_models
1
2
3

(b)

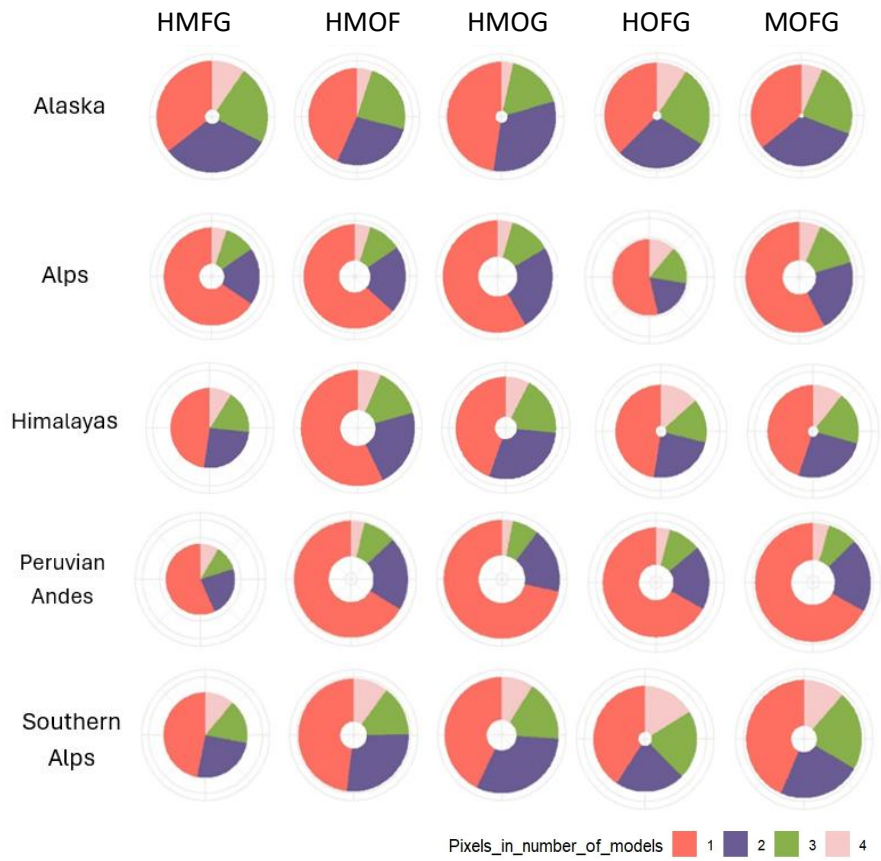

(c)

Figure 5.9: (a) Model combinations with 2 ice thickness models (b) Model combinations with 3 ice thickness models (c) Model combinations with 4 ice thickness models. The initial letters of the models have been used in the combination in each case. (H: Huss and Farinotti, F: Farinotti's Ensemble, M: Millan, O: OGGM, G: GlabTop2)

Table 5.2: Model combinations with the highest total pixels and the highest percentage of common pixels *(H: HF, F: Farinotti's Ensemble, M: Millan, O: OGGM, G: GlabTop2)*

Region	2 combinations		3 combinations		4 combinations	
	Highest Pixel Total	Percentage of common pixels	Highest Pixel Total	Percentage of common pixels	Highest Pixel Total	Percentage of common pixels
Alaska	HG	FG (52.9%)	HGM	FGH (20.6%)	HFMG	HFMG (9.6%)
Alps	MO	FG (43.8%)	GMO	FGO (24.6%)	HMOG	HOFG (11.26%)
Himalayas	MO	FG (40.8%)	HMO	FGO (23.5%)	HMOF	HOFG (13.5%)
Peruvian Andes	MO	FH (40.3%)	HMO	FGH (16.7%)	HMOG	HMOF (8.6%)
New Zealand Southern Alps	MO	FG (53.6%)	HMO	FGO (31.4%)	HMOG	HOFG (16.4%)

Table 5.3: Model combinations with the lowest total pixels and lowest percentage of common pixels *(H: HF, F: Farinotti's Ensemble, M: Millan, O: OGGM, G: GlabTop2)*

Region	2 combinations		3 combinations		4 combinations	
	Lowest Pixel Total	Percentage of common pixels	Lowest Pixel Total	Percentage of common pixels	Lowest Pixel Total	Percentage of common pixels
Alaska	OH	MO (16.6%)	HMO	HMO (6.2%)	HMOF	HMOG (3.4%)
Alps	FH	FM (11.75%)	FGH	HMO (6.91%)	HOFG	HMOG (4.3%)
Himalayas	FH	FM (21.2%)	FGM	HMO (9.6%)	HMGF	HMGF (9.1%)
Peruvian Andes	FG	GO (9.9%)	FGH	HMO (4.7%)	HMGF	HMOG (3.07%)
New Zealand Southern Alps	FH	FM (25.7%)	FGH	HMO (11.96%)	HMGF	HMOG (9.05%)

Millan and OGGM show the greatest consistency in their identification of overdeepenings (total pixels) for all regions except Alaska (Table 5.2). In contrast, Farinotti's Ensemble and GlabTop2 show the highest percentage of common pixels. The three model combinations for the highest and lowest percentage of common pixels are fairly consistent throughout. As seen from Table 5.3, Farinotti's Ensemble and Millan have the lowest common percentages for the Alps, Himalayas and the New Zealand Southern Alps. The agreement between Farinotti's Ensemble and GlabTop2 is the highest in the New Zealand Southern Alps (53.6%). The least overlap is between GlabTop2 and OGGM (9.9%) in the Peruvian Andes.

As it can be observed through the Figure 5.9 (a,b,c), it is can be observed that there is a disagreement between the models irrespective of the region.

When combined with the rest of the results in this chapter, it becomes clear that overdeepening locations and characteristics vary widely between regions, which may be expected, and between ice thickness models, with only around 50% agreement between any two models in any of the study

regions, and inconsistent patterns both within and between each region depending on the model choice.

6. DISCUSSION

This study has shown that the identification of subglacial overdeepenings using a GIS-based approach is largely insensitive to the choice of DEM, but is highly dependent on the ice thickness model that is used in the calculation. This raises questions about how robust previous studies that have presented future glacial lake locations using a single ice thickness model may be (e.g. Drenkhan et al. 2018; Viani et al. 2020; Magnin et al. 2020). This discussion will consider the influence of DEM and ice thickness model choice on the overdeepening characteristics, assess the uncertainties in doing so, and subsequently present a possible way forward for future studies pursuing a similar theme.

6.1. DEM AND ICE THICKNESS CHOICE

6.1.1. DEMs

There is an increasing amount of digital elevation data available for monitoring Earth's surfaces , along with those that are glacierised (Guth et al. 2021). Previous work has shown that uncertainties in DEMs are largely underestimated in the literature (Hugonnet et al. 2021), which makes the first key finding of this study, that DEM choice has little impact on overdeepening size and location, a little surprising.

There are relatively few studies that specifically address the influence of DEM choice on predicted overdeepening characteristics. Those that exist are locally focused; for example, DEM choice was found to affect the morphometry, location, accuracy and number of overdeepenings when applied with a single ice thickness model in the European Alps (Gharehchahi et al., 2020) and the Peruvian Andes (Drenkhan et al., 2018). For instance, for Gharehchahi et al. (2020), 125 overdeepenings are predicted by the swissALTI^{3D} and 113 by DHM25 L2. Findings like this are not necessarily widely applicable, since certain local DEMs like swissALTI^{3D}, DHM25L2 and Regione Autonoma Valle d'Aosta (RAVA) are only available for a given area, performing optimally within specific terrains. However, when globally available DEMs were analysed across multiple ice thickness models in the current study, the influence of the models became more pronounced in estimating overdeepenings, as discussed in Section 5.1.

Although the consistency of global DEMs is known to be variable (Li et al., 2018), the vertical differences (which are of the order of 1-10 m) are relatively small in comparison to the inconsistencies between ice thickness estimates. DEMs also tend to perform best over shallow-sloped terrain, making them more reliable over glacier tongues, as suggested by intercomparison studies of DEMs (Magnin et al. 2020; Gharechahi et al. 2020). These two factors together likely explain why there was little impact on overdeepening characteristics using different DEM choices in the current study.

Given the scale of analysis in this study, spanning five regions with over 150 glaciers each, the ALOS-PALSAR DEM was selected as an appropriate data source given its wide swath and a spatial resolution of 30 m (as mentioned in section 4.3.4) ALOS-PALSAR is an open-source DEM and it has been used in recent studies to estimate the overdeepenings (Furian et al. 2021, Furian et al. 2022). High-resolution DEMs have been shown elsewhere to provide more accurate estimates of both ice thickness (Ramsankaran et al. 2018) and overdeepenings location and size (Furian et al. 2021). This choice balances the need for robust data performance with the practical requirement of optimizing processing time. It seems likely that future studies could also adopt an approach of selecting the most appropriate choice of DEM for the scale of analysis, and anticipate that it plays only a minor role in the results that are derived.

6.1.2. Ice Thickness Models

The choice of ice thickness model appears to be a critical step when estimating overdeepening characteristics. When a single DEM is applied across all regions with various ice thickness models, OGGM consistently exhibits a wide range of overdeepening volumes and areas across all regions. Among the models, OGGM, GlabTop2, and Millan predict higher overdeepening volumes for all regions. GlabTop2, OGGM, and Farinotti's Ensemble produce higher mean values for the area. Although the range of median values of area across all regions and models is relatively similar, many large overdeepenings are found in Alaska, with the largest having an area of around 12 km^2 (Appendix G), predominantly predicted by Farinotti's Ensemble.

Previous studies have noted that HF tends to overestimate the number of overdeepenings compared to GlabTop2 in the Austrian Alps (Otto et al. 2022). A similar trend is observed in our study: HF predicts a greater number of overdeepenings and higher volumes of individual overdeepenings than

GlabTop2 across all regions. However, the total area of overdeepenings predicted by GlabTop2 remains higher than that of HF across most regions.

OGGM consistently predicts higher ice thickness volumes and the greatest pixel depths across all regions except for Alaska where GlabTop2 and Farinotti's Ensemble produces the higher volume (see Appendix F for reference). This overestimation (with respect to (wrt) other ice thickness models) may stem from OGGM's methodology, which uses temperature and precipitation as the main driver of the model. This is appropriate for studying long-term glacier fluctuations across broad scales of time and space but has been shown to be somewhat deficient on the scale of individual glaciers and using only limited climate records (Parkes and Goosse, 2020). Furthermore, the model employs inverse distance interpolation to estimate missing values especially of climate data (i.e. away from the centreline), potentially introducing errors that might contribute to overestimation (wrt other models).

Farinotti's Ensemble, on the other hand, tends to underestimate (wrt other models) both the number and volume of overdeepenings across all regions compared to other models, except for the volume in Alaska. This underestimation (wrt other models) could be attributed to its weighted average approach, which has a tendency to smooth out extreme values (Farinotti et al., 2017). Additionally, the models with high weights in Farinotti's Ensemble have primarily been tested and validated on glaciers in regions such as the Himalayas and the Alps, where their performance is well-established. This could explain why the ensemble tends to overestimate (wrt other models) overdeepening areas, and more generally to behave differently when applied to Alaska.

There is no consistent trend of models across all regions in terms of producing overdeepenings with the highest volumes or areas. Each model behaves differently depending on the region. OGGM estimates the highest total area across Himalayas, Peruvian Andes and New Zealand Southern Alps, suggesting that it is sensitive (in predicting the total area of overdeepenings) to regions which are dominated by valley-type glaciers, whereas Farinotti's ensemble predicts the highest total area for glaciers in Alaska, suggesting it is sensitive to larger glaciers, and Millan is sensitive to the region which is dominated by cirque glaciers. While models like GlabTop2 and OGGM tend to overestimate (wrt other models) values across most regions, their outputs do not follow a uniform pattern. Particularly for models like OGGM, which rely on numerous inputs, even small changes in input parameters can impact the estimated glacier thickness. Previous studies have shown that minor shifts in initial parameter values can lead to large variations in final ice thickness outputs

(Ramsankaran et al. 2018; Drenkhan et al. 2019; Pandit and Ramsankaran, 2020). For instance, Pandit and Ramsankaran, (2020), changed the shape factor from 0.6 to 0.9 for 31 times and averaged the ice thickness thus generated as the final output. This shows that even a small variability in shape factor can change the output.

The variability in glacier morphology across regions further complicates model predictions, and this may also account for the lack of any consistent trend in the model performance. For instance, the Alps and the Himalayas are characterized by predominantly flat-tongued valley glaciers, while glaciers in the tropical Andes are generally steeper (Drenkhan et al. 2018). Even within the European Alps, there are distinctions: the Swiss Alps host more valley glaciers, whereas cirque glaciers dominate the Austrian Alps (Cogley et al. 2010; Fischer et al. 2014; Otto et al. 2019; Otto et al. 2022). Similarly, glacier geography and type vary across the Himalayas, with the Eastern and Central Himalayas featuring more debris-covered glaciers compared to the Western Himalayas and the Karakoram. The general trend of glacier retreat in the Western, Central, and Eastern Himalayas contrasts with the Karakoram, which includes some advancing glaciers. The Alaskan glaciers have been reported to have long tunnel of troughs and is home to submarine landslides beneath the glaciers (Avidievitch and Coe, 2022). This might have attributed to the large and high voluminous overdeepenings in the Alaska as compared to other regions .

These regional differences highlight the importance of considering local glacier characteristics when interpreting model outputs. Hence if a similar study has to be done on one glacier or very few glaciers, then the local parameters of the glacier(s) like slope, aspect and debris cover can be taken into account.

Therefore, the finding that model outputs can vary both between and within regions leads to the recommendation that future studies should not assume that an ice thickness model performing well for one region can be considered representative elsewhere. Previous studies have compared the outputs of two ice thickness models (Otto et al. 2022). The findings of this study reveal that highly variable ranges of values for the area and depth of overdeepenings can extend both within and beyond the estimates provided by the two models alone. This broader spectrum of results, which incorporates five ice thickness models, adds a much more comprehensive analysis to the literature and provides a major advance in understanding the sensitivity of overdeepening estimates to the input datasets. Millan's dataset, which is not a part of Farinotti's ensemble was introduced into the study and it estimates the highest number of overdeepenings across all regions. The area and

volume of the majority of the overdeepenings estimated by Millan is similar to the area and volume of overdeepenings as predicted by other ice thickness models. This shows that recent models, which are not a part of any consensus may behave differently when compared with other ice thickness models that are a part of a consensus, in regard to some parameter(s).

These findings provide us with a chance to observe the differences in results from five different ice thickness models, they may also have value in a practical sense now that the effect of different models is better understood. In other words, future studies may decide to choose a specific ice thickness model because it fits best for their study purpose. Models that tend to overestimate values for area and volume of overdeepenings (like GlapTop2 or OGGM), may be deemed particularly suitable for predicting worst-case scenarios and serving as an upper limit for hazard planning. On the other hand, models that underestimate overdeepenings may help prioritize glaciers that require immediate attention, guiding more focused mitigation efforts. This assumes that the few(er) pixels defined as being overdeepening locations can be taken with high(er) confidence, but further work is required to establish whether this is actually the case when compared to field validation data. If field validation is not possible it will be best to stick to a model that is a combination of models with different approaches like Farinotti's Ensemble which is most likely to provide a solution with less uncertainty.

6.1.3. Uncertainties

Overdeepenings vary in size and contribute only a small fraction of the total glacier volume. In this study, they are shown to account for 0.1% to 10.9% of the total glacier volume (see Appendix A for reference). Alaska, with its substantial glacier volume ranging from 45 km^3 to 62.99 km^3, also has the highest total volume of overdeepenings, reaching up to 10.9% of the modelled ice volume. In contrast, the European Alps have a much lower proportion of overdeepenings, contributing only 0.1% to 1.7% of the glacier volume.

Despite their relatively small contribution to glacier volume, the potential downstream impact of these overdeepenings could be high, particularly if they evolve into glacial lakes, which is a likely scenario for those located towards a glacier terminus. One key purpose of identifying overdeepenings is to assess the future location, size and hazard potential posed by specific glaciers. The volume of overdeepenings has been shown to have a greater influence on their hazard potential than their area in previous work (Haeberli et al. 2016).

While overdeepenings detected in many cases have shown reliable performance regionally, significant uncertainties remain regarding their depth, volume, and area on a global scale. In most instances, the location of overdeepenings is accurately identified, but their morphometric characteristics are less well protected. The prediction of deeper and larger overdeepenings tend to be more robust (Cathala et al. 2021), probably because a high number of pixels are well within the modelled overdeepening position and those that are less certain around the periphery have a low impact, relative to the overall area and volume. Based on this rationale, the overdeepenings estimated by GlabTop2 in Alaska and the Himalayas in this study can be considered relatively high-confidence estimates, at least in terms of the location and the ultimate size and volume.

The accuracy of the overdeepening morphometry largely depends on the glacier type, and where along the glacier flowline the overdeepening is located (Sattar et al. 2019). The GlabTop2 model has shown particularly high uncertainties for depicting the morphometry of overdeepenings that are present beneath debris-covered glaciers (Linsbauer et al. 2016), most likely as a consequence of the methodological approach, which uses surface slope as a key input parameter. Debris-covered tongues tend to be very shallow in gradient, and inversions of the basal shear stress equation are increasingly uncertain as the slope approaches zero (Linsbauer et al. 2016). Overdeepenings located towards the termini of valley glaciers in the Austrian Alps were shown to be more accurate than the overdeepenings that were depicted beneath the cirque glaciers (Otto et al. 2022). These findings may be related to the ability of an individual model to correctly estimate ice thicknesses in both shallow and steep gradient terrain (Zorzut et al. 2020).

6.2. A POSSIBLE WAY FORWARD

6.2.1. Combining the models

Since overdeepenings can serve as a foundation for hazard mapping in a region, having confidence in the depiction of their initial morphometry is crucial. If the location and the morphometry of overdeepenings are highly uncertain themselves, these uncertainties will likely propagate during subsequent data processing and analysis. However, these uncertainties can potentially be reduced through various approaches, one of which involves combining multiple ice thickness models to achieve more reliable results. This method has been shown to provide more confident outcomes when combining two ice thickness models (Otto et al. 2022). It is reasonable to expect that

combining a larger number of models would further enhance the confidence in overdeepenings estimates, thereby reducing overall uncertainties.

In this approach, pixels can be ranked according to the number of models that depict them as being an overdeepening location. Pixels with a rank of 5 can therefore be considered to be those with the highest confidence (Figure 6.1). For example, in the Himalayas, the number of pixels that are present in all five models accounts for 5.92% of the total pixels in the overdeepenings that are depicted. Focusing attention on these areas may provide an improved judgement about the likely location and morphometry of the overdeepenings. It can also lay the foundation for further analysis of the regions where the pixels have high confidence, as well as provide a basis for communicating the uncertainty in predictions of lake development to communities who may depend on those results for water resource planning and/or hazard mitigation and preparation.

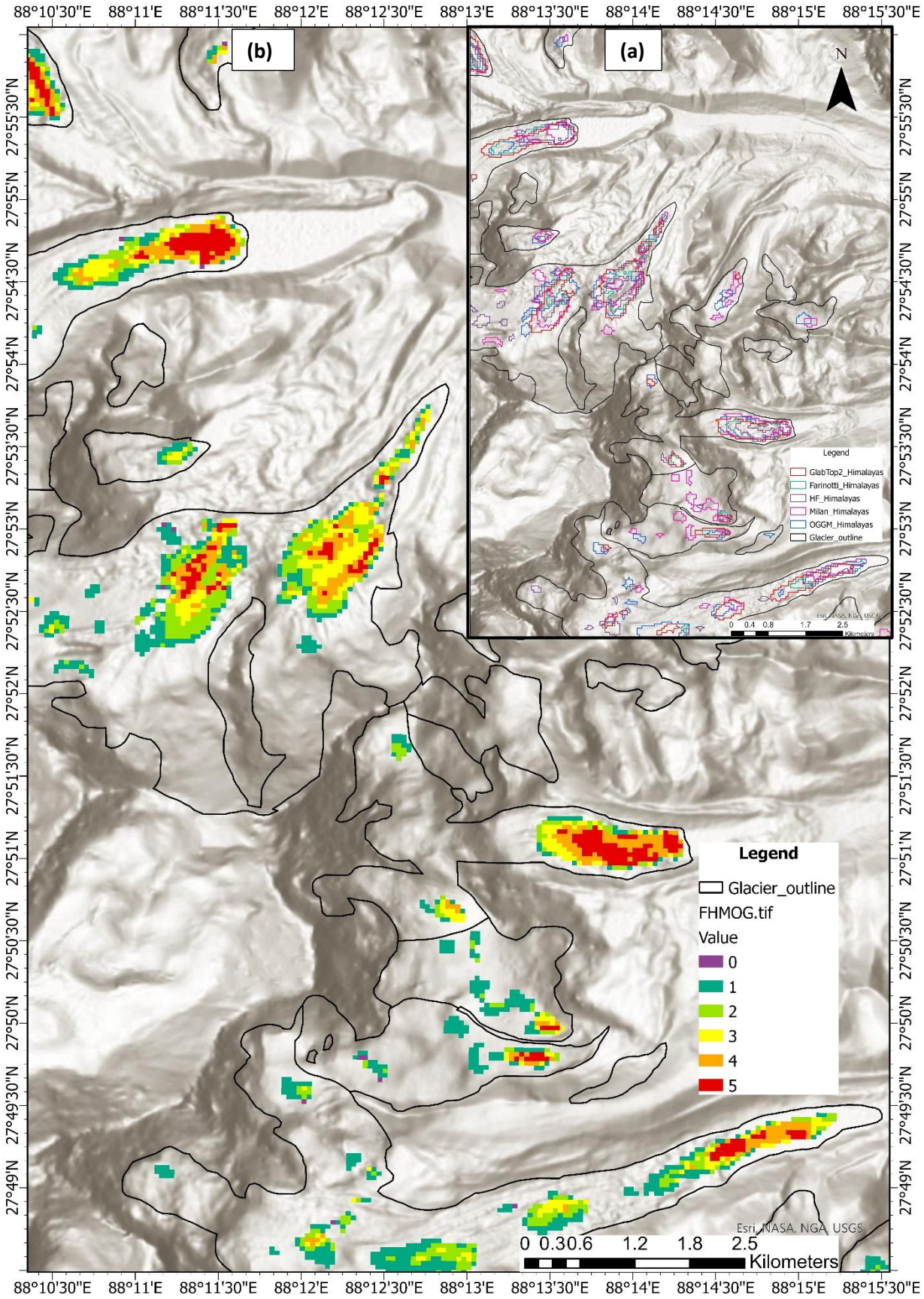

Figure 6.1: (a) Outlines of the overdeepenings determined by different five ice thickness models in part of the Central Himalayas (b) Pixels ranked according to the models that they fall in with rank 5 being the pixel that is present in all five models whereas rank 1 being the pixel that is present in only ice thickness model.

Section 5.4 showed that when two of the five models are used in combination, the number of pixels that are commonly identified as overdeepening locations rises to just over 50%. This low level of agreement highlights that overdeepenings predicted by different ice thickness models can vary significantly across regions. Since HF carries the highest weight (22%) in Farinotti's ensemble, it is perhaps not surprising that the highest overlap occurs between HF and Farinotti's Ensemble in some places. This overlap is most prominent in the Peruvian Andes, where the highest percentage (40.3%) is observed between these two models. Interestingly, Farinotti's Ensemble and GlabTop2 show the highest overlap in pixels across other regions, ranging from 53.6% in the New Zealand Southern Alps to 40.8% in the Himalayas. This difference in overlap percentages is likely due to GlabTop2's broader coverage, which results in more pixels than HF in all regions except the Peruvian Andes. Also, GlabTop2 is given the second-highest weight (19%) in Farinotti's ensemble, after HF, so again there may already be some level of correlation between these two datasets.

Overall, Farinotti's Ensemble, when combined with either HF, GlabTop2, or OGGM, gives strong agreement, most likely as a consequence of these three models being assigned the highest weightings in the ensemble, in that order. Additionally, the agreement between the HF model and GlabTop2 is noteworthy and aligns with findings from previous studies (Otto et al. 2022), further validating the consistency of these models in predicting overdeepenings.

In contrast, some models show minimal overlap, with Farinotti's Ensemble and Millan's model showing the least overlap in the Himalayas (21.2%), New Zealand Southern Alps (25.7%), and European Alps (11.75%). Farinotti's Ensemble consistently predicts smaller total overdeepening areas across all regions, except for in Alaska; Millan's model tends to show higher total area but in locations that are inconsistent with the ensemble outputs. In the European Alps, Millan's model estimates the highest total overdeepening area of all the models. This difference, between the ensemble outputs and those of Millan, are most likely to arise from the fundamental differences in how the ice thickness models are constructed. Specifically, Millan's model employs a velocity-based approach to derive its ice thicknesses. In contrast, the models within the ensemble rely on mass-conservation or shear-stress-based approaches, with the ensemble itself using a weighted method. This indicates that when assessing the potential for agreement or disagreement between two models, greater emphasis should be placed on the physical principles behind their functioning, rather than simply the number of pixels they generate.

6.2.2. Implications of the findings

Glacier mass loss is occurring now at a rate that has not been experienced since records began, and is accelerating globally due to rising temperatures and changes in precipitation (Hock et al., 2019). One of the clearest impacts of this is the growth of glacial lakes and associated hazard potential (Allen et al., 2016; Shugar et al., 2020). The Himalayas (Rao et al. 2014 ; Riaz et al. 2014 ; Westoby et al. 2014; Banerjee et al. 2024) and the Peruvian Andes (Emmer et al. 2014; Huggel et al. 2020; Vilca et al. 2021) have experienced numerous GLOFs in recent decades (Vilímek et al. 2014). The number and size of glacial lakes have been increasing globally, with those in High Mountain Asia expanding at a particularly fast rate. Between 2008 and 2017, the total glacial lake area in this region grew by approximately 6.90%, equating to an increase of around 90.14 km² (Zheng et al. 2021) .

The central and eastern Himalayas are emerging as hotspots for GLOFs (Gardelle et al. 2011; Veh et al. 2020), while glacial lakes in the Cordillera of the Peruvian Andes have grown by 18.3% in area and 9.7% in volume between 1988 and 2016 (Drenkhan et al. 2018). Young proglacial lakes, particularly those located at the glacier terminus, tend to be more unstable than older lakes that have fully developed and are no longer directly connected to glaciers. The dynamics of glaciers are influenced by these lakes, and conversely, the proglacial lake geometry is influenced by the glacier dynamics (Carrivick et al. 2022). The glacial lakes in the early stages of formation, typically found at the glacier tongues where the gradient changes sharply, are particularly prone to causing GLOFs (Emmer et al. 2015b).

One way to prepare for, and ultimately mitigate, the risk of such disasters is to create an inventory of potential future glacial lakes. Mapping overdeepenings can play a crucial role in this process. The first step in overdeepening mapping involves identifying regions with high confidence for the evolution of overdeepenings, which is where combining models can be particularly useful.

Several studies have begun ranking overdeepenings based on their hazard potential in regions like the Himalayas (Pandit and Ramsankaran, 2020) and the Peruvian Andes (Drenkhan et al. 2019; Davies, 2021; Gegg, 2021; Haeberli and Drenkhan, 2022). The current study contributes to this effort by suggesting a ranking of individual pixels; based on their occurrence across different ice thickness models, it can support future hazard assessment efforts.

The importance of subglacial overdeepenings extends beyond their potential to develop into glacial lakes. Subglacial overdeepenings are ubiquitous features in glacial systems, yet they remain enigmatic because their origins remain uncertain (Hooke, 1991; Alley et al. 2003; Cook and Swift, 2012). There have been numerous studies that have tried to answer questions regarding the evolution (Patton et al. 2016) sediment transfer (Swift et al. 2018), site and origin of formation of subglacial overdeepenings in a glacial system (Gegg and Preusser 2023; Lloyd et al. 2023). The estimation of area, volume and location of overdeepenings from this study when compared against the local climate, precipitation, bedrock geology (Magrani et al. 2020) and/or subglacial lithostratigraphic data (Preusser et al. 2010) might lead to a better understanding of the processes and factors that govern formation of subglacial overdeepenings (Huuse and Anderson 2000; Liebl et al. 2021; Swift et al. 2021; Evans 2023).

Apart from being important for hazard management and landscape evolution, overdeepenings also are a potential source of hydropower generation. These may act as reservoirs for meltwater and precipitation, accumulating water over time, after deglaciation (Cuellar and McKinney, 2017). A recent study in Mount Massif in the European Alps highlighted the high hydropower potential of future glacial lakes (Magnin et al. 2020). As glacial lakes increase in size and number, they can have both positive and negative impacts on downstream hydropower plants. While they may offer potential energy resources, they also pose risks to downstream areas, potentially leading to destruction and the loss of infrastructure and livelihoods (Rounce et al. 2017; Chettri et al. 2020).

Knowledge of future lake locations can be immensely valuable for mountain communities as well as businesses tasked with providing a sustainable power supply to remote regions (Farinotti et al., 2019a). By estimating the volume and area of overdeepenings, the approach developed in this study can help assess the potential hydropower capacity of these future lakes. Considering a range of values emphasizes the importance of using multiple volume estimates rather than relying on a single fixed value. It can also provide a means for communicating the range of power generation, and the longevity of that resource, to those who may be considering exploiting those locations for commercial benefit. This more nuanced approach – of ranking pixels – provides greater flexibility for decision-makers and stakeholders involved in policymaking for hydropower development. It allows for adjustments and refinements based on more varied projections of future glacial lake dynamics. By incorporating variability into hydropower assessments, this method ensures more adaptive and

resilient planning, helping to mitigate risks while optimising the potential benefits of glacial meltwater resources.

6.3. Limitations

There are a number of limitations within this study, which cannot be addressed within the scope of the work, but may prove fruitful for further investigation:

- Use of five ice thickness models produced estimates of overdeepening characteristics with greater confidence than has been possible in previous approaches. However, none of these results have been validated against existing glacial lake locations, known bed morphometries, or Ground Penetrating Radar (GPR) data, which limits the project to one of intercomparison, rather than being able to confirm their absolute accuracy.
- The ice thickness models used here were released in 2019 and rely on data collected prior to that year. Changes in ice thickness and bedrock topography occurring after 2019 have not been incorporated. Glacier dynamics, such as merging or splitting of glaciers over time can alter glacier outlines, bed topography, and ice thickness. These changes are not addressed in this study.
- Although it was possible to derive detailed insights into the location and volume of potential overdeepenings, it was not possible to evaluate the timing of when these features might develop. Predicting their temporal evolution remains a critical gap, but could be realized by combining these outputs with time-evolving glacier boundaries from a global dataset such as GloGEM (Huss and Hock, 2015). The estimation of overdeepening characteristics currently relies solely on an area threshold, without incorporating factors like slope and any evident surface features (e.g. crevasse fields), which affect and/or indicate the formation and distribution of overdeepenings (Frey et al. 2010). Including additional parameters such as slope could enhance the accuracy and reliability of our predictions.
- As with almost all previous studies, linking overdeepenings to potential future lakes is one thing, but linking those lakes, with reduced uncertainty, to a hazard is far more complex because then knowledge of the lake dam type and other catchment characteristics such as risk of avalanching must be incorporated.
- Combined, these points highlight the need for future studies to integrate updated datasets, validate findings with in-situ observations, and carefully consider the purpose of the work,

as well as the nuances of individual models to better capture the dynamics of glaciers and overdeepening evolution.

7. CONCLUSION

This study has shown for the first time that ice thickness model choice has a greater influence than DEM choice on the modelling of overdeepening location and size using a GIS-based approach. Future research can therefore focus on improving and refining ice thickness models providing a high-resolution, internally self-consistent and accurate glacier bed DEM that is used throughout the rest of the analysis. This work is the first to combine more than two ice thickness models to estimate overdeepenings across five diverse regions, providing a detailed assessment of their volume and area. The estimates reveal stark variations across all the models and regions, with the overdeepening area in Alaska being greatest at 12.11 km^2 as estimated by Farinotti's Ensemble, and volume ranging from 16.5 x 10^{-6} km^3 as estimated by Millan to 2 km^3 as estimated by GlabTop2. Despite the high uncertainty, these findings can offer insights into subglacial morphometry, as well as holding relevance for understanding hazard potential, sediment provenance, and glacier dynamics.

The results highlight significant differences in overdeepening characteristics derived from different ice thickness models. For the Himalayas, the overlap can be as high as 40.8% when combining two models but drops to as low as 5.9% with five models. Considering all regions, the agreement between any two models reached a maximum of just 53.6%. While no single model emerges as universally optimal, combining multiple models may provide a more reliable and flexible approach for estimating overdeepenings, balancing overestimation and underestimation.

It is impossible to eliminate uncertainties entirely when modelling overdeepenings, given the inherent complexities of glacier dynamics and ice thickness modelling. Therefore, the most practical approach would be to establish a range of estimates with varying confidence levels. This strategy provides a broader perspective while identifying regions with the highest reliability. Future research can aim to narrow this range and refine parameter estimates to improve accuracy further.

For small-scale studies requiring precision, local ice thickness models can be parameterized for enhanced accuracy. However, this study emphasizes the need to define clear objectives to ensure the correct model is employed, and to consider both overestimation and underestimation when analysing overdeepening locations and characteristics.

Finally, this study introduces a novel ranking system for regions based on pixel occurrences across different models, offering a fresh perspective on regional overdeepening assessments. The range of estimates, model overlaps, and the proposed ranking scheme provides a new framework for identifying overdeepenings, paving the way for more robust methodologies in future research. This framework can improve our ability to estimate hazard potential, understand glacial system evolution, and assess the water storage capacity of future glacial lakes for hydropower generation.

REFERENCES

Alifu, H., Tateishi, R., Nduati, E. and Maitiniyazi, A., 2016. Glacier changes in Glacier Bay, Alaska, during 2000–2012. *International Journal of Remote Sensing*, *37*(17), pp.4132-4147.

Allen, M., Dube, O.P., Solecki, W., Aragón-Durand, F., Cramer, W., Humphreys, S. and Kainuma, M., 2018. Special report: Global warming of 1.5 C. Intergovernmental Panel on Climate Change (IPCC), 677, p.393.Davaze, L., Rabatel, A., Dufour, A., Hugonnet, R. and Arnaud, Y., 2020. Region-wide annual glacier surface mass balance for the European Alps from 2000 to 2016. Frontiers in Earth Science, 8, p.149.

Allen, S.K., Linsbauer, A., Huggel, C., Randhawa, S.S., Schaub, Y. and Stoffel, M., 2016a. Current and future glacial lake outburst flood hazard: application of GIS-based modeling in Himachal Pradesh, India. *Climate Change, Glacier Response, and Vegetation Dynamics in the Himalaya: Contributions Toward Future Earth Initiatives*, pp.181-203.

Allen, S.K., Linsbauer, A., Randhawa, S.S., Huggel, C., Rana, P. and Kumari, A., 2016b. Glacial lake outburst flood risk in Himachal Pradesh, India: an integrative and anticipatory approach considering current and future threats. *Natural Hazards*, *84*, pp.1741-1763.

Alley, R.B., Lawson, D.E., Evenson, E.B. and Larson, G.J., 2003. Sediment, glaciohydraulic supercooling, and fast glacier flow. *Annals of Glaciology*, *36*, pp.135-141.

Alley, R.B., Cuffey, K.M. and Zoet, L.K., 2019. Glacial erosion: status and outlook. *Annals of Glaciology*, *60*(80), pp.1-13.

Anderson, B., Mackintosh, A.N., Dadić, R., Oerlemans, J., Zammit, C., Doughty, A., Sood, A. and Mullan, B., 2021. Modelled response of debris-covered and lake-calving glaciers to climate change, Kā Tiritiri o te Moana/Southern Alps, New Zealand. *Global and Planetary Change*, *205*, p.103593.

Avdievitch, N.N. and Coe, J.A., 2022. Submarine landslide susceptibility mapping in recently deglaciated terrain, Glacier Bay, Alaska. *Frontiers in Earth Science*, *10*, p.821188.

Banerjee, A., Kang, S., Guo, W., Meadows, M.E., Wang, W., Sengupta, D. and Zhang, T., 2024. Glacier retreat and lake outburst floods in the central Himalayan region from 2000 to 2022. *Natural Hazards*, *120*(6), pp.5485-5508.

Bhambri, R. and Bolch, T., 2009. Glacier mapping: a review with special reference to the Indian Himalayas. *Progress in Physical Geography*, *33*(5), pp.672-704.

Bhushan, S., Syed, T.H., Kulkarni, A.V., Gantayat, P. and Agarwal, V., 2017. Quantifying changes in the Gangotri Glacier of Central Himalaya: evidence for increasing mass loss and decreasing velocity. *IEEE Journal of Selected Topics in Applied Earth Observations and Remote Sensing*, *10*(12), pp.5295-5306.

Bolch, T., Kulkarni, A., Kääb, A., Huggel, C., Paul, F., Cogley, J.G., Frey, H., Kargel, J.S., Fujita, K., Scheel, M. and Bajracharya, S., 2012. The state and fate of Himalayan glaciers. *Science*, *336*(6079), pp.310-314.

Carrivick, J.L., Davies, B.J., James, W.H., Quincey, D.J. and Glasser, N.F., 2016. Distributed ice thickness and glacier volume in southern South America. *Global and Planetary Change*, *146*, pp.122-132.

Carrivick, J.L., Sutherland, J.L., Huss, M., Purdie, H., Stringer, C.D., Grimes, M., James, W.H. and Lorrey, A.M., 2022. Coincident evolution of glaciers and ice-marginal proglacial lakes across the Southern Alps, New Zealand: Past, present and future. *Global and Planetary Change*, *211*, p.103792.

Carrivick, J.L., James, W.H., Grimes, M., Sutherland, J.L. and Lorrey, A.M., 2020. Ice thickness and volume changes across the Southern Alps, New Zealand, from the little ice age to present. *Scientific reports*, *10*(1), p.13392.

Cathala, M., Magnin, F., Linsbauer, A. and Haeberli, W., 2021. Modelling and characterizing glacier-bed overdeepenings as sites for potential future lakes in the deglaciating French Alps. *Géomorphologie: relief, processus, environnement*, *27*(1), pp.19-36.

Chandler, B.M., Evans, D.J. and Roberts, D.H., 2016. Characteristics of recessional moraines at a temperate glacier in SE Iceland: Insights into patterns, rates and drivers of glacier retreat. Quaternary Science Reviews, 135, pp.171-205.

Chettri, N., Shrestha, A.B. and Sharma, E., 2020. Climate change trends and ecosystem resilience in the Hindu Kush Himalayas. *Himalayan Weather and Climate and their Impact on the Environment*, pp.525-552.

Chevallier, P., Pouyaud, B., Suarez, W. and Condom, T., 2011. Climate change threats to environment in the tropical Andes: glaciers and water resources. *Regional Environmental Change*, *11*, pp.179-187.

Chinn, T.J., 1999. New Zealand glacier response to climate change of the past 2 decades. Global and Planetary Change, 22(1-4), pp.155-168.Cogley, J.G., 2011. Present and future states of Himalaya and Karakoram glaciers. *Annals of Glaciology*, *52*(59), pp.69-73.

Cogley, J.G., 2016. Glacier shrinkage across high mountain Asia. *Annals of Glaciology*, *57*(71), pp.41-49.

Cogley, J.G., Arendt, A.A., Bauder, A., Braithwaite, R.J., Hock, R., Jansson, P., Kaser, G., Moller, M., Nicholson, L., Rasmussen, L.A. and Zemp, M., 2010. Glossary of glacier mass balance and related terms.

Colonia, D., Torres, J., Haeberli, W., Schauwecker, S., Braendle, E., Giraldez, C. and Cochachin, A., 2017. Compiling an inventory of glacier-bed overdeepenings and potential new lakes in de-glaciating areas of the Peruvian Andes: approach, first results, and perspectives for adaptation to climate change. *Water*, *9*(5), p.336.

Cook, S.J. and Swift, D.A., 2012. Subglacial basins: Their origin and importance in glacial systems and landscapes. *Earth-Science Reviews, 115(4)*, pp.332-372.

Cuellar, A.D. and McKinney, D.C., 2017. Decision-making methodology for risk management applied to Imja Lake in Nepal. *Water*, *9*(8), p.591.

Cuffey, K.M. and Paterson, W.S.B., 2010. *The physics of glaciers*. Academic Press., L., Rabatel, A., Dufour, A., Hugonnet, R. and Arnaud, Y., 2020. Region-wide annual glacier surface mass balance for the European Alps from 2000 to 2016. Frontiers in Earth Science, 8, p.149.

Dai, C., Higman, B., Lynett, P.J., Jacquemart, M., Howat, I.M., Liljedahl, A.K., Dufresne, A., Freymueller, J.T., Geertsema, M., Ward Jones, M. and Haeussler, P.J., 2020. Detection and assessment of a large and potentially tsunamigenic periglacial landslide in Barry Arm, Alaska. *Geophysical Research Letters*, *47*(22), p.e2020GL089800.

Davies, M.L., 2021. *Quantifying rates of glacier recession in the Peruvian Andes since the Little Ice Age* (Doctoral dissertation, University of Leeds).

Deline, P., Gardent, M., Magnin, F. and Ravanel, L., 2012. The morphodynamics of the Mont Blanc massif in a changing cryosphere: a comprehensive review. *Geografiska Annaler: Series A, Physical Geography*, *94*(2), pp.265-283.

Dorava, J.M. and Milner, A.M., 2000. Role of lake regulation on glacier-fed rivers in enhancing salmon productivity: the Cook Inlet watershed, south-central Alaska, USA. *Hydrological Processes*, *14*(16-17), pp.3149-3159.

Drenkhan, F., Guardamino, L., Huggel, C. and Frey, H., 2018. Current and future glacier and lake assessment in the deglaciating Vilcanota-Urubamba basin, Peruvian Andes. *Global and Planetary Change*, *169*, pp.105-118.

Drenkhan, F., Huggel, C., Guardamino, L. and Haeberli, W., 2019. Managing risks and future options from new lakes in the deglaciating Andes of Peru: The example of the Vilcanota-Urubamba basin. *Science of the Total Environment*, *665*, pp.465-483.

Emmer, A., Loarte, E.C., Klimeš, J. and Vilímek, V., 2015a. Recent evolution and degradation of the bent Jatunraju glacier (Cordillera Blanca, Peru). *Geomorphology*, *228*, pp.345-355.

Emmer, A., Merkl, S. and Mergili, M., 2015b. Spatiotemporal patterns of high-mountain lakes and related hazards in western Austria. *Geomorphology*, *246*, pp.602-616.

Emmer, A., Vilímek, V., Klimeš, J. and Cochachin, A., 2014. Glacier retreat, lakes development and associated natural hazards in Cordilera Blanca, Peru. Landslides in cold regions in the context of climate change, pp.231-252.

Evans, D.J., Clark, C.D. and Rea, B.R., 2008. Landform and sediment imprints of fast glacier flow in the southwest Laurentide Ice Sheet. *Journal of Quaternary Science: Published for the Quaternary Research Association*, *23*(3), pp.249-272.

Evans, D.J., Ewertowski, M.W., Tomczyk, A. and Chandler, B.M., 2023. Active temperate glacial landsystem evolution in association with outwash head/depositional overdeepenings. *Earth Surface Processes and Landforms*, *48*(8), pp.1573-1598.

Farinotti, D., Brinkerhoff, D.J., Clarke, G.K., Fürst, J.J., Frey, H., Gantayat, P., Gillet-Chaulet, F., Girard, C., Huss, M., Leclercq, P.W. and Linsbauer, A., 2017. How accurate are estimates of glacier ice thickness? Results from ITMIX, the Ice Thickness Models Intercomparison eXperiment. *The Cryosphere*, *11*(2), pp.949-970.

Farinotti, D., Huss, M., Fürst, J.J., Landmann, J., Machguth, H., Maussion, F. and Pandit, A., 2019a. A consensus estimate for the ice thickness distribution of all glaciers on Earth. *Nature Geoscience*, *12*(3), pp.168-173.

Farinotti, D., Round, V., Huss, M., Compagno, L. and Zekollari, H., 2019b. Large hydropower and water-storage potential in future glacier-free basins. *Nature*, *575*(7782), pp.341-344.

Fischer, M., Huss, M., Barboux, C. and Hoelzle, M., 2014. The new Swiss Glacier Inventory SGI2010: relevance of using high-resolution source data in areas dominated by very small glaciers. *Arctic, Antarctic, and Alpine Research*, *46*(4), pp.933-945.

Fountain, A.G. and Walder, J.S., 1998. Water flow through temperate glaciers. *Reviews of Geophysics*, *36*(3), pp.299-328.

Freudiger, D., Mennekes, D., Seibert, J. and Weiler, M., 2018. Historical glacier outlines from digitized topographic maps of the Swiss Alps. *Earth System Science Data*, *10*(2), pp.805-814.

Frey, H., Haeberli, W., Linsbauer, A., Huggel, C. and Paul, F., 2010. A multi-level strategy for anticipating future glacier lake formation and associated hazard potentials. *Natural Hazards and Earth System Sciences*, *10*(2), pp.339-352.

Frey, H., Machguth, H., Huss, M., Huggel, C., Bajracharya, S., Bolch, T., Kulkarni, A., Linsbauer, A., Salzmann, N. and Stoffel, M., 2014. Estimating the volume of glaciers in the Himalayan–Karakoram region using different methods. *The Cryosphere*, *8*(6), pp.2313-2333.

Fujisada, H., Sakuma, F., Ono, A. and Kudoh, M., 1998. Design and preflight performance of ASTER instrument protoflight model. *IEEE Transactions on Geoscience and Remote Sensing*, *36*(4), pp.1152-1160.

Fujita, K. and Nuimura, T., 2011. Spatially heterogeneous wastage of Himalayan glaciers. *Proceedings of the National Academy of Sciences*, *108*(34), pp.14011-14014.

Furian, W. and Sauter, T., 2025. Assessing economic impacts of future GLOFs in Nepal's Everest region under different SSP scenarios using three-dimensional simulations. *EGUsphere*, *2025*, pp.1-36.

Furian, W., Loibl, D. and Schneider, C., 2021. Future glacial lakes in High Mountain Asia: an inventory and assessment of hazard potential from surrounding slopes. *Journal of Glaciology*, *67*(264), pp.653-670..

Furian, W., Maussion, F. and Schneider, C., 2022. Projected 21st-century glacial lake evolution in High Mountain Asia. *Frontiers in Earth Science*, *10*, p.821798.

Gantayat, P., Kulkarni, A.V., Srinivasan, J. and Schmeits, M.J., 2017. Numerical modelling of past retreat and future evolution of Chhota Shigri glacier in Western Indian Himalaya. *Annals of Glaciology*, *58*(75pt2), pp.136-144.

Gopika, J.S., Kulkarni, A.V., Prasad, V., Srinivasalu, P. and Raman, A., 2021. Estimation of glacier stored water in the Bhaga basin using laminar flow and volume-area scaling methods. *Remote Sensing Applications: Society and Environment*, *24*, p.100656.

Gardelle, J., Berthier, E., Arnaud, Y. and Kääb, A., 2013. Region-wide glacier mass balances over the Pamir-Karakoram-Himalaya during 1999–2011. *The Cryosphere*, *7*(4), pp.1263-1286.

Gegg, L., 2021. *The Mid-Pleistocene landscape history of the Lower Aare Valley with emphasis on subglacial overdeepening* (Doctoral dissertation, University of Bern).

Gegg, L. and Preusser, F., 2023. Comparison of overdeepened structures in formerly glaciated areas of the northern Alpine foreland and northern central Europe. *E&G Quaternary Science Journal*, *72*(1), pp.23-36.

Gharehchahi, S., James, W.H., Bhardwaj, A., Jensen, J.L., Sam, L., Ballinger, T.J. and Butler, D.R., 2020. Glacier ice thickness estimation and future lake formation in Swiss Southwestern Alps—the Upper Rhône Catchment: a VOLTA application. *Remote Sensing*, *12*(20), p.3443.

Guth, P.L., Van Niekerk, A., Grohmann, C.H., Muller, J.P., Hawker, L., Florinsky, I.V., Gesch, D., Reuter, H.I., Herrera-Cruz, V., Riazanoff, S. and López-Vázquez, C., 2021. Digital elevation models: Terminology and definitions. *Remote Sensing*, *13*(18), p.3581.

Haeberli, W. and Drenkhan, F., 2022. Future lake development in deglaciating mountain ranges. In *Oxford Research Encyclopedia of Natural Hazard Science*.

Haeberli, W. and Hoelzle, M., 1995. Application of inventory data for estimating characteristics of and regional climate-change effects on mountain glaciers: a pilot study with the European Alps. *Annals of glaciology*, *21*, pp.206-212.

Haeberli, W., 2013. Mountain permafrost—research frontiers and a special long-term challenge. *Cold Regions Science and Technology*, *96*, pp.71-76.

Haeberli, W., Hoelzle, M., Paul, F. and Zemp, M., 2007. Integrated monitoring of mountain glaciers as key indicators of global climate change: the European Alps. *Annals of glaciology*, *46*, pp.150-160.

Haeberli, W., Linsbauer, A., Cochachin, A., Salazar, C. and Fischer, U.H., 2016. On the morphological characteristics of overdeepenings in high-mountain glacier beds. *Earth Surface Processes and Landforms*, *41*(13), pp.1980-1990.

Haeberli, W., Schaub, Y. and Huggel, C., 2017. Increasing risks related to landslides from degrading permafrost into new lakes in de-glaciating mountain ranges. *Geomorphology*, *293*, pp.405-417.

Harbor, J.M., 1992. Numerical modeling of the development of U-shaped valleys by glacial erosion. *Geological Society of America Bulletin*, *104*(10), pp.1364-1375.

Harrison, W.D. and Post, A.S., 2003. How much do we really know about glacier surging? *Annals of glaciology*, *36*, pp.1-6.

Henderson, R.D. and Thompson, S.M., 1999. Extreme rainfalls in the southern Alps of New Zealand. *Journal of Hydrology (New Zealand)*, pp.309-330.

Hock, R., Rasul, G., Adler, C., Cáceres, B., Gruber, S., Hirabayashi, Y., Jackson, M., Kääb, A., Kang, S., Kutuzov, S. and Milner, A., 2019. High mountain areas. In *IPCC special report on the ocean and cryosphere in a changing climate* (pp. 131-202). H.-O. Pörtner, DC Roberts, V. Masson-Delmotte, P. Zhai, M. Tignor, E. Poloczanska, K. Mintenbeck, A. Alegría, M. Nicolai, A. Okem, J. Petzold, B. Rama, NM Weyer (eds.).

Hoelzle, M., Chinn, T., Stumm, D., Paul, F., Zemp, M. and Haeberli, W., 2007. The application of glacier inventory data for estimating past climate change effects on mountain glaciers: A comparison between the European Alps and the Southern Alps of New Zealand. *Global and Planetary Change*, *56*(1-2), pp.69-82.

Hooke, R.L., 1991. Positive feedbacks associated with erosion of glacial cirques and overdeepenings. *Geological Society of America Bulletin*, *103*(8), pp.1104-1108.

Huggel, C., Carey, M., Emmer, A., Frey, H., Walker-Crawford, N. and Wallimann-Helmer, I., 2020. Anthropogenic climate change and glacier lake outburst flood risk: local and global drivers and responsibilities for the case of lake Palcacocha, Peru. *Natural Hazards and Earth System Sciences*, *20*(8), pp.2175-2193.

Hugonnet, R., McNabb, R., Berthier, E., Menounos, B., Nuth, C., Girod, L., Farinotti, D., Huss, M., Dussaillant, I., Brun, F. and Kääb, A., 2021. Accelerated global glacier mass loss in the early twenty-first century. *Nature*, *592*(7856), pp.726-731.

Huss, M. and Farinotti, D., 2012. Distributed ice thickness and volume of all glaciers around the globe. *Journal of Geophysical Research: Earth Surface*, *117*(F4).

Huss, M. and Hock, R., 2015. A new model for global glacier change and sea-level rise. *Frontiers in Earth Science*, *3*, p.54.

Huss, M. and Hock, R., 2018. Global-scale hydrological response to future glacier mass loss. *Nature Climate Change*, *8*(2), pp.135-140.

Huuse, M. and Lykke-Andersen, H., 2000. Overdeepened Quaternary valleys in the eastern Danish North Sea: morphology and origin. *Quaternary Science Reviews*, *19*(12), pp.1233-1253.

Hutchinson, M.F., Xu, T. and Stein, J.A., 2011. Recent progress in the ANUDEM elevation gridding procedure. *Geomorphometry*, *2011*, pp.19-22.

James, W.H. and Carrivick, J.L., 2016. Automated modelling of spatially-distributed glacier ice thickness and volume. *Computers & Geosciences*, *92*, pp.90-103.

Johnson, A.J., Larsen, C.F., Murphy, N., Arendt, A.A. and Zirnheld, S.L., 2013. Mass balance in the Glacier Bay area of Alaska, USA, and British Columbia, Canada, 1995–2011, using airborne laser altimetry. *Journal of Glaciology*, *59*(216), pp.632-648.

Jomelli, V., Favier, V., Rabatel, A., Brunstein, D., Hoffmann, G. and Francou, B., 2009. Fluctuations of glaciers in the tropical Andes over the last millennium and palaeoclimatic implications: A review. Palaeogeography, Palaeoclimatology, Palaeoecology, 281(3-4), pp.269-282.

Kapitsa, V., Shahgedanova, M., Machguth, H., Severskiy, I. and Medeu, A., 2017. Assessment of evolution and risks of glacier lake outbursts in the Djungarskiy Alatau, Central Asia, using Landsat imagery and glacier bed topography modelling. *Natural Hazards and Earth System Sciences*, *17*(10), pp.1837-1856.

Kaser, G., 1999. A review of the modern fluctuations of tropical glaciers. *Global and Planetary Change*, *22*(1-4), pp.93-103.

Khatri, B., 2025. Impacts of Glacial Lake Outburst Floods on Nepal's National Security. *Unity Journal*, *6*(1), pp.63-78.

Kienholz, C., Rich, J.L., Arendt, A.A. and Hock, R., 2014. A new method for deriving glacier centerlines applied to glaciers in Alaska and northwest Canada. *The Cryosphere*, *8*(2), pp.503-519.

King, O., Bhattacharya, A., Ghuffar, S., Tait, A., Guilford, S., Elmore, A.C. and Bolch, T., 2020. Six decades of glacier mass changes around Mt. Everest are revealed by historical and contemporary images. *One Earth*, *3*(5), pp.608-620.

Kulkarni, A.V. and Karyakarte, Y., 2014. Observed changes in Himalayan glaciers. *Current science*, pp.237-244.

Li, H. and Zhao, J., 2018. Evaluation of the newly released worldwide AW3D30 DEM over typical landforms of China using two global DEMs and ICESat/GLAS data. *IEEE Journal of Selected Topics in Applied Earth Observations and Remote Sensing*, *11*(11), pp.4430-4440.

Liebl, M., Robl, J., Egholm, D.L., Prasicek, G., Stüwe, K., Gradwohl, G. and Hergarten, S., 2021. Topographic signatures of progressive glacial landscape transformation. *Earth Surface Processes and Landforms*, *46*(10), pp.1964-1980.

Linsbauer, A., Frey, H., Haeberli, W., Machguth, H., Azam, M.F. and Allen, S., 2016. Modelling glacier-bed overdeepenings and possible future lakes for the glaciers in the Himalaya—Karakoram region. *Annals of Glaciology*, *57*(71), pp.119-130.

Linsbauer, A., Paul, F. and Haeberli, W., 2012. Modeling glacier thickness distribution and bed topography over entire mountain ranges with GlabTop: Application of a fast and robust approach. *Journal of Geophysical Research: Earth Surface*, *117*(F3).

Lloyd, C.T., Clark, C.D. and Swift, D.A., 2023. The effect of valley confluence and bedrock geology upon the location and depth of glacial overdeepenings. *Geografiska Annaler: Series A, Physical Geography*, *105*(2-3), pp.65-90.

Magnin, F., Haeberli, W., Linsbauer, A., Deline, P. and Ravanel, L., 2020. Estimating glacier-bed overdeepenings as possible sites of future lakes in the de-glaciating Mont Blanc massif (Western European Alps). *Geomorphology*, *350*, p.106913.

Magrani, F., Valla, P.G., Gribenski, N. and Serra, E., 2020. Glacial overdeepenings in the Swiss Alps and foreland: Spatial distribution and morphometrics. *Quaternary Science Reviews*, *243*, p.106483.

Majeed, U., Rashid, I., Najar, N.A. and Gul, N., 2021a. Spatiotemporal dynamics and geodetic mass changes of glaciers with varying debris cover in the Pangong Region of Trans-Himalayan Ladakh, India between 1990 and 2019. *Frontiers in Earth Science*, *9*, p.748107.

Majeed, U., Rashid, I., Sattar, A., Allen, S., Stoffel, M., Nüsser, M. and Schmidt, S., 2021b. Recession of Gya Glacier and the 2014 glacial lake outburst flood in the Trans-Himalayan region of Ladakh, India. *Science of the Total Environment*, *756*, p.144008.

Marzeion, B., Hofer, M., Jarosch, A.H., Kaser, G. and Mölg, T., 2012. A minimal model for reconstructing interannual mass balance variability of glaciers in the European Alps. *The Cryosphere*, *6*(1), pp.71-84.

Maussion, F., Butenko, A., Champollion, N., Dusch, M., Eis, J., Fourteau, K., Gregor, P., Jarosch, A.H., Landmann, J., Oesterle, F. and Recinos, B., 2019. The open global glacier model (OGGM) v1. 1. *Geoscientific Model Development*, *12*(3), pp.909-931.

Meier, M.F., Rasmussen, L.A., Krimmel, R.M., Olsen, R.W. and Frank, D., 1985. *Photogrammetric determination of surface altitude, terminus position, and ice velocity of Columbia Glacier, Alaska* (No. 1258-F).

Millan, R., Mouginot, J., Rabatel, A. and Morlighem, M., 2022. Ice velocity and thickness of the world's glaciers. *Nature Geoscience*, *15*(2), pp.124-129.

Moore, R.D., Fleming, S.W., Menounos, B., Wheate, R., Fountain, A., Stahl, K., Holm, K. and Jakob, M., 2009. Glacier change in western North America: influences on hydrology, geomorphic hazards and water quality. *Hydrological Processes: An International Journal*, *23*(1), pp.42-61.

Nye, J.F., 1965. The frequency response of glaciers. *Journal of Glaciology*, *5*(41), pp.567-587.

Otto, J.C., 2019. Proglacial lakes in high mountain environments. *Geomorphology of proglacial systems: landform and sediment dynamics in recently deglaciated alpine landscapes*, pp.231-247.

Otto, J.C., Helfricht, K., Prasicek, G., Binder, D. and Keuschnig, M., 2022. Testing the performance of ice thickness models to estimate the formation of potential future glacial lakes in Austria. *Earth Surface Processes and Landforms*, *47*(3), pp.723-741.

Pandey, P. and Venkataraman, G., 2013. Changes in the glaciers of Chandra–Bhaga basin, Himachal Himalaya, India, between 1980 and 2010 measured using remote sensing. *International Journal of Remote Sensing*, *34*(15), pp.5584-5597.

Pandit, A. and Ramsankaran, R.A.A.J., 2020. Identification of potential sites for future lake formation and expansion of existing lakes in glaciers of Chandra Basin, Western Himalayas, India. *Frontiers in Earth Science*, *8*, p.500116.

Parkes, D. and Goosse, H., 2020. Modelling regional glacier length changes over the last millennium using the Open Global Glacier Model. *The Cryosphere, 14(9),* pp.3135-3153.

Patterson, C.J., 1998. Laurentide glacial landscapes: the role of ice streams. *Geology*, *26*(7), pp.643-646.

Patton, H., Swift, D.A., Clark, C.D., Livingstone, S.J. and Cook, S.J., 2016. Distribution and characteristics of overdeepenings beneath the Greenland and Antarctic ice sheets: Implications for overdeepening origin and evolution. *Quaternary Science Reviews*, *148*, pp.128-145.

Paul, F. and Linsbauer, A., 2012. Modeling of glacier bed topography from glacier outlines, central branch lines, and a DEM. *International Journal of Geographical Information Science*, *26*(7), pp.1173-1190.

Paul, F., Rastner, P., Azzoni, R.S., Diolaiuti, G., Fugazza, D., Le Bris, R., Nemec, J., Rabatel, A., Ramusovic, M., Schwaizer, G. and Smiraglia, C., 2019. Glacier shrinkage in the Alps continues unabated as revealed by a new glacier inventory from Sentinel-2. *Earth System Science Data Discussions*, *2019*, pp.1-28.

Penk, A. and Brückner, E., 1909. Die alpen im Eiszeitalter. *Die Eiszeiten in den Südalpen und im Bereich der*.

Pfeffer, W.T., Arendt, A.A., Bliss, A., Bolch, T., Cogley, J.G., Gardner, A.S., Hagen, J.O., Hock, R., Kaser, G., Kienholz, C. and Miles, E.S., 2014. The Randolph Glacier Inventory: a globally complete inventory of glaciers. *Journal of glaciology*, *60*(221), pp.537-552.

Preusser, F., Reitner, J.M. and Schlüchter, C., 2010. Distribution, geometry, age and origin of overdeepened valleys and basins in the Alps and their foreland. *Swiss Journal of Geosciences*, *103*, pp.407-426.

Prothro, L.O., Simkins, L.M., Majewski, W. and Anderson, J.B., 2018. Glacial retreat patterns and processes determined from integrated sedimentology and geomorphology records. *Marine Geology*, *395*, pp.104-119.

Purdie, H., 2013. Glacier retreat and tourism: Insights from New Zealand. *Mountain Research and Development*, *33*(4), pp.463-472.

Rabatel, A., Francou, B., Soruco, A., Gomez, J., Cáceres, B., Ceballos, J.L., Basantes, R., Vuille, M., Sicart, J.E., Huggel, C. and Scheel, M., 2013. Current state of glaciers in the tropical Andes: a multi-century perspective on glacier evolution and climate change. *The Cryosphere*, *7*(1), pp.81-102.

Rabus, B., Eineder, M., Roth, A. and Bamler, R., 2003. The shuttle radar topography mission—a new class of digital elevation models acquired by spaceborne radar. *ISPRS journal of photogrammetry and remote sensing*, *57*(4), pp.241-262.

Ragettli, S., Bolch, T. and Pellicciotti, F., 2016. Heterogeneous glacier thinning patterns over the last 40 years in Langtang Himal, Nepal. *The Cryosphere*, *10*(5), pp.2075-2097.

Ramsankaran, R.A.A.J., Navinkumar, P.J., Dashora, A. and Kulkarni, A., 2020. UAV-based survey of Glaciers in Himalayas: opportunities and challenges. *Preprints*.

Ramsankaran, R.A.A.J., Pandit, A. and Azam, M.F., 2018. Spatially distributed ice-thickness modelling for Chhota Shigri Glacier in western Himalayas, India. *International Journal of Remote Sensing*, *39*(10), pp.3320-3343.

Rana, A.S., Kunmar, P., Mehta, M. and Kumar, V., 2023. Glacier retreat, dynamics and bed overdeepenings of Parkachik Glacier, Ladakh Himalaya, India. *Annals of Glaciology*, *64*(92), pp.254-267.

Rao, K.D., Rao, V.V., Dadhwal, V.K. and Diwakar, P.G., 2014. Kedarnath flash floods: a hydrological and hydraulic simulation study. *Current Science*, pp.598-603.

Rashid, I., Najar, N.A., Majeed, U. and Rasool, W., 2022. Ascertaining glacier dynamics and geodetic mass changes in the Pangong Region of Trans-Himalayan Ladakh using remote sensing data. *Data in Brief*, *42*, p.108176.

Raup, B., Racoviteanu, A., Khalsa, S.J.S., Helm, C., Armstrong, R. and Arnaud, Y., 2007. The GLIMS geospatial glacier database: A new tool for studying glacier change. *Global and Planetary Change*, *56*(1-2), pp.101-110.

Regmi, S. and Bookhagen, B., 2022. The spatial pattern of extreme precipitation from 40 years of gauge data in the central Himalaya. *Weather and Climate Extremes*, *37*, p.100470.

Riaz, S., Ali, A. and Baig, M.N., 2014. Increasing risk of glacial lake outburst floods as a consequence of climate change in the Himalayan region.

Rounce, D.R., Watson, C.S. and McKinney, D.C., 2017. Identification of hazard and risk for glacial lakes in the Nepal Himalaya using satellite imagery from 2000–2015. *Remote Sensing*, *9*(7), p.654.

Sattar, A., Cook, K.L., Rai, S.K., Berthier, E., Allen, S., Rinzin, S., Van Wyk de Vries, M., Haeberli, W., Kushwaha, P., Shugar, D.H. and Emmer, A., 2025. The Sikkim flood of October 2023: Drivers, causes and impacts of a multihazard cascade. *Science*, p.eads2659.

Sattar, A., Goswami, A., Kulkarni, A.V. and Das, P., 2019. Glacier-surface velocity derived ice volume and retreat assessment in the dhauliganga basin, central himalaya–A remote sensing and modeling based approach. *Frontiers in Earth Science*, *7*, p.105.

Schlunegger, F., Kissling, E., Bandou, D.T., Douillet, G.A., Mair, D., Marti, U., Reber, R., Schläfli, P. and Schwenk, M.A., 2024. The Aare main overdeepening on the northern margin of the European Alps: basins, riegels, and slot canyons. Earth Surface Dynamics, 12(6), pp.1371-1389.

Shruti, K. and Geetha Priya, M., 2025. Estimation of Ice Thickness and Glacier-Stored Water of the Teesta Basin, Eastern Himalayas, Sikkim, India. *Water Resources Management in Mountain Regions*, pp.237-255.

Shugar, D.H., Burr, A., Haritashya, U.K., Kargel, J.S., Watson, C.S., Kennedy, M.C., Bevington, A.R., Betts, R.A., Harrison, S. and Strattman, K., 2020. Rapid worldwide growth of glacial lakes since 1990. *Nature climate change*, *10*(10), pp.939-945.

Silverio Torres, W.C. and Jaquet, J.M., 2017. Evaluating glacier fluctuations in Cordillera Blanca (Peru) by remote sensing between 1987 and 2016 in the context of ENSO. *Arch Sci*, *69*, pp.145-162.

Sommer, C., Malz, P., Seehaus, T.C., Lippl, S., Zemp, M. and Braun, M.H., 2020. Rapid glacier retreat and downwasting throughout the European Alps in the early 21st century. *Nature communications*, *11*(1), p.3209.

Srinivasalu, P., Kulkarni, A.V., Remya, S.N., Shirsat, T. and Goswami, A., 2024. Himalayan glacier thickness mapper (HIGTHIM) tool: An automated approach to map potential glacier lakes and expansion of existing lakes. *Polar Science*, *39*, p.101008.

Strahler, A.N., 1957. Quantitative analysis of watershed geomorphology. *Eos, Transactions American Geophysical Union*, *38*(6), pp.913-920.

Swift, D.A., Cook, S.J., Graham, D.J., Midgley, N.G., Fallick, A.E., Storrar, R., Rodrigo, M.T. and Evans, D.J.A., 2018. Terminal zone glacial sediment transfer at a temperate overdeepened glacier system. *Quaternary Science Reviews*, *180*, pp.111-131.

Swift, D.A., Tallentire, G.D., Farinotti, D., Cook, S.J., Higson, W.J. and Bryant, R.G., 2021. The hydrology of glacier-bed overdeepenings: Sediment transport mechanics, drainage system morphology, and geomorphological implications. *Earth Surface Processes and Landforms*, *46*(11), pp.2264-2278.

Taylor, L.S., Quincey, D.J., Smith, M.W., Potter, E.R., Castro, J. and Fyffe, C.L., 2022. Multi-decadal glacier area and mass balance change in the Southern Peruvian Andes. *Frontiers in Earth Science*, *10*, p.863933.

Tweed, F.S. and Carrivick, J.L., 2015. Deglaciation and proglacial lakes. *Geology Today*, *31*(3), pp.96-102.

Veh, G., Korup, O. and Walz, A., 2020. Hazard from Himalayan glacier lake outburst floods. *Proceedings of the National Academy of Sciences*, *117*(2), pp.907-912.

Viani, C., Machguth, H., Huggel, C., Godio, A., Franco, D., Perotti, L. and Giardino, M., 2020. Potential future lakes from continued glacier shrinkage in the Aosta Valley Region (Western Alps, Italy). *Geomorphology*, *355*, p.107068.

Vilca, O., Mergili, M., Emmer, A., Frey, H. and Huggel, C., 2021. The 2020 glacial lake outburst flood process chain at Lake Salkantaycocha (Cordillera Vilcabamba, Peru). *Landslides*, *18*, pp.2211-2223.

Vilímek, V., Klimeš, J., Emmer, A. and Novotný, J., 2014. Natural hazards in the Cordillera Blanca of Peru during the time of global climate change. In *Landslide Science for a Safer Geoenvironment: Vol. 1: The International Programme on Landslides (IPL)* (pp. 261-266). Springer International Publishing.

Vincent, C., Peyaud, V., Laarman, O., Six, D., Gilbert, A., Gillet-Chaulet, F., Berthier, É., Morin, S., Verfaillie, D., Rabatel, A. and Jourdain, B., 2019. Decline of the two largest glaciers in the French Alps during the 21st century: Argentière and Mer de Glace. *La Météorologie* , (106), pp.49-58.

Vuille, M., Carey, M., Huggel, C., Buytaert, W., Rabatel, A., Jacobsen, D., Soruco, A., Villacis, M., Yarleque, C., Timm, O.E. and Condom, T., 2018. Rapid decline of snow and ice in the tropical Andes–Impacts, uncertainties and challenges ahead. *Earth-science reviews*, *176*, pp.195-213.

Westoby, M.J., Glasser, N.F., Brasington, J., Hambrey, M.J., Quincey, D.J. and Reynolds, J.M., 2014. Modelling outburst floods from moraine-dammed glacial lakes. *Earth-Science Reviews*, *134*, pp.137-159.

Yang, Y., Li, Z., Huang, L., Tian, B. and Chen, Q., 2016. Extraction of glacier outlines and water-eroded stripes using high-resolution SAR imagery. *International Journal of Remote Sensing*, *37*(5), pp.1016-1034.

Yao, T., Thompson, L.G., Mosbrugger, V., Zhang, F., Ma, Y., Luo, T., Xu, B., Yang, X., Joswiak, D.R., Wang, W. and Joswiak, M.E., 2012. Third pole environment (TPE). Environmental Development, 3, pp.52-64.

Zemp, M., 2006. *Glaciers and climate change: spatio-temporal analysis of glacier fluctuations in the European Alps after 1850* (Doctoral dissertation, University of Zurich).

Zemp, M., Huss, M., Thibert, E., Eckert, N., McNabb, R., Huber, J., Barandun, M., Machguth, H., Nussbaumer, S.U., Gärtner-Roer, I. and Thomson, L., 2019. Global glacier mass changes and their contributions to sea-level rise from 1961 to 2016. *Nature*, *568*(7752), pp.382-386.

Zhang, G., Bolch, T., Allen, S., Linsbauer, A., Chen, W. and Wang, W., 2019. Glacial lake evolution and glacier–lake interactions in the Poiqu River basin, central Himalaya, 1964–2017. *Journal of Glaciology*, *65*(251), pp.347-365.

Zhang, S., Zhao, H., Sheng, Y., Zhang, J., Zhang, J., Sun, A., Wang, L., Huang, L., Hou, J. and Chen, F., 2022. Mega-lakes in the northwestern Tibetan Plateau formed by melting glaciers during the last deglacial. *Quaternary Science Reviews*, *285*, p.107528.

Zheng, W., 2021. Glacier geometry and flow speed determine how Arctic marine-terminating glaciers respond to lubricated beds. *The Cryosphere Discussions*, *2021*, pp.1-23.

Zorzut, V., Ruiz, L., Rivera, A., Pitte, P., Villalba, R. and Medrzycka, D., 2020. Slope estimation influences on ice thickness inversion models: a case study for Monte Tronador glaciers, North Patagonian Andes. *Journal of Glaciology*, *66*(260), pp.996-1005.

APPENDIX A

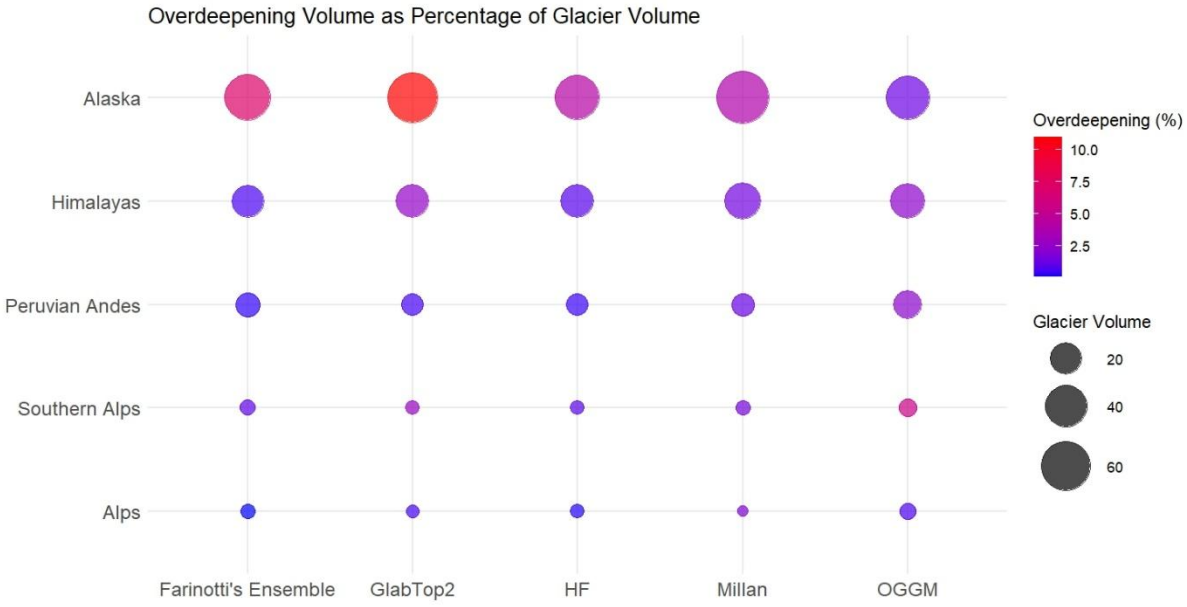
Overdeepening Volume as Percentage of Glacier Volume
Alaska
Himalayas
Peruvian Andes
Southern Alps
Alps
Farinotti's Ensemble
GlabTop2
HF
Millan
OGGM
Overdeepening (%)
10.0
7.5
5.0
2.5
Glacier Volume
20
40
60

APPENDIX B

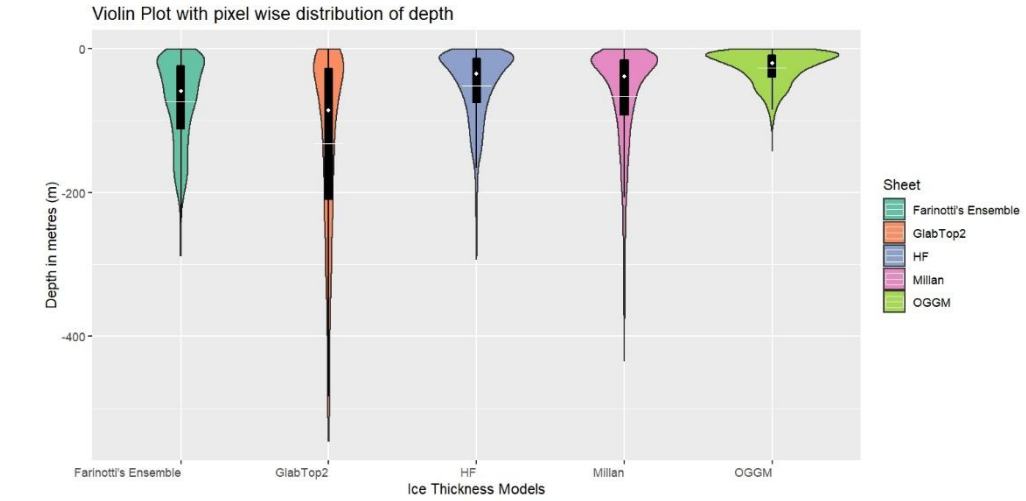

Alaska

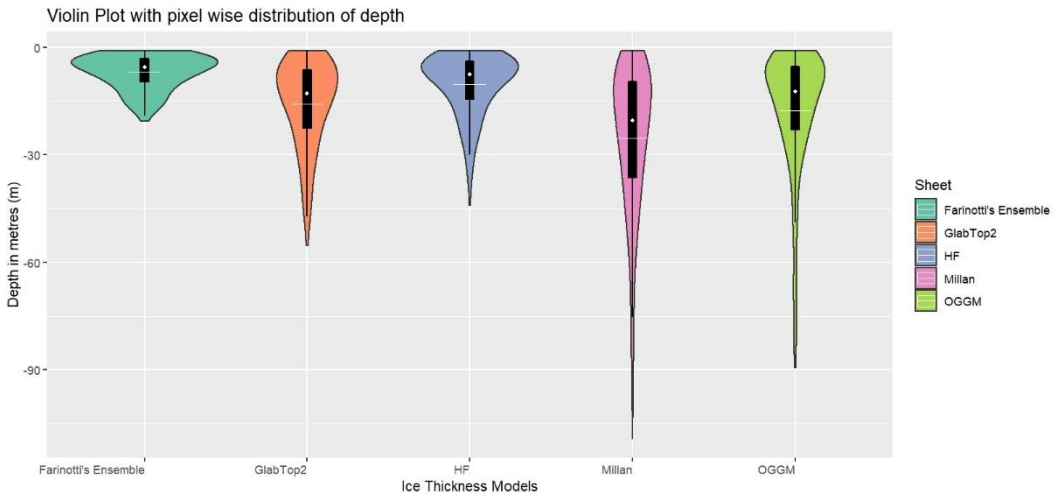

European Alps

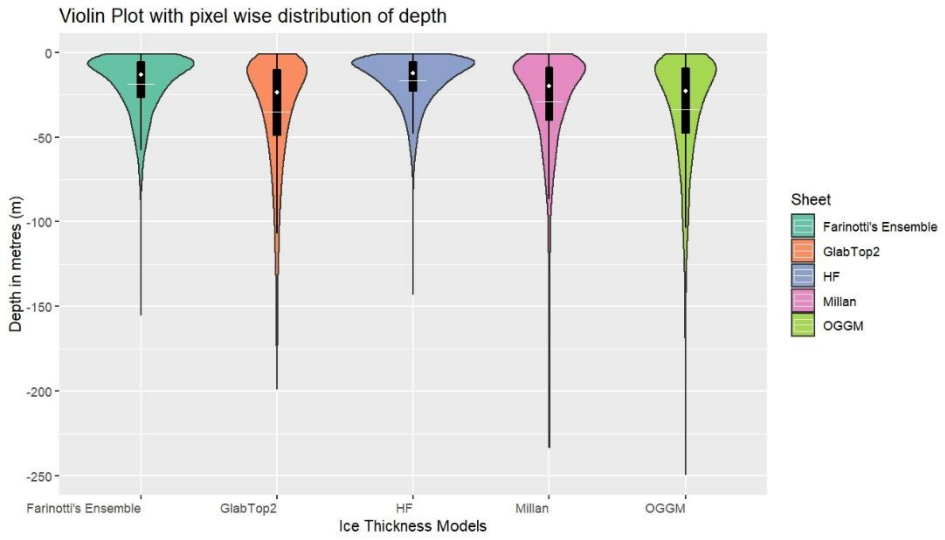

Himalayas

Nb: The violin plots represent the distribution of pixel depth of overdeepenings with the white dot representing the median whereas the line represents the mean of the pixel depths

APPENDIX C

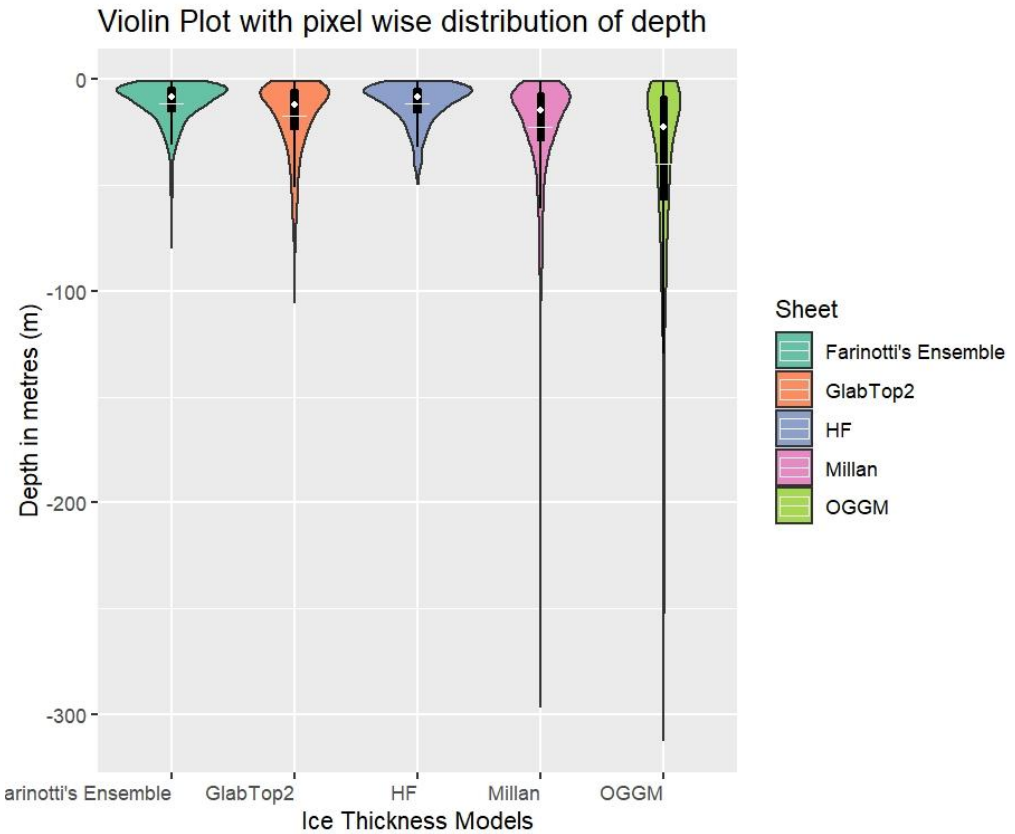

Peruvian Andes

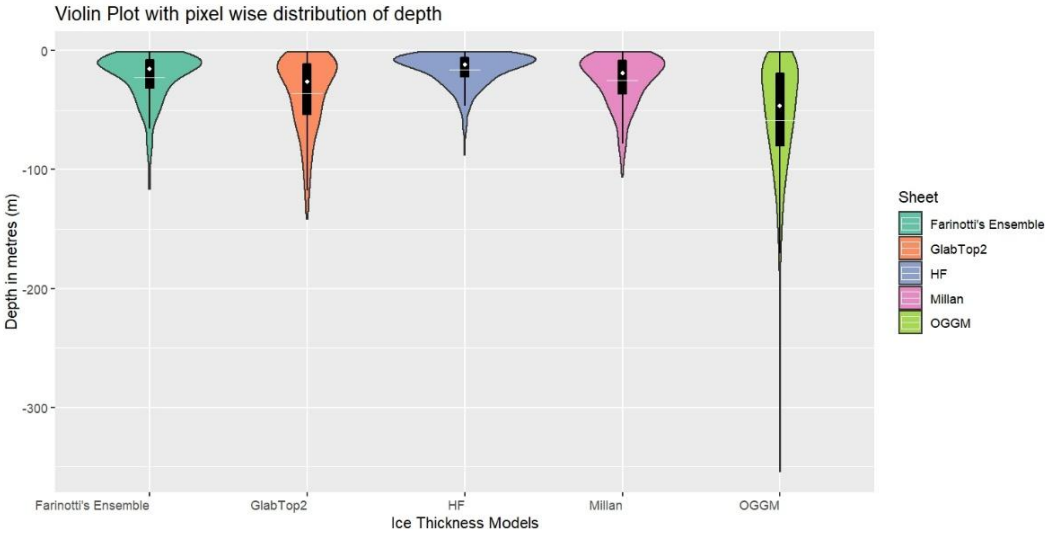

New Zealand Southern Alps

APPENDIX D

Value for boxplots for area of the overdeepenings (in m^2)

	Region	Model	Median	Mean
	<fct>	<fct>	<dbl>	<dbl>
1	Alaska	Farinottis' Ensemble	24985.	375944.
2	Alaska	GlabTop2	41226.	343766.
3	Alaska	HF	23736.	174885.
4	Alaska	Millan	17490.	100590.
5	Alaska	OGGM	22487.	185104.
6	Alps	Farinottis' Ensemble	29999.	39281.
7	Alps	GlabTop2	39999.	62201.
8	Alps	HF	21249.	30335.
9	Alps	Millan	14999.	34122.
10	Alps	OGGM	34999.	64385.
11	Himalayas	Farinottis' Ensemble	22500.	70480.
12	Himalayas	GlabTop2	28750.	110363.
13	Himalayas	HF	25000.	59824.
14	Himalayas	Millan	22500.	49936.
15	Himalayas	OGGM	40000.	108292.
16	Peruvian Andes	Farinottis' Ensemble	19994.	37804.
17	Peruvian Andes	GlabTop2	17494.	39045.
18	Peruvian Andes	HF	21243.	32518.
19	Peruvian Andes	Millan	19994.	42156.
20	Peruvian Andes	OGGM	24992.	84667.
21	Southern Alps	Farinottis' Ensemble	36143.	116262.
22	Southern Alps	GlabTop2	17448.	118595.
23	Southern Alps	HF	34896.	64703.
24	Southern Alps	Millan	23680.	64724.
25	Southern Alps	OGGM	33650.	225579.

APPENDIX E

Variance in different volume and area of the overdeepenings

	Region	Model	Volume_Variance	Area_Variance
	<chr>	<chr>	<dbl>	<dbl>
1	Alaska	Farinotti's Ensemble	2.18e16	2.46e12
2	Alaska	GlabTop2	4.05e16	1.02e12
3	Alaska	HF	3.75e15	6.32e11
4	Alaska	Millan	4.82e15	4.99e11
5	Alaska	OGGM	8.33e14	6.93e11
6	Alps	Farinotti's Ensemble	8.82e10	8.10e 8
7	Alps	GlabTop2	2.63e12	4.94e 9
8	Alps	HF	2.16e11	9.15e 8
9	Alps	Millan	3.28e12	2.41e 9
10	Alps	OGGM	4.96e12	3.63e 9
11	Himalayas	Farinotti's Ensemble	1.20e13	1.70e10
12	Himalayas	GlabTop2	1.52e14	4.59e10
13	Himalayas	HF	5.62e12	1.01e10
14	Himalayas	Millan	1.22e13	7.65e 9
15	Himalayas	OGGM	1.08e14	3.57e10
16	Peruvian Andes	Farinotti's Ensemble	4.78e11	1.73e 9
17	Peruvian Andes	GlabTop2	2.81e12	2.58e 9
18	Peruvian Andes	HF	6.06e11	1.68e 9
19	Peruvian Andes	Millan	3.31e12	3.30e 9
20	Peruvian Andes	OGGM	2.05e14	4.13e10
21	Southern Alps	Farinotti's Ensemble	2.48e13	3.67e10
22	Southern Alps	GlabTop2	2.52e14	1.06e11
23	Southern Alps	HF	6.13e12	1.08e10
24	Southern Alps	Millan	2.27e13	1.76e10
25	Southern Alps	OGGM	1.15e15	2.40e11

p-value for ANOVA test of area and volume of overdeepenings across regions

	Region	Volume_p_value	Area_p_value
1	Alaska	9.074045e-04	1.144949e-02
2	Alps	3.298525e-01	5.767190e-02
3	Himalayas	8.485426e-05	1.269341e-05
4	Peruvian Andes	1.851389e-02	4.984693e-03
5	Southern Alps	8.900406e-02	3.069962e-01

APPENDIX F

Region	Model	Volume (in cu m)	Area (in sq m)
Alaska	Farinotti's Ensemble	20702.7558	9994.0762
Alaska	Farinotti's Ensemble	25059.4569	9994.0762
Alaska	Farinotti's Ensemble	27613.0276	9994.0762
Alaska	Farinotti's Ensemble	28046.4255	9994.0762
Alaska	Farinotti's Ensemble	28765.9087	9994.0762
Alaska	Farinotti's Ensemble	33032.4838	9994.0762
Alaska	Farinotti's Ensemble	35981.7854	9994.0762
Alaska	Farinotti's Ensemble	40443.5573	9994.0762
Alaska	Farinotti's Ensemble	41001.0882	9994.0762
Alaska	Farinotti's Ensemble	41594.3035	9994.0762
Alaska	Farinotti's Ensemble	42072.5356	9994.0762
Alaska	Farinotti's Ensemble	42946.6513	9994.0762
Alaska	Farinotti's Ensemble	57033.7605	9994.0762
Alaska	Farinotti's Ensemble	66287.4614	9994.0762
Alaska	Farinotti's Ensemble	66303.4736	9994.0762
Alaska	Farinotti's Ensemble	75889.4665	9994.0762
Alaska	Farinotti's Ensemble	77756.7984	9994.0762
Alaska	Farinotti's Ensemble	83902.6002	9994.0762
Alaska	Farinotti's Ensemble	84078.8873	9994.0762
Alaska	Farinotti's Ensemble	105236.0857	9994.0762
Alaska	Farinotti's Ensemble	112046.6241	9994.0762
Alaska	Farinotti's Ensemble	139397.0509	9994.0762
Alaska	Farinotti's Ensemble	174064.6129	9994.0762
Alaska	Farinotti's Ensemble	287042.0817	9994.0762
Alaska	Farinotti's Ensemble	19688.3424	12492.595
Alaska	Farinotti's Ensemble	35352.5807	12492.595
Alaska	Farinotti's Ensemble	48876.3641	12492.595
Alaska	Farinotti's Ensemble	64929.4711	12492.595
Alaska	Farinotti's Ensemble	68313.0857	12492.595
Alaska	Farinotti's Ensemble	69007.2543	12492.595
Alaska	Farinotti's Ensemble	77199.4201	12492.595
Alaska	Farinotti's Ensemble	80694.0528	12492.595
Alaska	Farinotti's Ensemble	82486.5084	12492.595
Alaska	Farinotti's Ensemble	95377.1222	12492.595
Alaska	Farinotti's Ensemble	119148.4327	12492.595
Alaska	Farinotti's Ensemble	119633.3748	12492.595
Alaska	Farinotti's Ensemble	120150.3413	12492.595
Alaska	Farinotti's Ensemble	144479.1827	12492.595
Alaska	Farinotti's Ensemble	157601.2877	12492.595
Alaska	Farinotti's Ensemble	38914.3124	14991.114
Alaska	Farinotti's Ensemble	40452.0972	14991.114
Alaska	Farinotti's Ensemble	71969.3658	14991.114

Alaska	Farinotti's Ensemble	94437.1276	14991.114
Alaska	Farinotti's Ensemble	99656.5071	14991.114
Alaska	Farinotti's Ensemble	111309.4512	14991.114
Alaska	Farinotti's Ensemble	139447.6801	14991.114
Alaska	Farinotti's Ensemble	230718.3496	14991.114
Alaska	Farinotti's Ensemble	252071.6597	14991.114
Alaska	Farinotti's Ensemble	62722.8323	17489.633
Alaska	Farinotti's Ensemble	68075.7996	17489.633
Alaska	Farinotti's Ensemble	82077.8151	17489.633
Alaska	Farinotti's Ensemble	102945.5732	17489.633
Alaska	Farinotti's Ensemble	115705.0391	17489.633
Alaska	Farinotti's Ensemble	142084.0569	17489.633
Alaska	Farinotti's Ensemble	187380.0847	17489.633
Alaska	Farinotti's Ensemble	278758.1125	17489.633
Alaska	Farinotti's Ensemble	47394.6984	19988.153
Alaska	Farinotti's Ensemble	49509.5338	19988.153
Alaska	Farinotti's Ensemble	148610.34	19988.153
Alaska	Farinotti's Ensemble	254880.6637	19988.153
Alaska	Farinotti's Ensemble	386205.7169	19988.153
Alaska	Farinotti's Ensemble	420859.8591	19988.153
Alaska	Farinotti's Ensemble	59643.2977	22486.672
Alaska	Farinotti's Ensemble	195762.8724	22486.672
Alaska	Farinotti's Ensemble	264498.9861	22486.672
Alaska	Farinotti's Ensemble	69700.2029	24985.191
Alaska	Farinotti's Ensemble	71950.4561	24985.191
Alaska	Farinotti's Ensemble	95762.3309	24985.191
Alaska	Farinotti's Ensemble	207671.7072	24985.191
Alaska	Farinotti's Ensemble	75528.0475	27483.71
Alaska	Farinotti's Ensemble	268155.5712	27483.71
Alaska	Farinotti's Ensemble	88340.8875	29982.229
Alaska	Farinotti's Ensemble	471374.9614	29982.229
Alaska	Farinotti's Ensemble	139546.8035	32480.748
Alaska	Farinotti's Ensemble	400873.5366	34979.267
Alaska	Farinotti's Ensemble	206624.3544	37477.786
Alaska	Farinotti's Ensemble	257203.2007	37477.786
Alaska	Farinotti's Ensemble	359136.8004	37477.786
Alaska	Farinotti's Ensemble	342920.2162	39976.305
Alaska	Farinotti's Ensemble	1077676.052	39976.305
Alaska	Farinotti's Ensemble	255420.1999	42474.824
Alaska	Farinotti's Ensemble	275700.2326	42474.824
Alaska	Farinotti's Ensemble	323477.6997	42474.824
Alaska	Farinotti's Ensemble	479761.409	42474.824
Alaska	Farinotti's Ensemble	279554.7594	44973.343
Alaska	Farinotti's Ensemble	641807.9988	44973.343
Alaska	Farinotti's Ensemble	177279.1077	49970.381
Alaska	Farinotti's Ensemble	270856.6069	49970.381

Alaska	Farinotti's Ensemble	655889.3131	49970.381
Alaska	Farinotti's Ensemble	1254096.141	49970.381
Alaska	Farinotti's Ensemble	911985.9919	54967.419
Alaska	Farinotti's Ensemble	499972.8178	62462.977
Alaska	Farinotti's Ensemble	1252102.084	67460.015
Alaska	Farinotti's Ensemble	796940.0469	72457.053
Alaska	Farinotti's Ensemble	946310.7394	72457.053
Alaska	Farinotti's Ensemble	1468123.182	72457.053
Alaska	Farinotti's Ensemble	476041.6899	77454.091
Alaska	Farinotti's Ensemble	821706.8611	87448.167
Alaska	Farinotti's Ensemble	593142.9962	94943.724
Alaska	Farinotti's Ensemble	650533.2958	99940.762
Alaska	Farinotti's Ensemble	1382114.744	107436.32
Alaska	Farinotti's Ensemble	1186497.354	109934.84
Alaska	Farinotti's Ensemble	2289063.133	112433.36
Alaska	Farinotti's Ensemble	1283527.854	127424.47
Alaska	Farinotti's Ensemble	2230989.95	129922.99
Alaska	Farinotti's Ensemble	1367834.878	139917.07
Alaska	Farinotti's Ensemble	1629187.84	142415.59
Alaska	Farinotti's Ensemble	4054933.264	142415.59
Alaska	Farinotti's Ensemble	4112528.978	147412.62
Alaska	Farinotti's Ensemble	1517417.847	149911.14
Alaska	Farinotti's Ensemble	1199530.4	157406.7
Alaska	Farinotti's Ensemble	2257641.023	157406.7
Alaska	Farinotti's Ensemble	1342746.599	167400.78
Alaska	Farinotti's Ensemble	1714938.863	167400.78
Alaska	Farinotti's Ensemble	2472218.732	242356.35
Alaska	Farinotti's Ensemble	4851749.025	257347.46
Alaska	Farinotti's Ensemble	6322811.291	289828.21
Alaska	Farinotti's Ensemble	6251043.07	294825.25
Alaska	Farinotti's Ensemble	9267353.977	312314.88
Alaska	Farinotti's Ensemble	5892090.181	332303.04
Alaska	Farinotti's Ensemble	9230973.563	379774.9
Alaska	Farinotti's Ensemble	7775309.274	407258.61
Alaska	Farinotti's Ensemble	10219098.2	447234.91
Alaska	Farinotti's Ensemble	8001102.565	454730.47
Alaska	Farinotti's Ensemble	35064320.05	592149.02
Alaska	Farinotti's Ensemble	11731343.03	707080.89
Alaska	Farinotti's Ensemble	20471921.53	861989.08
Alaska	Farinotti's Ensemble	110682238.7	1791438.2
Alaska	Farinotti's Ensemble	133380255.9	1796435.2
Alaska	Farinotti's Ensemble	136013258.6	1973830.1
Alaska	Farinotti's Ensemble	98521903.12	2258661.2
Alaska	Farinotti's Ensemble	255383278.7	2498519.1
Alaska	Farinotti's Ensemble	418408277.2	6718517.8
Alaska	Farinotti's Ensemble	1201792412	11475698

Alaska	Farinotti's Ensemble	1131865190	12115319
Alaska	GlabTop2	22388.7682	9994.0762
Alaska	GlabTop2	23463.5705	9994.0762
Alaska	GlabTop2	43451.113	9994.0762
Alaska	GlabTop2	47936.9795	9994.0762
Alaska	GlabTop2	51862.5702	9994.0762
Alaska	GlabTop2	53734.6295	9994.0762
Alaska	GlabTop2	55523.1202	9994.0762
Alaska	GlabTop2	61815.3196	9994.0762
Alaska	GlabTop2	64108.8821	9994.0762
Alaska	GlabTop2	75026.0257	9994.0762
Alaska	GlabTop2	104332.3855	9994.0762
Alaska	GlabTop2	112816.279	9994.0762
Alaska	GlabTop2	114771.1444	9994.0762
Alaska	GlabTop2	123706.888	9994.0762
Alaska	GlabTop2	143957.0312	9994.0762
Alaska	GlabTop2	270456.1485	9994.0762
Alaska	GlabTop2	22417.4377	12492.595
Alaska	GlabTop2	23173.2153	12492.595
Alaska	GlabTop2	28153.4787	12492.595
Alaska	GlabTop2	31422.1101	12492.595
Alaska	GlabTop2	32011.208	12492.595
Alaska	GlabTop2	32795.9601	12492.595
Alaska	GlabTop2	32985.2095	12492.595
Alaska	GlabTop2	34595.5831	12492.595
Alaska	GlabTop2	39294.3362	12492.595
Alaska	GlabTop2	52734.2459	12492.595
Alaska	GlabTop2	59386.7969	12492.595
Alaska	GlabTop2	69573.63	12492.595
Alaska	GlabTop2	72891.0607	12492.595
Alaska	GlabTop2	103161.2047	12492.595
Alaska	GlabTop2	104075.2747	12492.595
Alaska	GlabTop2	126566.8262	12492.595
Alaska	GlabTop2	135350.0723	12492.595
Alaska	GlabTop2	33319.789	14991.114
Alaska	GlabTop2	39981.7949	14991.114
Alaska	GlabTop2	77873.459	14991.114
Alaska	GlabTop2	79537.8168	14991.114
Alaska	GlabTop2	86559.7167	14991.114
Alaska	GlabTop2	87268.2201	14991.114
Alaska	GlabTop2	220454.0478	14991.114
Alaska	GlabTop2	336419.4002	14991.114
Alaska	GlabTop2	74918.3624	17489.633
Alaska	GlabTop2	83305.42	17489.633
Alaska	GlabTop2	86442.5986	17489.633
Alaska	GlabTop2	88685.5319	17489.633

Alaska	GlabTop2	89075.9255	17489.633
Alaska	GlabTop2	99590.3232	17489.633
Alaska	GlabTop2	65806.3317	19988.153
Alaska	GlabTop2	179989.1408	19988.153
Alaska	GlabTop2	389767.906	19988.153
Alaska	GlabTop2	486621.6616	19988.153
Alaska	GlabTop2	73316.2237	22486.672
Alaska	GlabTop2	120319.6135	22486.672
Alaska	GlabTop2	209766.4129	22486.672
Alaska	GlabTop2	257805.8708	22486.672
Alaska	GlabTop2	296826.6264	22486.672
Alaska	GlabTop2	120781.071	24985.191
Alaska	GlabTop2	172701.2852	27483.71
Alaska	GlabTop2	296194.6768	29982.229
Alaska	GlabTop2	642636.3652	29982.229
Alaska	GlabTop2	659483.6792	29982.229
Alaska	GlabTop2	107960.606	32480.748
Alaska	GlabTop2	155319.0101	32480.748
Alaska	GlabTop2	196783.6906	32480.748
Alaska	GlabTop2	317389.6945	32480.748
Alaska	GlabTop2	116761.8468	34979.267
Alaska	GlabTop2	160686.3121	34979.267
Alaska	GlabTop2	204762.2074	34979.267
Alaska	GlabTop2	213007.2898	34979.267
Alaska	GlabTop2	233644.4717	34979.267
Alaska	GlabTop2	177071.8636	37477.786
Alaska	GlabTop2	306362.4477	37477.786
Alaska	GlabTop2	121567.9581	39976.305
Alaska	GlabTop2	479992.9002	39976.305
Alaska	GlabTop2	473367.1887	42474.824
Alaska	GlabTop2	774911.1729	42474.824
Alaska	GlabTop2	471212.0941	44973.343
Alaska	GlabTop2	275371.143	47471.862
Alaska	GlabTop2	466773.0443	47471.862
Alaska	GlabTop2	861850.3033	47471.862
Alaska	GlabTop2	388372.0964	49970.381
Alaska	GlabTop2	419545.0256	49970.381
Alaska	GlabTop2	480720.0083	49970.381
Alaska	GlabTop2	1356741.904	52468.9
Alaska	GlabTop2	1442646.797	52468.9
Alaska	GlabTop2	263308.2856	54967.419
Alaska	GlabTop2	352150.5849	57465.938
Alaska	GlabTop2	745602.9831	57465.938
Alaska	GlabTop2	699646.3361	59964.458
Alaska	GlabTop2	379457.3975	62462.977
Alaska	GlabTop2	511651.6864	64961.496

Alaska	GlabTop2	989331.1995	64961.496
Alaska	GlabTop2	1076694.426	69958.534
Alaska	GlabTop2	923914.3464	72457.053
Alaska	GlabTop2	1556919.579	77454.091
Alaska	GlabTop2	1706627.901	77454.091
Alaska	GlabTop2	1417645.442	82451.129
Alaska	GlabTop2	1185686.677	97442.243
Alaska	GlabTop2	852705.0282	102439.28
Alaska	GlabTop2	848853.5513	109934.84
Alaska	GlabTop2	3317261.066	109934.84
Alaska	GlabTop2	1305312.885	124925.95
Alaska	GlabTop2	1407064.86	132421.51
Alaska	GlabTop2	1377709.701	142415.59
Alaska	GlabTop2	2697422.467	147412.62
Alaska	GlabTop2	1316365.751	157406.7
Alaska	GlabTop2	8208755.667	159905.22
Alaska	GlabTop2	3443305.893	172397.82
Alaska	GlabTop2	2179010.871	182391.89
Alaska	GlabTop2	4968475.645	187388.93
Alaska	GlabTop2	3615039.887	189887.45
Alaska	GlabTop2	7065474.275	194884.49
Alaska	GlabTop2	3289533.513	214872.64
Alaska	GlabTop2	2295296.621	227365.23
Alaska	GlabTop2	2383739.377	229863.75
Alaska	GlabTop2	4788277.43	254848.94
Alaska	GlabTop2	7082682.093	257347.46
Alaska	GlabTop2	9332786.385	277335.62
Alaska	GlabTop2	6418431.952	294825.25
Alaska	GlabTop2	15749231.14	294825.25
Alaska	GlabTop2	9476325.725	312314.88
Alaska	GlabTop2	14872944.05	334801.55
Alaska	GlabTop2	9234541.09	344795.63
Alaska	GlabTop2	12100858.66	374777.86
Alaska	GlabTop2	8735565.91	379774.9
Alaska	GlabTop2	12597910.08	382273.42
Alaska	GlabTop2	32190906.01	387270.45
Alaska	GlabTop2	46231447.48	397264.53
Alaska	GlabTop2	12122097.14	482214.18
Alaska	GlabTop2	18355773.79	492208.26
Alaska	GlabTop2	15749878.19	494706.77
Alaska	GlabTop2	12110941.03	509697.89
Alaska	GlabTop2	19061285.64	544677.16
Alaska	GlabTop2	46743728.6	667104.59
Alaska	GlabTop2	47350025.5	794529.06
Alaska	GlabTop2	58669771.98	799526.1
Alaska	GlabTop2	120384977.6	1259253.6

Alaska	GlabTop2	117591028.2	1369188.4
Alaska	GlabTop2	351818341.5	1616541.8
Alaska	GlabTop2	373253988.8	1619040.4
Alaska	GlabTop2	381241819.8	1634031.5
Alaska	GlabTop2	485284229.7	2013806.4
Alaska	GlabTop2	406983216	2403575.3
Alaska	GlabTop2	401346870.8	2965742.1
Alaska	GlabTop2	358523942.7	3467944.5
Alaska	GlabTop2	414240686.8	3517914.8
Alaska	GlabTop2	978603804.1	5531721.2
Alaska	GlabTop2	2001663636	8797285.6
Alaska	HF	17384.7151	9994.0762
Alaska	HF	23789.9152	9994.0762
Alaska	HF	26179.551	9994.0762
Alaska	HF	32063.9721	9994.0762
Alaska	HF	39603.6011	9994.0762
Alaska	HF	48452.1161	9994.0762
Alaska	HF	52925.4778	9994.0762
Alaska	HF	55132.4216	9994.0762
Alaska	HF	55213.2453	9994.0762
Alaska	HF	56076.3812	9994.0762
Alaska	HF	56638.487	9994.0762
Alaska	HF	58246.7256	9994.0762
Alaska	HF	58652.369	9994.0762
Alaska	HF	62852.1501	9994.0762
Alaska	HF	63817.7643	9994.0762
Alaska	HF	68284.7211	9994.0762
Alaska	HF	71049.1958	9994.0762
Alaska	HF	80795.0062	9994.0762
Alaska	HF	86376.4147	9994.0762
Alaska	HF	86791.8179	9994.0762
Alaska	HF	89078.9754	9994.0762
Alaska	HF	92141.1252	9994.0762
Alaska	HF	112548.6459	9994.0762
Alaska	HF	113525.2399	9994.0762
Alaska	HF	123805.0964	9994.0762
Alaska	HF	123860.3005	9994.0762
Alaska	HF	149379.5374	9994.0762
Alaska	HF	150195.094	9994.0762
Alaska	HF	155283.3256	9994.0762
Alaska	HF	158498.888	9994.0762
Alaska	HF	181746.217	9994.0762
Alaska	HF	213673.0939	9994.0762
Alaska	HF	234747.3336	9994.0762
Alaska	HF	473170.162	9994.0762
Alaska	HF	23386.4068	12492.595

Alaska	HF	27535.8638	12492.595
Alaska	HF	31504.4588	12492.595
Alaska	HF	32228.5169	12492.595
Alaska	HF	32488.0677	12492.595
Alaska	HF	34810.6046	12492.595
Alaska	HF	35399.855	12492.595
Alaska	HF	35418.1547	12492.595
Alaska	HF	36766.8426	12492.595
Alaska	HF	41278.9386	12492.595
Alaska	HF	53127.3845	12492.595
Alaska	HF	54991.8189	12492.595
Alaska	HF	56272.798	12492.595
Alaska	HF	60363.6959	12492.595
Alaska	HF	74819.5441	12492.595
Alaska	HF	81823.4493	12492.595
Alaska	HF	84388.1523	12492.595
Alaska	HF	104781.6431	12492.595
Alaska	HF	108340.6298	12492.595
Alaska	HF	114246.553	12492.595
Alaska	HF	116628.869	12492.595
Alaska	HF	153829.7195	12492.595
Alaska	HF	165347.2457	12492.595
Alaska	HF	166073.4388	12492.595
Alaska	HF	167600.8538	12492.595
Alaska	HF	211601.5678	12492.595
Alaska	HF	288305.981	12492.595
Alaska	HF	312659.832	12492.595
Alaska	HF	533374.9555	12492.595
Alaska	HF	50697.1843	14991.114
Alaska	HF	55345.3082	14991.114
Alaska	HF	72247.2162	14991.114
Alaska	HF	72341.7647	14991.114
Alaska	HF	77025.5729	14991.114
Alaska	HF	112813.9915	14991.114
Alaska	HF	118805.0083	14991.114
Alaska	HF	121398.9908	14991.114
Alaska	HF	148187.4644	14991.114
Alaska	HF	162073.4294	14991.114
Alaska	HF	188065.7135	14991.114
Alaska	HF	207473.7655	14991.114
Alaska	HF	208784.329	14991.114
Alaska	HF	243884.9839	14991.114
Alaska	HF	304363.9679	14991.114
Alaska	HF	306510.5227	14991.114
Alaska	HF	404742.3982	14991.114
Alaska	HF	70543.8191	17489.633

Alaska	HF	72959.6845	17489.633
Alaska	HF	74679.8563	17489.633
Alaska	HF	80959.3985	17489.633
Alaska	HF	89079.8904	17489.633
Alaska	HF	89391.9003	17489.633
Alaska	HF	105073.5233	17489.633
Alaska	HF	146699.5463	17489.633
Alaska	HF	189579.7087	17489.633
Alaska	HF	227699.2041	17489.633
Alaska	HF	276565.8084	17489.633
Alaska	HF	287791.1495	17489.633
Alaska	HF	307967.1789	17489.633
Alaska	HF	530546.7368	17489.633
Alaska	HF	889626.5032	17489.633
Alaska	HF	50817.3523	19988.153
Alaska	HF	62090.5776	19988.153
Alaska	HF	98022.3439	19988.153
Alaska	HF	114881.5526	19988.153
Alaska	HF	183759.489	19988.153
Alaska	HF	191712.5387	19988.153
Alaska	HF	337685.5869	19988.153
Alaska	HF	769694.5383	19988.153
Alaska	HF	61347.9148	22486.672
Alaska	HF	77384.857	22486.672
Alaska	HF	156532.1277	22486.672
Alaska	HF	168737.8752	22486.672
Alaska	HF	171002.4631	22486.672
Alaska	HF	188116.0377	22486.672
Alaska	HF	236412.3013	22486.672
Alaska	HF	164590.8581	24985.191
Alaska	HF	183867.7623	24985.191
Alaska	HF	224119.1727	24985.191
Alaska	HF	231194.4468	24985.191
Alaska	HF	396600.8616	24985.191
Alaska	HF	411128.841	24985.191
Alaska	HF	435544.1485	24985.191
Alaska	HF	437110.6028	24985.191
Alaska	HF	546578.4942	24985.191
Alaska	HF	1275141.711	24985.191
Alaska	HF	90461.8228	27483.71
Alaska	HF	176858.0621	27483.71
Alaska	HF	204417.4106	27483.71
Alaska	HF	535174.731	27483.71
Alaska	HF	83217.2765	29982.229
Alaska	HF	145397.9801	29982.229
Alaska	HF	222528.0138	29982.229

Alaska	HF	238491.7572	29982.229
Alaska	HF	516511.1718	29982.229
Alaska	HF	1118657.621	29982.229
Alaska	HF	92102.2384	32480.748
Alaska	HF	440385.9442	32480.748
Alaska	HF	359545.1888	34979.267
Alaska	HF	373826.5797	34979.267
Alaska	HF	388573.3931	34979.267
Alaska	HF	418914.296	34979.267
Alaska	HF	497049.7457	34979.267
Alaska	HF	549214.871	34979.267
Alaska	HF	155784.4324	37477.786
Alaska	HF	355675.7172	37477.786
Alaska	HF	224283.2601	39976.305
Alaska	HF	382160.2632	39976.305
Alaska	HF	611107.8118	39976.305
Alaska	HF	818367.1658	39976.305
Alaska	HF	965217.6846	39976.305
Alaska	HF	274019.8626	42474.824
Alaska	HF	468291.7669	42474.824
Alaska	HF	364240.5868	44973.343
Alaska	HF	2989163.912	44973.343
Alaska	HF	5806582.088	44973.343
Alaska	HF	367789.8137	47471.862
Alaska	HF	571747.2918	47471.862
Alaska	HF	676697.2921	47471.862
Alaska	HF	1036667.644	47471.862
Alaska	HF	916989.7399	49970.381
Alaska	HF	2340242.21	49970.381
Alaska	HF	452800.7657	52468.9
Alaska	HF	618637.5284	52468.9
Alaska	HF	3913888.935	52468.9
Alaska	HF	1375879.731	54967.419
Alaska	HF	335120.579	57465.938
Alaska	HF	482055.5814	57465.938
Alaska	HF	2355607.858	57465.938
Alaska	HF	244565.4277	59964.458
Alaska	HF	647093.4097	59964.458
Alaska	HF	822233.2825	59964.458
Alaska	HF	221274.0269	62462.977
Alaska	HF	1093225.917	62462.977
Alaska	HF	1744642.174	62462.977
Alaska	HF	702460.525	64961.496
Alaska	HF	220816.3819	69958.534
Alaska	HF	452482.351	69958.534
Alaska	HF	730799.7456	69958.534

Alaska	HF	828945.6125	69958.534
Alaska	HF	1000038.659	69958.534
Alaska	HF	889295.8886	74955.572
Alaska	HF	1182083.161	77454.091
Alaska	HF	1358496.846	77454.091
Alaska	HF	485149.4507	79952.61
Alaska	HF	981452.7211	82451.129
Alaska	HF	656577.3818	84949.648
Alaska	HF	2013053.026	84949.648
Alaska	HF	1614326.654	89946.686
Alaska	HF	1159824.321	92445.205
Alaska	HF	1490440.581	92445.205
Alaska	HF	1375910.84	99940.762
Alaska	HF	1385973.235	102439.28
Alaska	HF	3076407.122	119928.91
Alaska	HF	1370591.728	124925.95
Alaska	HF	6766914.667	124925.95
Alaska	HF	7540163.922	127424.47
Alaska	HF	2757074.305	129922.99
Alaska	HF	1630956.964	139917.07
Alaska	HF	1864134.946	147412.62
Alaska	HF	3222051.233	149911.14
Alaska	HF	3687453.478	149911.14
Alaska	HF	3374899.021	157406.7
Alaska	HF	2500797.374	162403.74
Alaska	HF	3143345.9	192385.97
Alaska	HF	3823551.55	204878.56
Alaska	HF	4202212.301	227365.23
Alaska	HF	13436494.45	244854.87
Alaska	HF	3510764.535	247353.39
Alaska	HF	7035268.79	272338.58
Alaska	HF	5682100.817	277335.62
Alaska	HF	8117658.845	327306
Alaska	HF	11751711.81	462226.03
Alaska	HF	4869373.619	497205.29
Alaska	HF	18170451.51	507199.37
Alaska	HF	33688692.7	532184.56
Alaska	HF	14209328	539680.12
Alaska	HF	11882418.95	644617.92
Alaska	HF	87422944.05	1261752.1
Alaska	HF	83135863.23	1314221
Alaska	HF	83362570.59	1356695.9
Alaska	HF	58058468.36	2188702.7
Alaska	HF	203649688.7	2698400.6
Alaska	HF	167161755.9	3575380.8
Alaska	HF	188584978.5	4362414.3

Alaska	HF	840051859.3	9664271.7
Alaska	Millan	16513.9544	9994.0762
Alaska	Millan	21081.8646	9994.0762
Alaska	Millan	32069.0045	9994.0762
Alaska	Millan	33381.703	9994.0762
Alaska	Millan	35238.8176	9994.0762
Alaska	Millan	35805.4983	9994.0762
Alaska	Millan	37495.7806	9994.0762
Alaska	Millan	39446.8337	9994.0762
Alaska	Millan	39639.8955	9994.0762
Alaska	Millan	43211.692	9994.0762
Alaska	Millan	43337.3499	9994.0762
Alaska	Millan	45264.0033	9994.0762
Alaska	Millan	47093.9734	9994.0762
Alaska	Millan	52393.414	9994.0762
Alaska	Millan	53677.2905	9994.0762
Alaska	Millan	54784.4223	9994.0762
Alaska	Millan	55660.673	9994.0762
Alaska	Millan	57331.4356	9994.0762
Alaska	Millan	59305.5158	9994.0762
Alaska	Millan	60260.9126	9994.0762
Alaska	Millan	60476.8491	9994.0762
Alaska	Millan	62124.4321	9994.0762
Alaska	Millan	65603.5101	9994.0762
Alaska	Millan	67381.3259	9994.0762
Alaska	Millan	69589.7948	9994.0762
Alaska	Millan	69630.3591	9994.0762
Alaska	Millan	70474.8902	9994.0762
Alaska	Millan	70736.576	9994.0762
Alaska	Millan	70851.5591	9994.0762
Alaska	Millan	73461.4013	9994.0762
Alaska	Millan	73546.4949	9994.0762
Alaska	Millan	73688.3176	9994.0762
Alaska	Millan	76992.0235	9994.0762
Alaska	Millan	77816.73	9994.0762
Alaska	Millan	82857.9923	9994.0762
Alaska	Millan	83078.8087	9994.0762
Alaska	Millan	83616.2099	9994.0762
Alaska	Millan	91475.9311	9994.0762
Alaska	Millan	94758.8973	9994.0762
Alaska	Millan	96213.1135	9994.0762
Alaska	Millan	96911.8571	9994.0762
Alaska	Millan	102328.5683	9994.0762
Alaska	Millan	103601.9225	9994.0762
Alaska	Millan	104674.2849	9994.0762
Alaska	Millan	105288.6973	9994.0762

Alaska	Millan	106086.1067	9994.0762
Alaska	Millan	116544.9954	9994.0762
Alaska	Millan	119556.821	9994.0762
Alaska	Millan	119660.5193	9994.0762
Alaska	Millan	120840.24	9994.0762
Alaska	Millan	123392.8957	9994.0762
Alaska	Millan	126001.6704	9994.0762
Alaska	Millan	130240.186	9994.0762
Alaska	Millan	132722.2353	9994.0762
Alaska	Millan	133281.5961	9994.0762
Alaska	Millan	133639.3553	9994.0762
Alaska	Millan	133670.4648	9994.0762
Alaska	Millan	136476.7238	9994.0762
Alaska	Millan	138257.5896	9994.0762
Alaska	Millan	138901.4341	9994.0762
Alaska	Millan	141182.4917	9994.0762
Alaska	Millan	141267.5853	9994.0762
Alaska	Millan	145631.1488	9994.0762
Alaska	Millan	154228.6529	9994.0762
Alaska	Millan	155686.834	9994.0762
Alaska	Millan	158141.4338	9994.0762
Alaska	Millan	158293.0163	9994.0762
Alaska	Millan	161803.5088	9994.0762
Alaska	Millan	167179.9607	9994.0762
Alaska	Millan	168637.5318	9994.0762
Alaska	Millan	170985.3834	9994.0762
Alaska	Millan	172414.2849	9994.0762
Alaska	Millan	173719.9685	9994.0762
Alaska	Millan	175255.0084	9994.0762
Alaska	Millan	177871.713	9994.0762
Alaska	Millan	183993.4202	9994.0762
Alaska	Millan	184260.5958	9994.0762
Alaska	Millan	189644.8251	9994.0762
Alaska	Millan	198063.7547	9994.0762
Alaska	Millan	201699.6001	9994.0762
Alaska	Millan	219130.3695	9994.0762
Alaska	Millan	236792.6301	9994.0762
Alaska	Millan	253680.8134	9994.0762
Alaska	Millan	256770.7177	9994.0762
Alaska	Millan	274549.4864	9994.0762
Alaska	Millan	289449.4073	9994.0762
Alaska	Millan	293979.8031	9994.0762
Alaska	Millan	295163.7937	9994.0762
Alaska	Millan	299721.029	9994.0762
Alaska	Millan	309551.3229	9994.0762
Alaska	Millan	417378.3411	9994.0762

Alaska	Millan	422638.285	9994.0762
Alaska	Millan	510464.6459	9994.0762
Alaska	Millan	546402.817	9994.0762
Alaska	Millan	655812.7593	9994.0762
Alaska	Millan	843118.4253	9994.0762
Alaska	Millan	32772.628	12492.595
Alaska	Millan	40064.601	12492.595
Alaska	Millan	43529.8018	12492.595
Alaska	Millan	43796.9774	12492.595
Alaska	Millan	50691.3894	12492.595
Alaska	Millan	55069.8977	12492.595
Alaska	Millan	58167.4269	12492.595
Alaska	Millan	62114.6722	12492.595
Alaska	Millan	65278.3854	12492.595
Alaska	Millan	82175.7185	12492.595
Alaska	Millan	96031.9465	12492.595
Alaska	Millan	102805.2755	12492.595
Alaska	Millan	103930.7071	12492.595
Alaska	Millan	105928.4243	12492.595
Alaska	Millan	107626.6365	12492.595
Alaska	Millan	108357.4045	12492.595
Alaska	Millan	112843.576	12492.595
Alaska	Millan	119065.3216	12492.595
Alaska	Millan	120919.8437	12492.595
Alaska	Millan	125556.3777	12492.595
Alaska	Millan	130561.1932	12492.595
Alaska	Millan	138302.1189	12492.595
Alaska	Millan	139804.5243	12492.595
Alaska	Millan	141012.3045	12492.595
Alaska	Millan	147419.0295	12492.595
Alaska	Millan	151121.3638	12492.595
Alaska	Millan	160806.7851	12492.595
Alaska	Millan	164404.8112	12492.595
Alaska	Millan	166872.0683	12492.595
Alaska	Millan	175904.3428	12492.595
Alaska	Millan	177649.9817	12492.595
Alaska	Millan	187423.394	12492.595
Alaska	Millan	192048.6432	12492.595
Alaska	Millan	195083.0385	12492.595
Alaska	Millan	208206.0585	12492.595
Alaska	Millan	218486.22	12492.595
Alaska	Millan	225213.4948	12492.595
Alaska	Millan	234976.6898	12492.595
Alaska	Millan	239566.5596	12492.595
Alaska	Millan	240686.5013	12492.595
Alaska	Millan	245508.7773	12492.595

Alaska	Millan	250569.8643	12492.595
Alaska	Millan	282719.3876	12492.595
Alaska	Millan	286588.5542	12492.595
Alaska	Millan	368121.3432	12492.595
Alaska	Millan	369509.3755	12492.595
Alaska	Millan	391480.9105	12492.595
Alaska	Millan	392245.8379	12492.595
Alaska	Millan	406283.5379	12492.595
Alaska	Millan	409552.7794	12492.595
Alaska	Millan	638888.5866	12492.595
Alaska	Millan	57318.1683	14991.114
Alaska	Millan	62946.3936	14991.114
Alaska	Millan	64093.1748	14991.114
Alaska	Millan	80407.9675	14991.114
Alaska	Millan	81569.0835	14991.114
Alaska	Millan	81686.8115	14991.114
Alaska	Millan	102679.0076	14991.114
Alaska	Millan	104011.5307	14991.114
Alaska	Millan	107235.3279	14991.114
Alaska	Millan	109107.3872	14991.114
Alaska	Millan	113132.7113	14991.114
Alaska	Millan	119012.4049	14991.114
Alaska	Millan	125822.6384	14991.114
Alaska	Millan	142599.4985	14991.114
Alaska	Millan	149086.7422	14991.114
Alaska	Millan	153632.3877	14991.114
Alaska	Millan	157618.8249	14991.114
Alaska	Millan	181467.1466	14991.114
Alaska	Millan	215609.5072	14991.114
Alaska	Millan	232515.9902	14991.114
Alaska	Millan	241155.8886	14991.114
Alaska	Millan	241398.9696	14991.114
Alaska	Millan	245475.2278	14991.114
Alaska	Millan	246901.232	14991.114
Alaska	Millan	249785.7222	14991.114
Alaska	Millan	261932.7582	14991.114
Alaska	Millan	348576.0435	14991.114
Alaska	Millan	357959.8247	14991.114
Alaska	Millan	367296.6367	14991.114
Alaska	Millan	373325.9304	14991.114
Alaska	Millan	383150.582	14991.114
Alaska	Millan	388321.4672	14991.114
Alaska	Millan	423608.779	14991.114
Alaska	Millan	424530.7789	14991.114
Alaska	Millan	462809.6342	14991.114
Alaska	Millan	595458.5182	14991.114

Alaska	Millan	1133279.691	14991.114
Alaska	Millan	67966.3064	17489.633
Alaska	Millan	99850.7889	17489.633
Alaska	Millan	107687.6355	17489.633
Alaska	Millan	147353.4556	17489.633
Alaska	Millan	149904.7388	17489.633
Alaska	Millan	158049.0203	17489.633
Alaska	Millan	159233.6209	17489.633
Alaska	Millan	192142.2767	17489.633
Alaska	Millan	199882.4399	17489.633
Alaska	Millan	206099.0005	17489.633
Alaska	Millan	216474.473	17489.633
Alaska	Millan	220582.4507	17489.633
Alaska	Millan	233161.6646	17489.633
Alaska	Millan	254357.9023	17489.633
Alaska	Millan	256455.3529	17489.633
Alaska	Millan	260467.8672	17489.633
Alaska	Millan	261392.002	17489.633
Alaska	Millan	265894.9482	17489.633
Alaska	Millan	279103.3668	17489.633
Alaska	Millan	301381.4218	17489.633
Alaska	Millan	312162.0801	17489.633
Alaska	Millan	313263.4171	17489.633
Alaska	Millan	330882.6734	17489.633
Alaska	Millan	362978.5175	17489.633
Alaska	Millan	375258.5313	17489.633
Alaska	Millan	396560.1447	17489.633
Alaska	Millan	413777.8751	17489.633
Alaska	Millan	425597.9565	17489.633
Alaska	Millan	447807.9975	17489.633
Alaska	Millan	487148.3879	17489.633
Alaska	Millan	1008040.966	17489.633
Alaska	Millan	97417.8438	19988.153
Alaska	Millan	133206.5674	19988.153
Alaska	Millan	133817.7774	19988.153
Alaska	Millan	137570.1309	19988.153
Alaska	Millan	148587.1604	19988.153
Alaska	Millan	148825.9714	19988.153
Alaska	Millan	170703.263	19988.153
Alaska	Millan	220880.4308	19988.153
Alaska	Millan	280773.8244	19988.153
Alaska	Millan	284319.6963	19988.153
Alaska	Millan	293723.9123	19988.153
Alaska	Millan	294730.7008	19988.153
Alaska	Millan	301380.2018	19988.153
Alaska	Millan	320122.4497	19988.153

Alaska	Millan	394223.578	19988.153
Alaska	Millan	409591.8187	19988.153
Alaska	Millan	431560.3038	19988.153
Alaska	Millan	443763.1538	19988.153
Alaska	Millan	520741.4525	19988.153
Alaska	Millan	544990.3852	19988.153
Alaska	Millan	766133.4167	19988.153
Alaska	Millan	793006.3739	19988.153
Alaska	Millan	954817.965	19988.153
Alaska	Millan	1106656.982	19988.153
Alaska	Millan	71313.9315	22486.672
Alaska	Millan	126363.3945	22486.672
Alaska	Millan	130359.744	22486.672
Alaska	Millan	150586.7076	22486.672
Alaska	Millan	181244.5003	22486.672
Alaska	Millan	217661.5136	22486.672
Alaska	Millan	239996.2976	22486.672
Alaska	Millan	358395.0526	22486.672
Alaska	Millan	366922.8654	22486.672
Alaska	Millan	582750.2915	22486.672
Alaska	Millan	819860.4214	22486.672
Alaska	Millan	934983.53	22486.672
Alaska	Millan	1064102.097	22486.672
Alaska	Millan	232366.8476	24985.191
Alaska	Millan	242012.3146	24985.191
Alaska	Millan	269183.8618	24985.191
Alaska	Millan	270949.6304	24985.191
Alaska	Millan	278749.5726	24985.191
Alaska	Millan	368457.4477	24985.191
Alaska	Millan	431549.0189	24985.191
Alaska	Millan	442833.834	24985.191
Alaska	Millan	504418.73	24985.191
Alaska	Millan	520873.8203	24985.191
Alaska	Millan	669464.0306	24985.191
Alaska	Millan	746330.3962	24985.191
Alaska	Millan	919105.1852	24985.191
Alaska	Millan	1227197.107	24985.191
Alaska	Millan	1248426.284	24985.191
Alaska	Millan	1403454.024	24985.191
Alaska	Millan	88748.6658	27483.71
Alaska	Millan	128282.4231	27483.71
Alaska	Millan	196739.1614	27483.71
Alaska	Millan	273335.9113	27483.71
Alaska	Millan	347447.867	27483.71
Alaska	Millan	403913.4218	27483.71
Alaska	Millan	465533.6971	27483.71

Alaska	Millan	564768.3961	27483.71
Alaska	Millan	611684.2524	27483.71
Alaska	Millan	723457.4484	27483.71
Alaska	Millan	868034.382	27483.71
Alaska	Millan	940166.3101	27483.71
Alaska	Millan	1118162.614	27483.71
Alaska	Millan	1196034.853	27483.71
Alaska	Millan	213346.4443	29982.229
Alaska	Millan	235708.0679	29982.229
Alaska	Millan	349601.7417	29982.229
Alaska	Millan	357522.1569	29982.229
Alaska	Millan	367031.9011	29982.229
Alaska	Millan	483454.5935	29982.229
Alaska	Millan	490352.9704	29982.229
Alaska	Millan	539682.4047	29982.229
Alaska	Millan	582184.8307	29982.229
Alaska	Millan	583029.6669	29982.229
Alaska	Millan	584192.0028	29982.229
Alaska	Millan	795927.1585	29982.229
Alaska	Millan	1035550.219	29982.229
Alaska	Millan	1131321.928	29982.229
Alaska	Millan	994688.7417	32480.748
Alaska	Millan	1211392.876	32480.748
Alaska	Millan	1449382.307	32480.748
Alaska	Millan	159083.2584	34979.267
Alaska	Millan	367940.9387	34979.267
Alaska	Millan	439821.0934	34979.267
Alaska	Millan	440409.4288	34979.267
Alaska	Millan	472073.0949	34979.267
Alaska	Millan	539765.2108	34979.267
Alaska	Millan	604944.1678	34979.267
Alaska	Millan	643225.9206	34979.267
Alaska	Millan	889078.7322	34979.267
Alaska	Millan	1068177.593	34979.267
Alaska	Millan	257025.6936	37477.786
Alaska	Millan	322288.3717	37477.786
Alaska	Millan	409891.6288	37477.786
Alaska	Millan	500587.3827	37477.786
Alaska	Millan	869454.1337	37477.786
Alaska	Millan	988158.4937	37477.786
Alaska	Millan	1054541.571	37477.786
Alaska	Millan	1260727.038	37477.786
Alaska	Millan	621753.9674	39976.305
Alaska	Millan	695625.282	39976.305
Alaska	Millan	893228.1892	39976.305
Alaska	Millan	2138404.752	39976.305

Alaska	Millan	253047.1863	42474.824
Alaska	Millan	815003.0709	42474.824
Alaska	Millan	837566.2962	42474.824
Alaska	Millan	1091872.959	42474.824
Alaska	Millan	1411617.978	42474.824
Alaska	Millan	2370591.042	42474.824
Alaska	Millan	1186246.343	44973.343
Alaska	Millan	1339961.689	44973.343
Alaska	Millan	2238829.541	44973.343
Alaska	Millan	959437.1144	47471.862
Alaska	Millan	312782.745	49970.381
Alaska	Millan	525318.2075	49970.381
Alaska	Millan	791404.8451	49970.381
Alaska	Millan	1200841.116	49970.381
Alaska	Millan	1357255.516	49970.381
Alaska	Millan	1237938.726	52468.9
Alaska	Millan	1420864.054	52468.9
Alaska	Millan	1242403.243	54967.419
Alaska	Millan	2602259.146	54967.419
Alaska	Millan	2950163.438	54967.419
Alaska	Millan	1124070.062	62462.977
Alaska	Millan	1178552.844	62462.977
Alaska	Millan	1765089.649	62462.977
Alaska	Millan	718739.6332	64961.496
Alaska	Millan	1847834.793	64961.496
Alaska	Millan	1929497.205	64961.496
Alaska	Millan	1614670.688	67460.015
Alaska	Millan	4350189.471	67460.015
Alaska	Millan	470968.4031	72457.053
Alaska	Millan	2710928.561	72457.053
Alaska	Millan	1118825.063	74955.572
Alaska	Millan	1190893.857	74955.572
Alaska	Millan	1805017.154	74955.572
Alaska	Millan	2489431.43	77454.091
Alaska	Millan	1065122.153	84949.648
Alaska	Millan	1561121.191	84949.648
Alaska	Millan	1912118.894	84949.648
Alaska	Millan	1914434.417	84949.648
Alaska	Millan	1525257.743	87448.167
Alaska	Millan	1699500.168	87448.167
Alaska	Millan	1000157.302	89946.686
Alaska	Millan	1038133.45	92445.205
Alaska	Millan	2799715.046	92445.205
Alaska	Millan	2581568.895	94943.724
Alaska	Millan	993017.9791	97442.243
Alaska	Millan	3743823.721	97442.243

Alaska	Millan	2406758.57	99940.762
Alaska	Millan	1198908.668	102439.28
Alaska	Millan	2015091.612	102439.28
Alaska	Millan	3472334.86	104937.8
Alaska	Millan	4483652.234	107436.32
Alaska	Millan	866215.2393	109934.84
Alaska	Millan	1677446.285	109934.84
Alaska	Millan	2762261.05	109934.84
Alaska	Millan	6470620.257	112433.36
Alaska	Millan	5887676.294	117430.4
Alaska	Millan	2236111.731	119928.91
Alaska	Millan	4908158.918	122427.43
Alaska	Millan	5018355.138	124925.95
Alaska	Millan	3681579.731	127424.47
Alaska	Millan	3164689.146	129922.99
Alaska	Millan	1481952.113	134920.03
Alaska	Millan	1848624.425	134920.03
Alaska	Millan	6408920.073	142415.59
Alaska	Millan	1827366.883	152409.66
Alaska	Millan	4647277.783	154908.18
Alaska	Millan	1786669.265	167400.78
Alaska	Millan	9922027.275	169899.3
Alaska	Millan	3105335.288	172397.82
Alaska	Millan	5317109.79	189887.45
Alaska	Millan	7981450.212	257347.46
Alaska	Millan	7355981.71	277335.62
Alaska	Millan	9984356.054	289828.21
Alaska	Millan	7533184.417	294825.25
Alaska	Millan	5603421.561	312314.88
Alaska	Millan	6052611.796	319810.44
Alaska	Millan	8646449.726	319810.44
Alaska	Millan	8397829.389	332303.04
Alaska	Millan	11733794.58	399763.05
Alaska	Millan	7980590.888	402261.57
Alaska	Millan	26908517.46	452231.95
Alaska	Millan	23034822.9	504700.85
Alaska	Millan	17278781.08	519691.96
Alaska	Millan	39158050.2	584653.46
Alaska	Millan	28564358.81	587151.98
Alaska	Millan	28820444.21	637122.36
Alaska	Millan	44723852.31	657110.51
Alaska	Millan	36576526.29	1119336.5
Alaska	Millan	159529432.8	1853901.1
Alaska	Millan	995618607.9	7807872.1
Alaska	Millan	987265581.5	11815497
Alaska	OGGM	21775.5757	9994.0762

Alaska	OGGM	23388.2368	9994.0762
Alaska	OGGM	23564.8289	9994.0762
Alaska	OGGM	26244.21	9994.0762
Alaska	OGGM	27583.443	9994.0762
Alaska	OGGM	30737.0914	9994.0762
Alaska	OGGM	42519.9633	9994.0762
Alaska	OGGM	65698.0585	9994.0762
Alaska	OGGM	65953.6443	9994.0762
Alaska	OGGM	66419.9817	9994.0762
Alaska	OGGM	94241.6258	9994.0762
Alaska	OGGM	98727.7973	9994.0762
Alaska	OGGM	98824.4807	9994.0762
Alaska	OGGM	103342.9817	9994.0762
Alaska	OGGM	139030.7519	9994.0762
Alaska	OGGM	150764.5197	9994.0762
Alaska	OGGM	165024.866	9994.0762
Alaska	OGGM	168678.4012	9994.0762
Alaska	OGGM	226284.0273	9994.0762
Alaska	OGGM	341308.9276	9994.0762
Alaska	OGGM	16598.133	12492.595
Alaska	OGGM	18210.1841	12492.595
Alaska	OGGM	37993.8375	12492.595
Alaska	OGGM	45500.3745	12492.595
Alaska	OGGM	62474.5663	12492.595
Alaska	OGGM	111161.8336	12492.595
Alaska	OGGM	134860.7078	12492.595
Alaska	OGGM	142644.0277	12492.595
Alaska	OGGM	157393.7386	12492.595
Alaska	OGGM	36231.5763	14991.114
Alaska	OGGM	46064.9202	14991.114
Alaska	OGGM	51657.9186	14991.114
Alaska	OGGM	52079.7267	14991.114
Alaska	OGGM	52290.7832	14991.114
Alaska	OGGM	107115.7699	14991.114
Alaska	OGGM	151048.47	14991.114
Alaska	OGGM	159819.8213	14991.114
Alaska	OGGM	202387.9738	14991.114
Alaska	OGGM	233348.0165	14991.114
Alaska	OGGM	302824.6581	14991.114
Alaska	OGGM	357902.7907	14991.114
Alaska	OGGM	28924.8111	17489.633
Alaska	OGGM	40854.6906	17489.633
Alaska	OGGM	43785.0826	17489.633
Alaska	OGGM	87749.5022	17489.633
Alaska	OGGM	101881.7506	17489.633
Alaska	OGGM	144393.1741	17489.633

Alaska	OGGM	150028.5667	17489.633
Alaska	OGGM	155063.8817	17489.633
Alaska	OGGM	200352.1322	17489.633
Alaska	OGGM	35120.4795	19988.153
Alaska	OGGM	74231.9712	19988.153
Alaska	OGGM	106784.5453	19988.153
Alaska	OGGM	186164.3746	19988.153
Alaska	OGGM	218153.013	19988.153
Alaska	OGGM	265257.5087	19988.153
Alaska	OGGM	505985.4893	19988.153
Alaska	OGGM	161704.3854	22486.672
Alaska	OGGM	280755.9822	22486.672
Alaska	OGGM	556152.8973	22486.672
Alaska	OGGM	43899.1507	24985.191
Alaska	OGGM	48561.9143	24985.191
Alaska	OGGM	51518.8408	24985.191
Alaska	OGGM	171931.7828	24985.191
Alaska	OGGM	301592.1733	24985.191
Alaska	OGGM	150561.088	27483.71
Alaska	OGGM	319577.4236	27483.71
Alaska	OGGM	428331.3217	27483.71
Alaska	OGGM	256495.3073	29982.229
Alaska	OGGM	313065.6278	29982.229
Alaska	OGGM	539971.3874	29982.229
Alaska	OGGM	308209.6499	32480.748
Alaska	OGGM	521033.9427	32480.748
Alaska	OGGM	306513.8777	34979.267
Alaska	OGGM	377116.8658	34979.267
Alaska	OGGM	533216.3581	34979.267
Alaska	OGGM	221283.6342	37477.786
Alaska	OGGM	404439.8431	37477.786
Alaska	OGGM	217878.67	39976.305
Alaska	OGGM	287081.4261	39976.305
Alaska	OGGM	164827.5343	42474.824
Alaska	OGGM	297000.4736	42474.824
Alaska	OGGM	674193.5881	42474.824
Alaska	OGGM	447541.1269	44973.343
Alaska	OGGM	175383.1063	47471.862
Alaska	OGGM	761090.3243	49970.381
Alaska	OGGM	139489.7694	52468.9
Alaska	OGGM	270886.8014	52468.9
Alaska	OGGM	740109.4131	54967.419
Alaska	OGGM	503185.3302	59964.458
Alaska	OGGM	1117864.939	59964.458
Alaska	OGGM	1898154.088	67460.015
Alaska	OGGM	824168.4758	69958.534

Alaska	OGGM	3001143.2	72457.053
Alaska	OGGM	1100672.065	82451.129
Alaska	OGGM	558172.7267	84949.648
Alaska	OGGM	1493254.008	94943.724
Alaska	OGGM	2404527.836	94943.724
Alaska	OGGM	311297.1143	97442.243
Alaska	OGGM	255242.0828	102439.28
Alaska	OGGM	1032761.573	129922.99
Alaska	OGGM	4285083.408	144914.11
Alaska	OGGM	1515798.018	159905.22
Alaska	OGGM	2857381.061	164902.26
Alaska	OGGM	5110160.769	184890.41
Alaska	OGGM	2880075.892	232362.27
Alaska	OGGM	3188656.568	249851.91
Alaska	OGGM	4409511.914	249851.91
Alaska	OGGM	2464251.348	259845.98
Alaska	OGGM	3041583.708	262344.5
Alaska	OGGM	6083201.728	307317.84
Alaska	OGGM	7215890.491	332303.04
Alaska	OGGM	8062858.868	374777.86
Alaska	OGGM	9044335.836	389768.97
Alaska	OGGM	65936565.22	3635345.2
Alaska	OGGM	166474932.1	5284367.8
Alaska	OGGM	259060235.9	6498648.1
Alps	Farinotti’s Ensemble	76351.2863	12499.562
Alps	Farinotti’s Ensemble	49623.8756	14977.704
Alps	Farinotti’s Ensemble	48473.0366	14999.474
Alps	Farinotti’s Ensemble	71504.7177	19970.271
Alps	Farinotti’s Ensemble	73004.2368	22499.211
Alps	Farinotti’s Ensemble	85319.2556	22499.211
Alps	Farinotti’s Ensemble	139208.216	29998.949
Alps	Farinotti’s Ensemble	208363.8951	29998.949
Alps	Farinotti’s Ensemble	378064.061	37498.686
Alps	Farinotti’s Ensemble	162790.089	42498.51
Alps	Farinotti’s Ensemble	501530.2847	52498.16
Alps	Farinotti’s Ensemble	407523.0991	54998.072
Alps	Farinotti’s Ensemble	615776.5647	84997.021
Alps	Farinotti’s Ensemble	1085145.646	109996.14
Alps	GlabTop2	39371.1786	9999.6495
Alps	GlabTop2	67110.6849	9999.6495
Alps	GlabTop2	75592.4259	12481.42
Alps	GlabTop2	88301.3484	12499.562
Alps	GlabTop2	124638.5758	14999.474
Alps	GlabTop2	152181.5557	17499.387
Alps	GlabTop2	161429.6107	19970.271
Alps	GlabTop2	129867.8847	34998.773

Alps	GlabTop2	258695.1564	39998.598
Alps	GlabTop2	227300.9931	44998.423
Alps	GlabTop2	650474.6375	47498.335
Alps	GlabTop2	884441.6568	52498.16
Alps	GlabTop2	1000460.54	67497.634
Alps	GlabTop2	1572172.679	77497.284
Alps	GlabTop2	1666307.563	147494.83
Alps	GlabTop2	3111157.434	199992.99
Alps	GlabTop2	6392830.132	247491.33
Alps	HF	41227.1927	9999.6495
Alps	HF	50721.4888	9999.6495
Alps	HF	56929.157	9999.6495
Alps	HF	57306.9514	9999.6495
Alps	HF	124337.683	9999.6495
Alps	HF	65390.328	12481.42
Alps	HF	50819.752	12499.562
Alps	HF	57713.4313	12499.562
Alps	HF	88273.8836	17499.387
Alps	HF	83668.9424	19999.299
Alps	HF	97000.9947	19999.299
Alps	HF	76729.4884	22499.211
Alps	HF	124740.5009	22499.211
Alps	HF	143815.1497	22499.211
Alps	HF	125925.2131	24962.839
Alps	HF	137959.0318	27499.036
Alps	HF	395128.3474	32451.691
Alps	HF	252481.9953	32498.861
Alps	HF	667613.319	44998.423
Alps	HF	1418257.786	64997.722
Alps	HF	1431639.275	102496.41
Alps	HF	1352650.344	124995.62
Alps	Millan	40706.9789	9999.6495
Alps	Millan	57708.233	9999.6495
Alps	Millan	64515.8119	9999.6495
Alps	Millan	80124.1907	9999.6495
Alps	Millan	97027.8276	9999.6495
Alps	Millan	103843.948	9999.6495
Alps	Millan	109427.6514	9999.6495
Alps	Millan	117073.5179	9999.6495
Alps	Millan	122377.1819	9999.6495
Alps	Millan	140063.5867	9999.6495
Alps	Millan	147411.7207	9999.6495
Alps	Millan	160865.8101	9999.6495
Alps	Millan	217180.5578	9999.6495
Alps	Millan	125613.1776	12481.42
Alps	Millan	259032.7275	12481.42

Alps	Millan	65867.1999	12499.562
Alps	Millan	129386.0962	12499.562
Alps	Millan	130814.3578	12499.562
Alps	Millan	109618.615	14999.474
Alps	Millan	111542.8939	14999.474
Alps	Millan	115273.0908	14999.474
Alps	Millan	134950.2762	14999.474
Alps	Millan	158224.655	14999.474
Alps	Millan	202143.2395	14999.474
Alps	Millan	224794.0886	14999.474
Alps	Millan	299316.8828	14999.474
Alps	Millan	355066.0608	14999.474
Alps	Millan	419727.0783	14999.474
Alps	Millan	458403.9036	17473.988
Alps	Millan	550877.6053	17499.387
Alps	Millan	345411.7084	19970.271
Alps	Millan	296929.5324	22499.211
Alps	Millan	336115.5135	22499.211
Alps	Millan	429295.3934	22499.211
Alps	Millan	510949.7336	24999.124
Alps	Millan	833256.0751	24999.124
Alps	Millan	270118.3607	27499.036
Alps	Millan	695662.8135	27499.036
Alps	Millan	1713505.676	27499.036
Alps	Millan	142783.6618	34947.975
Alps	Millan	301684.6881	39940.543
Alps	Millan	635922.3126	39998.598
Alps	Millan	869187.743	39998.598
Alps	Millan	922668.5416	39998.598
Alps	Millan	946827.5762	49998.248
Alps	Millan	1456599.802	52498.16
Alps	Millan	2348440.654	74888.518
Alps	Millan	2354238.686	77497.284
Alps	Millan	1499896.688	82497.109
Alps	Millan	5276652.391	182228.73
Alps	Millan	8256789.677	202492.9
Alps	Millan	9244668.943	259990.89
Alps	OGGM	27289.0882	9985.1357
Alps	OGGM	45326.1024	9999.6495
Alps	OGGM	56961.4615	19999.299
Alps	OGGM	253632.0372	22499.211
Alps	OGGM	120714.4642	24962.839
Alps	OGGM	140848.1848	24999.124
Alps	OGGM	88072.0604	29998.949
Alps	OGGM	191742.7379	29998.949
Alps	OGGM	216478.3241	32498.861

Alps	OGGM	216860.8615	32498.861
Alps	OGGM	233477.7479	34998.773
Alps	OGGM	345914.4491	34998.773
Alps	OGGM	540841.9479	54998.072
Alps	OGGM	744923.4988	59997.897
Alps	OGGM	822844.9014	74888.518
Alps	OGGM	1262996.847	87496.933
Alps	OGGM	1272077.076	99996.495
Alps	OGGM	2277532.927	114995.97
Alps	OGGM	2459400.353	142288.18
Alps	OGGM	2515645.662	162494.3
Alps	OGGM	10199414.49	247491.33
Himalayas	Farinotti's Ensemble	22504.625	9999.8854
Himalayas	Farinotti's Ensemble	27539.9677	9999.8854
Himalayas	Farinotti's Ensemble	27699.878	9999.8854
Himalayas	Farinotti's Ensemble	30006.9804	9999.8854
Himalayas	Farinotti's Ensemble	30839.4904	9999.8854
Himalayas	Farinotti's Ensemble	37104.0671	9999.8854
Himalayas	Farinotti's Ensemble	37947.5633	9999.8854
Himalayas	Farinotti's Ensemble	38258.839	9999.8854
Himalayas	Farinotti's Ensemble	40889.4241	9999.8854
Himalayas	Farinotti's Ensemble	42199.2236	9999.8854
Himalayas	Farinotti's Ensemble	43278.3128	9999.8854
Himalayas	Farinotti's Ensemble	47822.9384	9999.8854
Himalayas	Farinotti's Ensemble	49966.4686	9999.8854
Himalayas	Farinotti's Ensemble	63392.8284	9999.8854
Himalayas	Farinotti's Ensemble	128754.6284	9999.8854
Himalayas	Farinotti's Ensemble	38371.1424	12499.857
Himalayas	Farinotti's Ensemble	39807.8935	12499.857
Himalayas	Farinotti's Ensemble	41463.148	12499.857
Himalayas	Farinotti's Ensemble	42493.4096	12499.857
Himalayas	Farinotti's Ensemble	52959.5983	12499.857
Himalayas	Farinotti's Ensemble	58698.058	12499.857
Himalayas	Farinotti's Ensemble	60349.6504	12499.857
Himalayas	Farinotti's Ensemble	61190.7052	12499.857
Himalayas	Farinotti's Ensemble	84706.0608	12499.857
Himalayas	Farinotti's Ensemble	91512.6234	12499.857
Himalayas	Farinotti's Ensemble	34705.4129	14999.828
Himalayas	Farinotti's Ensemble	42428.7131	14999.828
Himalayas	Farinotti's Ensemble	46065.1461	14999.828
Himalayas	Farinotti's Ensemble	56956.1346	14999.828
Himalayas	Farinotti's Ensemble	69962.5773	14999.828
Himalayas	Farinotti's Ensemble	70122.4876	14999.828
Himalayas	Farinotti's Ensemble	115495.5029	14999.828
Himalayas	Farinotti's Ensemble	123144.3411	14999.828
Himalayas	Farinotti's Ensemble	149163.3301	14999.828

Himalayas	Farinotti's Ensemble	29692.0426	17499.8
Himalayas	Farinotti's Ensemble	65383.7724	17499.8
Himalayas	Farinotti's Ensemble	73780.893	17499.8
Himalayas	Farinotti's Ensemble	75351.9199	17499.8
Himalayas	Farinotti's Ensemble	94511.8566	17499.8
Himalayas	Farinotti's Ensemble	113069.9936	17499.8
Himalayas	Farinotti's Ensemble	118650.9844	17499.8
Himalayas	Farinotti's Ensemble	121603.8314	17499.8
Himalayas	Farinotti's Ensemble	122538.8793	17499.8
Himalayas	Farinotti's Ensemble	168805.439	17499.8
Himalayas	Farinotti's Ensemble	210666.5317	17499.8
Himalayas	Farinotti's Ensemble	432707.4448	17499.8
Himalayas	Farinotti's Ensemble	70471.6047	19999.771
Himalayas	Farinotti's Ensemble	100982.7298	19999.771
Himalayas	Farinotti's Ensemble	145678.2626	19999.771
Himalayas	Farinotti's Ensemble	163776.1998	19999.771
Himalayas	Farinotti's Ensemble	139294.0584	22499.742
Himalayas	Farinotti's Ensemble	215053.6885	22499.742
Himalayas	Farinotti's Ensemble	400360.4033	22499.742
Himalayas	Farinotti's Ensemble	125226.8368	24999.714
Himalayas	Farinotti's Ensemble	135066.8119	24999.714
Himalayas	Farinotti's Ensemble	165311.8267	24999.714
Himalayas	Farinotti's Ensemble	343342.0136	24999.714
Himalayas	Farinotti's Ensemble	239828.7953	27499.685
Himalayas	Farinotti's Ensemble	268071.8799	27499.685
Himalayas	Farinotti's Ensemble	294485.1515	27499.685
Himalayas	Farinotti's Ensemble	243611.7109	29999.656
Himalayas	Farinotti's Ensemble	112278.9871	32499.628
Himalayas	Farinotti's Ensemble	159826.0497	32499.628
Himalayas	Farinotti's Ensemble	255438.968	32499.628
Himalayas	Farinotti's Ensemble	258468.7184	32499.628
Himalayas	Farinotti's Ensemble	1687605.177	32499.628
Himalayas	Farinotti's Ensemble	112093.4423	34999.599
Himalayas	Farinotti's Ensemble	150524.3985	37499.57
Himalayas	Farinotti's Ensemble	222717.1749	37499.57
Himalayas	Farinotti's Ensemble	253800.8031	39999.542
Himalayas	Farinotti's Ensemble	268905.6106	42499.513
Himalayas	Farinotti's Ensemble	278247.5445	42499.513
Himalayas	Farinotti's Ensemble	660621.0934	42499.513
Himalayas	Farinotti's Ensemble	498375.6378	44999.484
Himalayas	Farinotti's Ensemble	323393.5117	49999.427
Himalayas	Farinotti's Ensemble	202658.811	52499.399
Himalayas	Farinotti's Ensemble	588626.0686	52499.399
Himalayas	Farinotti's Ensemble	530759.3	54999.37
Himalayas	Farinotti's Ensemble	708192.5698	59999.313
Himalayas	Farinotti's Ensemble	929961.2693	62499.284

Himalayas	Farinotti's Ensemble	273124.3122	67499.227
Himalayas	Farinotti's Ensemble	408261.9241	67499.227
Himalayas	Farinotti's Ensemble	458256.4685	69999.198
Himalayas	Farinotti's Ensemble	498103.4241	69999.198
Himalayas	Farinotti's Ensemble	693064.5693	72499.169
Himalayas	Farinotti's Ensemble	1411032.418	82499.055
Himalayas	Farinotti's Ensemble	585292.3666	84999.026
Himalayas	Farinotti's Ensemble	544348.0115	89998.969
Himalayas	Farinotti's Ensemble	503528.1666	94998.912
Himalayas	Farinotti's Ensemble	923184.0032	94998.912
Himalayas	Farinotti's Ensemble	1353887.076	97498.883
Himalayas	Farinotti's Ensemble	1486184.145	114998.68
Himalayas	Farinotti's Ensemble	1488275.185	142498.37
Himalayas	Farinotti's Ensemble	2434843.32	162498.14
Himalayas	Farinotti's Ensemble	4640924.612	202497.68
Himalayas	Farinotti's Ensemble	5772577.907	234997.31
Himalayas	Farinotti's Ensemble	8755777.371	309996.45
Himalayas	Farinotti's Ensemble	4868165.661	319996.33
Himalayas	Farinotti's Ensemble	5471315.489	337496.13
Himalayas	Farinotti's Ensemble	11611276.88	404995.36
Himalayas	Farinotti's Ensemble	15219247.02	497494.3
Himalayas	Farinotti's Ensemble	11089240.63	532493.9
Himalayas	Farinotti's Ensemble	18405990.29	584993.3
Himalayas	Farinotti's Ensemble	19254011.58	794990.89
Himalayas	GlabTop2	17136.0341	9999.8854
Himalayas	GlabTop2	26012.8856	9999.8854
Himalayas	GlabTop2	26371.7682	9999.8854
Himalayas	GlabTop2	31205.6972	9999.8854
Himalayas	GlabTop2	31422.9798	9999.8854
Himalayas	GlabTop2	33047.7171	9999.8854
Himalayas	GlabTop2	33611.6755	9999.8854
Himalayas	GlabTop2	44982.3948	9999.8854
Himalayas	GlabTop2	55630.4662	9999.8854
Himalayas	GlabTop2	55767.1833	9999.8854
Himalayas	GlabTop2	56306.7279	9999.8854
Himalayas	GlabTop2	60437.54	9999.8854
Himalayas	GlabTop2	63856.6903	9999.8854
Himalayas	GlabTop2	73500.1345	9999.8854
Himalayas	GlabTop2	82855.496	9999.8854
Himalayas	GlabTop2	85785.15	9999.8854
Himalayas	GlabTop2	89524.1208	9999.8854
Himalayas	GlabTop2	91820.2371	9999.8854
Himalayas	GlabTop2	107099.603	9999.8854
Himalayas	GlabTop2	158617.5675	9999.8854
Himalayas	GlabTop2	161848.7316	9999.8854
Himalayas	GlabTop2	26569.5198	12499.857

Himalayas	GlabTop2	32549.6759	12499.857
Himalayas	GlabTop2	37344.5428	12499.857
Himalayas	GlabTop2	43589.5885	12499.857
Himalayas	GlabTop2	49390.3033	12499.857
Himalayas	GlabTop2	51978.1643	12499.857
Himalayas	GlabTop2	63035.1665	12499.857
Himalayas	GlabTop2	63960.4488	12499.857
Himalayas	GlabTop2	69420.5914	12499.857
Himalayas	GlabTop2	83877.2128	12499.857
Himalayas	GlabTop2	101079.1642	12499.857
Himalayas	GlabTop2	111482.4874	12499.857
Himalayas	GlabTop2	112983.3247	12499.857
Himalayas	GlabTop2	116721.0748	12499.857
Himalayas	GlabTop2	139696.8858	12499.857
Himalayas	GlabTop2	159401.2499	12499.857
Himalayas	GlabTop2	39966.5831	14999.828
Himalayas	GlabTop2	48926.4414	14999.828
Himalayas	GlabTop2	53961.7841	14999.828
Himalayas	GlabTop2	55870.9419	14999.828
Himalayas	GlabTop2	74404.6651	14999.828
Himalayas	GlabTop2	107459.7063	14999.828
Himalayas	GlabTop2	115608.4167	14999.828
Himalayas	GlabTop2	123204.1549	14999.828
Himalayas	GlabTop2	126465.8362	14999.828
Himalayas	GlabTop2	143223.4567	14999.828
Himalayas	GlabTop2	295736.3578	14999.828
Himalayas	GlabTop2	96015.7457	17499.8
Himalayas	GlabTop2	119365.0875	17499.8
Himalayas	GlabTop2	193320.539	17499.8
Himalayas	GlabTop2	198211.8404	17499.8
Himalayas	GlabTop2	201872.6871	17499.8
Himalayas	GlabTop2	285986.7137	17499.8
Himalayas	GlabTop2	86267.9325	19999.771
Himalayas	GlabTop2	109542.202	19999.771
Himalayas	GlabTop2	183922.4534	19999.771
Himalayas	GlabTop2	195706.9863	19999.771
Himalayas	GlabTop2	284361.9764	19999.771
Himalayas	GlabTop2	214273.6681	22499.742
Himalayas	GlabTop2	218265.3216	22499.742
Himalayas	GlabTop2	220757.9688	22499.742
Himalayas	GlabTop2	265618.2947	22499.742
Himalayas	GlabTop2	218673.0318	24999.714
Himalayas	GlabTop2	226717.3732	24999.714
Himalayas	GlabTop2	286201.555	24999.714
Himalayas	GlabTop2	147340.8412	27499.685
Himalayas	GlabTop2	204354.3482	27499.685

Himalayas	GlabTop2	236525.6104	27499.685
Himalayas	GlabTop2	256760.9743	27499.685
Himalayas	GlabTop2	320961.8989	27499.685
Himalayas	GlabTop2	358075.7315	27499.685
Himalayas	GlabTop2	114131.9932	29999.656
Himalayas	GlabTop2	535186.7395	29999.656
Himalayas	GlabTop2	87191.3839	32499.628
Himalayas	GlabTop2	235456.2868	32499.628
Himalayas	GlabTop2	286250.3825	32499.628
Himalayas	GlabTop2	322882.0429	32499.628
Himalayas	GlabTop2	246564.5579	34999.599
Himalayas	GlabTop2	931180.7377	34999.599
Himalayas	GlabTop2	1630285.277	37499.57
Himalayas	GlabTop2	181385.8613	39999.542
Himalayas	GlabTop2	454640.7873	39999.542
Himalayas	GlabTop2	709277.7625	42499.513
Himalayas	GlabTop2	477551.9017	44999.484
Himalayas	GlabTop2	364137.6738	47499.456
Himalayas	GlabTop2	477158.8398	47499.456
Himalayas	GlabTop2	833375.4618	47499.456
Himalayas	GlabTop2	1144482.737	47499.456
Himalayas	GlabTop2	282969.1701	49999.427
Himalayas	GlabTop2	641477.0256	49999.427
Himalayas	GlabTop2	866050.8687	49999.427
Himalayas	GlabTop2	351343.6309	54999.37
Himalayas	GlabTop2	384949.2029	54999.37
Himalayas	GlabTop2	501705.6777	54999.37
Himalayas	GlabTop2	1344014.143	54999.37
Himalayas	GlabTop2	624118.826	57499.341
Himalayas	GlabTop2	686515.5721	57499.341
Himalayas	GlabTop2	530831.3206	59999.313
Himalayas	GlabTop2	567065.0364	62499.284
Himalayas	GlabTop2	511698.239	64999.255
Himalayas	GlabTop2	886969.8185	72499.169
Himalayas	GlabTop2	1151115.962	77499.112
Himalayas	GlabTop2	686123.7309	79999.084
Himalayas	GlabTop2	2523147.362	82499.055
Himalayas	GlabTop2	707196.4875	84999.026
Himalayas	GlabTop2	1007046.568	92498.94
Himalayas	GlabTop2	2191442.178	94998.912
Himalayas	GlabTop2	1289771.6	97498.883
Himalayas	GlabTop2	964809.5028	99998.854
Himalayas	GlabTop2	2833866.458	107498.77
Himalayas	GlabTop2	2758842.904	117498.65
Himalayas	GlabTop2	1442717.846	122498.6
Himalayas	GlabTop2	2776614.917	129998.51

Himalayas	GlabTop2	2707208.974	139998.4
Himalayas	GlabTop2	1720762.756	142498.37
Himalayas	GlabTop2	4157585.423	142498.37
Himalayas	GlabTop2	2552565.97	162498.14
Himalayas	GlabTop2	2675850.691	162498.14
Himalayas	GlabTop2	2591494.968	164998.11
Himalayas	GlabTop2	2222691.82	167498.08
Himalayas	GlabTop2	5341889.482	172498.02
Himalayas	GlabTop2	8311425.162	172498.02
Himalayas	GlabTop2	2355530.874	174998
Himalayas	GlabTop2	4300326.708	174998
Himalayas	GlabTop2	3692704.275	222497.45
Himalayas	GlabTop2	5136207.024	247497.16
Himalayas	GlabTop2	12760500.78	252497.11
Himalayas	GlabTop2	6945442.887	254997.08
Himalayas	GlabTop2	3209103.858	272496.88
Himalayas	GlabTop2	4951688.874	284996.73
Himalayas	GlabTop2	16266843.66	364995.82
Himalayas	GlabTop2	11473470.84	387495.56
Himalayas	GlabTop2	9861427.545	392495.5
Himalayas	GlabTop2	12156055.8	447494.87
Himalayas	GlabTop2	26906279.87	542493.78
Himalayas	GlabTop2	13917837.37	594993.18
Himalayas	GlabTop2	26796268.92	627492.81
Himalayas	GlabTop2	44045849.13	667492.35
Himalayas	GlabTop2	40950714.91	682492.18
Himalayas	GlabTop2	21532581.67	732491.61
Himalayas	GlabTop2	25037900.4	737491.55
Himalayas	GlabTop2	71157310.97	1137487
Himalayas	GlabTop2	106194868.5	1567482
Himalayas	HF	20319.5914	9999.8854
Himalayas	HF	23586.1556	9999.8854
Himalayas	HF	26209.4165	9999.8854
Himalayas	HF	28987.705	9999.8854
Himalayas	HF	33263.7791	9999.8854
Himalayas	HF	36842.8396	9999.8854
Himalayas	HF	37091.8602	9999.8854
Himalayas	HF	37964.6529	9999.8854
Himalayas	HF	39446.5695	9999.8854
Himalayas	HF	40296.1692	9999.8854
Himalayas	HF	41623.0583	9999.8854
Himalayas	HF	42145.5132	9999.8854
Himalayas	HF	43235.5886	9999.8854
Himalayas	HF	44175.5193	9999.8854
Himalayas	HF	48927.6621	9999.8854
Himalayas	HF	50208.165	9999.8854

Himalayas	HF	50274.0822	9999.8854
Himalayas	HF	50380.2822	9999.8854
Himalayas	HF	50997.9509	9999.8854
Himalayas	HF	51958.6332	9999.8854
Himalayas	HF	52164.9297	9999.8854
Himalayas	HF	52764.2881	9999.8854
Himalayas	HF	53247.681	9999.8854
Himalayas	HF	64858.8761	9999.8854
Himalayas	HF	65299.5448	9999.8854
Himalayas	HF	71916.9007	9999.8854
Himalayas	HF	79145.8217	9999.8854
Himalayas	HF	83215.5993	9999.8854
Himalayas	HF	85898.6741	9999.8854
Himalayas	HF	103678.0114	9999.8854
Himalayas	HF	181705.6819	9999.8854
Himalayas	HF	334981.5137	9999.8854
Himalayas	HF	29261.1394	12499.857
Himalayas	HF	38916.7905	12499.857
Himalayas	HF	45087.3741	12499.857
Himalayas	HF	61906.029	12499.857
Himalayas	HF	65527.8137	12499.857
Himalayas	HF	71960.8455	12499.857
Himalayas	HF	74864.8649	12499.857
Himalayas	HF	79775.6973	12499.857
Himalayas	HF	80500.7867	12499.857
Himalayas	HF	82035.1929	12499.857
Himalayas	HF	85304.1985	12499.857
Himalayas	HF	92467.2023	12499.857
Himalayas	HF	100360.1783	12499.857
Himalayas	HF	135243.8118	12499.857
Himalayas	HF	27760.9124	14999.828
Himalayas	HF	32107.7864	14999.828
Himalayas	HF	43773.9125	14999.828
Himalayas	HF	47858.3384	14999.828
Himalayas	HF	48958.1793	14999.828
Himalayas	HF	57332.1068	14999.828
Himalayas	HF	57830.148	14999.828
Himalayas	HF	67626.1783	14999.828
Himalayas	HF	90060.0033	14999.828
Himalayas	HF	106569.824	14999.828
Himalayas	HF	120512.5353	14999.828
Himalayas	HF	152078.3358	14999.828
Himalayas	HF	60425.3331	17499.8
Himalayas	HF	70477.7082	17499.8
Himalayas	HF	78718.5805	17499.8
Himalayas	HF	84712.1642	17499.8

Himalayas	HF	86789.7771	17499.8
Himalayas	HF	96314.8145	17499.8
Himalayas	HF	99168.7857	17499.8
Himalayas	HF	103366.7357	17499.8
Himalayas	HF	103906.2803	17499.8
Himalayas	HF	107178.9478	17499.8
Himalayas	HF	117377.8056	17499.8
Himalayas	HF	131783.1581	17499.8
Himalayas	HF	135616.122	17499.8
Himalayas	HF	153292.9215	17499.8
Himalayas	HF	156221.3547	17499.8
Himalayas	HF	160275.2633	17499.8
Himalayas	HF	302168.1689	17499.8
Himalayas	HF	47372.5041	19999.771
Himalayas	HF	72817.7692	19999.771
Himalayas	HF	81166.0623	19999.771
Himalayas	HF	86371.0808	19999.771
Himalayas	HF	107252.1892	19999.771
Himalayas	HF	107784.4096	19999.771
Himalayas	HF	128150.3873	19999.771
Himalayas	HF	128199.2148	19999.771
Himalayas	HF	146792.7518	19999.771
Himalayas	HF	212917.4825	19999.771
Himalayas	HF	518846.5946	19999.771
Himalayas	HF	131574.4203	22499.742
Himalayas	HF	134820.2327	22499.742
Himalayas	HF	215035.3781	22499.742
Himalayas	HF	222247.2096	22499.742
Himalayas	HF	298198.4878	22499.742
Himalayas	HF	300331.0318	22499.742
Himalayas	HF	336063.0443	22499.742
Himalayas	HF	452299.5055	22499.742
Himalayas	HF	86827.6185	24999.714
Himalayas	HF	178877.3451	24999.714
Himalayas	HF	185487.3768	24999.714
Himalayas	HF	189844.0164	24999.714
Himalayas	HF	195379.8416	24999.714
Himalayas	HF	267356.556	24999.714
Himalayas	HF	296996.109	24999.714
Himalayas	HF	1334442.719	24999.714
Himalayas	HF	138283.3278	27499.685
Himalayas	HF	139328.2377	27499.685
Himalayas	HF	233838.8736	27499.685
Himalayas	HF	274128.9394	27499.685
Himalayas	HF	338600.857	27499.685
Himalayas	HF	128656.9732	29999.656

Himalayas	HF	136567.0389	29999.656
Himalayas	HF	167776.3981	29999.656
Himalayas	HF	184374.1083	29999.656
Himalayas	HF	240760.1811	29999.656
Himalayas	HF	311857.9993	29999.656
Himalayas	HF	397814.0458	29999.656
Himalayas	HF	400001.5207	29999.656
Himalayas	HF	195940.1379	32499.628
Himalayas	HF	271581.3612	32499.628
Himalayas	HF	301988.7276	32499.628
Himalayas	HF	350530.6519	32499.628
Himalayas	HF	292455.1454	34999.599
Himalayas	HF	294585.248	34999.599
Himalayas	HF	306165.9259	34999.599
Himalayas	HF	345860.2953	34999.599
Himalayas	HF	363039.0536	34999.599
Himalayas	HF	414926.8868	34999.599
Himalayas	HF	477328.5156	34999.599
Himalayas	HF	298801.5083	37499.57
Himalayas	HF	269932.2101	39999.542
Himalayas	HF	291509.1114	39999.542
Himalayas	HF	318864.755	39999.542
Himalayas	HF	358792.276	39999.542
Himalayas	HF	560779.708	39999.542
Himalayas	HF	810011.4717	39999.542
Himalayas	HF	245039.9172	42499.513
Himalayas	HF	293351.1313	42499.513
Himalayas	HF	302567.3343	42499.513
Himalayas	HF	394534.0541	42499.513
Himalayas	HF	413535.3012	42499.513
Himalayas	HF	457521.6137	42499.513
Himalayas	HF	493664.9984	42499.513
Himalayas	HF	423701.2004	44999.484
Himalayas	HF	649992.553	44999.484
Himalayas	HF	823773.521	47499.456
Himalayas	HF	516484.5612	49999.427
Himalayas	HF	875640.6026	49999.427
Himalayas	HF	360565.9374	52499.399
Himalayas	HF	475455.9785	54999.37
Himalayas	HF	722911.6395	57499.341
Himalayas	HF	1694077.271	57499.341
Himalayas	HF	544350.4528	59999.313
Himalayas	HF	685010.4624	59999.313
Himalayas	HF	715889.0149	59999.313
Himalayas	HF	746483.1468	59999.313
Himalayas	HF	610082.1216	64999.255

Himalayas	HF	988520.1687	64999.255
Himalayas	HF	537938.1728	67499.227
Himalayas	HF	569164.6217	67499.227
Himalayas	HF	2012797.984	69999.198
Himalayas	HF	629420.279	72499.169
Himalayas	HF	857105.6587	72499.169
Himalayas	HF	845656.8152	77499.112
Himalayas	HF	1150244.39	77499.112
Himalayas	HF	1259443.578	79999.084
Himalayas	HF	1364613.272	79999.084
Himalayas	HF	590236.1576	82499.055
Himalayas	HF	1163188.578	82499.055
Himalayas	HF	1232106.245	82499.055
Himalayas	HF	1164526.453	84999.026
Himalayas	HF	2416183.255	87498.998
Himalayas	HF	599277.8021	89998.969
Himalayas	HF	1846359.462	89998.969
Himalayas	HF	1244554.833	92498.94
Himalayas	HF	1058007.898	97498.883
Himalayas	HF	969086.7976	99998.854
Himalayas	HF	1501111.952	99998.854
Himalayas	HF	1015730.55	102498.83
Himalayas	HF	1109287.828	104998.8
Himalayas	HF	1014024.027	107498.77
Himalayas	HF	1342769.04	107498.77
Himalayas	HF	1755321.686	109998.74
Himalayas	HF	1164569.177	124998.57
Himalayas	HF	2686322.983	132498.48
Himalayas	HF	4280748.075	132498.48
Himalayas	HF	2490840.603	144998.34
Himalayas	HF	5743485.222	169998.05
Himalayas	HF	4140373.706	172498.02
Himalayas	HF	2663863.523	177497.97
Himalayas	HF	3119190.338	182497.91
Himalayas	HF	3264499.952	194997.77
Himalayas	HF	2660036.663	227497.39
Himalayas	HF	5045950.489	302496.53
Himalayas	HF	9465128.375	322496.31
Himalayas	HF	5928728.461	324996.28
Himalayas	HF	8457965.841	324996.28
Himalayas	HF	6261246.624	334996.16
Himalayas	HF	10995983.64	394995.47
Himalayas	HF	7600661.21	462494.7
Himalayas	HF	12496584.12	582493.33
Himalayas	HF	16116012.87	652492.52
Himalayas	HF	16731186.49	684992.15

Himalayas	Millan	24834.9205	9999.8854
Himalayas	Millan	28113.6916	9999.8854
Himalayas	Millan	31098.2765	9999.8854
Himalayas	Millan	35891.9228	9999.8854
Himalayas	Millan	42919.4301	9999.8854
Himalayas	Millan	44596.657	9999.8854
Himalayas	Millan	46729.201	9999.8854
Himalayas	Millan	51126.1232	9999.8854
Himalayas	Millan	51937.8815	9999.8854
Himalayas	Millan	52102.6745	9999.8854
Himalayas	Millan	52548.2261	9999.8854
Himalayas	Millan	56782.7967	9999.8854
Himalayas	Millan	57918.0376	9999.8854
Himalayas	Millan	59731.9817	9999.8854
Himalayas	Millan	60986.8501	9999.8854
Himalayas	Millan	61965.8428	9999.8854
Himalayas	Millan	61997.5807	9999.8854
Himalayas	Millan	63307.3802	9999.8854
Himalayas	Millan	68164.5022	9999.8854
Himalayas	Millan	71686.1904	9999.8854
Himalayas	Millan	75316.5199	9999.8854
Himalayas	Millan	77042.5744	9999.8854
Himalayas	Millan	88990.6797	9999.8854
Himalayas	Millan	93365.6295	9999.8854
Himalayas	Millan	99182.2133	9999.8854
Himalayas	Millan	99746.1717	9999.8854
Himalayas	Millan	102385.3016	9999.8854
Himalayas	Millan	103717.0734	9999.8854
Himalayas	Millan	109418.3021	9999.8854
Himalayas	Millan	115494.2823	9999.8854
Himalayas	Millan	128666.7388	9999.8854
Himalayas	Millan	154116.8866	9999.8854
Himalayas	Millan	154514.8313	9999.8854
Himalayas	Millan	157637.3541	9999.8854
Himalayas	Millan	176998.7046	9999.8854
Himalayas	Millan	177939.8559	9999.8854
Himalayas	Millan	216783.405	9999.8854
Himalayas	Millan	217462.1082	9999.8854
Himalayas	Millan	225112.167	9999.8854
Himalayas	Millan	232771.9913	9999.8854
Himalayas	Millan	296551.7782	9999.8854
Himalayas	Millan	423282.504	9999.8854
Himalayas	Millan	494337.5981	9999.8854
Himalayas	Millan	37334.7773	12499.857
Himalayas	Millan	46446.0011	12499.857
Himalayas	Millan	51748.6747	12499.857

Himalayas	Millan	51914.6884	12499.857
Himalayas	Millan	53118.2879	12499.857
Himalayas	Millan	65510.7241	12499.857
Himalayas	Millan	82052.2826	12499.857
Himalayas	Millan	86650.6186	12499.857
Himalayas	Millan	88817.3418	12499.857
Himalayas	Millan	103234.9012	12499.857
Himalayas	Millan	112783.742	12499.857
Himalayas	Millan	125479.5194	12499.857
Himalayas	Millan	127212.898	12499.857
Himalayas	Millan	127240.9738	12499.857
Himalayas	Millan	127635.2564	12499.857
Himalayas	Millan	128237.0562	12499.857
Himalayas	Millan	176829.0288	12499.857
Himalayas	Millan	189851.3405	12499.857
Himalayas	Millan	213452.1443	12499.857
Himalayas	Millan	222892.9541	12499.857
Himalayas	Millan	223012.5817	12499.857
Himalayas	Millan	232167.7502	12499.857
Himalayas	Millan	236525.6104	12499.857
Himalayas	Millan	239548.0368	12499.857
Himalayas	Millan	285171.2933	12499.857
Himalayas	Millan	368593.1891	12499.857
Himalayas	Millan	418747.6438	12499.857
Himalayas	Millan	505613.1037	12499.857
Himalayas	Millan	507058.3996	12499.857
Himalayas	Millan	560502.6115	12499.857
Himalayas	Millan	615198.0298	12499.857
Himalayas	Millan	50165.4409	14999.828
Himalayas	Millan	74404.6651	14999.828
Himalayas	Millan	75336.0509	14999.828
Himalayas	Millan	78514.7255	14999.828
Himalayas	Millan	84974.6124	14999.828
Himalayas	Millan	86303.9429	14999.828
Himalayas	Millan	86407.7014	14999.828
Himalayas	Millan	107661.12	14999.828
Himalayas	Millan	107724.5959	14999.828
Himalayas	Millan	112351.0077	14999.828
Himalayas	Millan	129366.1936	14999.828
Himalayas	Millan	153871.5281	14999.828
Himalayas	Millan	157283.3543	14999.828
Himalayas	Millan	171761.9481	14999.828
Himalayas	Millan	186642.1488	14999.828
Himalayas	Millan	192882.3116	14999.828
Himalayas	Millan	224361.4432	14999.828
Himalayas	Millan	245850.4548	14999.828

Himalayas	Millan	303083.6858	14999.828
Himalayas	Millan	319636.2305	14999.828
Himalayas	Millan	344450.3993	14999.828
Himalayas	Millan	358297.8969	14999.828
Himalayas	Millan	370144.685	14999.828
Himalayas	Millan	380569.3703	14999.828
Himalayas	Millan	412724.7636	14999.828
Himalayas	Millan	504867.2626	14999.828
Himalayas	Millan	582473.7954	14999.828
Himalayas	Millan	685232.6278	14999.828
Himalayas	Millan	1092183.532	14999.828
Himalayas	Millan	63851.8075	17499.8
Himalayas	Millan	64670.8899	17499.8
Himalayas	Millan	142727.857	17499.8
Himalayas	Millan	148700.6889	17499.8
Himalayas	Millan	184418.0531	17499.8
Himalayas	Millan	198421.799	17499.8
Himalayas	Millan	256582.7537	17499.8
Himalayas	Millan	291958.325	17499.8
Himalayas	Millan	303647.6442	17499.8
Himalayas	Millan	340613.7734	17499.8
Himalayas	Millan	397804.2803	17499.8
Himalayas	Millan	451060.506	17499.8
Himalayas	Millan	473040.2347	17499.8
Himalayas	Millan	527365.7842	17499.8
Himalayas	Millan	78519.6082	19999.771
Himalayas	Millan	120662.6801	19999.771
Himalayas	Millan	147954.8479	19999.771
Himalayas	Millan	170985.5898	19999.771
Himalayas	Millan	198490.1575	19999.771
Himalayas	Millan	211427.021	19999.771
Himalayas	Millan	220589.5137	19999.771
Himalayas	Millan	220704.2585	19999.771
Himalayas	Millan	333367.7626	19999.771
Himalayas	Millan	422729.5318	19999.771
Himalayas	Millan	455507.4766	19999.771
Himalayas	Millan	525943.6813	19999.771
Himalayas	Millan	718259.5932	19999.771
Himalayas	Millan	777179.8166	19999.771
Himalayas	Millan	820206.6674	19999.771
Himalayas	Millan	1068515.59	19999.771
Himalayas	Millan	96879.9936	22499.742
Himalayas	Millan	179634.1724	22499.742
Himalayas	Millan	204862.1549	22499.742
Himalayas	Millan	254939.7061	22499.742
Himalayas	Millan	279977.2611	22499.742

Himalayas	Millan	286075.824	22499.742
Himalayas	Millan	377898.5025	22499.742
Himalayas	Millan	390370.2834	22499.742
Himalayas	Millan	458003.7859	22499.742
Himalayas	Millan	467653.3335	22499.742
Himalayas	Millan	482048.9205	22499.742
Himalayas	Millan	528802.5353	22499.742
Himalayas	Millan	559999.6876	22499.742
Himalayas	Millan	562129.7902	22499.742
Himalayas	Millan	674555.2599	22499.742
Himalayas	Millan	792886.4237	22499.742
Himalayas	Millan	224142.9398	24999.714
Himalayas	Millan	603149.828	24999.714
Himalayas	Millan	691725.4734	24999.714
Himalayas	Millan	1296897.983	24999.714
Himalayas	Millan	144151.1805	27499.685
Himalayas	Millan	174149.6161	27499.685
Himalayas	Millan	178678.3728	27499.685
Himalayas	Millan	187561.3277	27499.685
Himalayas	Millan	195883.9862	27499.685
Himalayas	Millan	212305.9172	27499.685
Himalayas	Millan	222065.3269	27499.685
Himalayas	Millan	253062.2862	27499.685
Himalayas	Millan	342686.5035	27499.685
Himalayas	Millan	385492.4096	27499.685
Himalayas	Millan	422899.2076	27499.685
Himalayas	Millan	423070.1041	27499.685
Himalayas	Millan	492541.9644	27499.685
Himalayas	Millan	536048.546	27499.685
Himalayas	Millan	632696.6086	27499.685
Himalayas	Millan	288577.016	29999.656
Himalayas	Millan	442012.7581	29999.656
Himalayas	Millan	456506.0003	29999.656
Himalayas	Millan	472924.2692	29999.656
Himalayas	Millan	766307.1384	29999.656
Himalayas	Millan	1042496.601	29999.656
Himalayas	Millan	1252046.202	29999.656
Himalayas	Millan	1579057.837	29999.656
Himalayas	Millan	164895.5717	32499.628
Himalayas	Millan	227762.2831	32499.628
Himalayas	Millan	322044.6502	32499.628
Himalayas	Millan	618879.6283	32499.628
Himalayas	Millan	695043.3064	32499.628
Himalayas	Millan	757556.018	32499.628
Himalayas	Millan	783267.3933	32499.628
Himalayas	Millan	1073633.94	32499.628

Himalayas	Millan	1406806.392	32499.628
Himalayas	Millan	1652257.681	32499.628
Himalayas	Millan	256287.3469	34999.599
Himalayas	Millan	1315528.141	34999.599
Himalayas	Millan	1480892.457	34999.599
Himalayas	Millan	2002126.72	34999.599
Himalayas	Millan	606462.7783	37499.57
Himalayas	Millan	885963.9706	37499.57
Himalayas	Millan	1195956.757	37499.57
Himalayas	Millan	1232136.762	37499.57
Himalayas	Millan	1792530.733	37499.57
Himalayas	Millan	2094827.074	37499.57
Himalayas	Millan	304135.9198	39999.542
Himalayas	Millan	320035.3959	39999.542
Himalayas	Millan	333686.3625	39999.542
Himalayas	Millan	432547.5345	39999.542
Himalayas	Millan	558603.2192	39999.542
Himalayas	Millan	2601348.37	39999.542
Himalayas	Millan	549716.6023	42499.513
Himalayas	Millan	1062976.103	42499.513
Himalayas	Millan	1730635.69	42499.513
Himalayas	Millan	1958784.931	42499.513
Himalayas	Millan	341448.7247	44999.484
Himalayas	Millan	736728.0095	44999.484
Himalayas	Millan	1290764.02	44999.484
Himalayas	Millan	1592906.555	44999.484
Himalayas	Millan	530191.6795	47499.456
Himalayas	Millan	850778.8269	47499.456
Himalayas	Millan	1471351.551	47499.456
Himalayas	Millan	3200672.559	47499.456
Himalayas	Millan	3943900.127	47499.456
Himalayas	Millan	530679.9552	49999.427
Himalayas	Millan	3836708.973	49999.427
Himalayas	Millan	357279.8422	52499.399
Himalayas	Millan	1090302.45	52499.399
Himalayas	Millan	1226925.64	52499.399
Himalayas	Millan	1314615.065	52499.399
Himalayas	Millan	1925689.607	52499.399
Himalayas	Millan	2009491.138	52499.399
Himalayas	Millan	2674627.56	52499.399
Himalayas	Millan	223587.5263	54999.37
Himalayas	Millan	572028.3584	54999.37
Himalayas	Millan	695801.3544	57499.341
Himalayas	Millan	807914.3277	57499.341
Himalayas	Millan	1523295.536	57499.341
Himalayas	Millan	2137689.132	57499.341

Himalayas	Millan	2297490.768	57499.341
Himalayas	Millan	443013.7232	59999.313
Himalayas	Millan	475608.5646	59999.313
Himalayas	Millan	476246.9851	59999.313
Himalayas	Millan	1133423.294	59999.313
Himalayas	Millan	1945110.772	59999.313
Himalayas	Millan	2439347.053	59999.313
Himalayas	Millan	3047828.851	59999.313
Himalayas	Millan	486982.946	62499.284
Himalayas	Millan	926395.6363	64999.255
Himalayas	Millan	1729269.739	64999.255
Himalayas	Millan	3190302.804	64999.255
Himalayas	Millan	4893731.774	64999.255
Himalayas	Millan	737325.5369	67499.227
Himalayas	Millan	682079.5878	72499.169
Himalayas	Millan	869460.2535	72499.169
Himalayas	Millan	2234018.594	82499.055
Himalayas	Millan	4850873.379	87498.998
Himalayas	Millan	2845403.191	89998.969
Himalayas	Millan	732868.8008	92498.94
Himalayas	Millan	3709821.999	94998.912
Himalayas	Millan	1091364.449	99998.854
Himalayas	Millan	4596188.797	107498.77
Himalayas	Millan	1788602.555	112498.71
Himalayas	Millan	5694188.912	114998.68
Himalayas	Millan	1339522.007	137498.42
Himalayas	Millan	1785146.784	159998.17
Himalayas	Millan	9167663.521	167498.08
Himalayas	Millan	1932756.177	174998
Himalayas	Millan	3227979.375	174998
Himalayas	Millan	3941965.335	194997.77
Himalayas	Millan	7915484.264	209997.59
Himalayas	Millan	2172333.51	212497.57
Himalayas	Millan	7096365.23	212497.57
Himalayas	Millan	23612136.7	212497.57
Himalayas	Millan	19435962.63	214997.54
Himalayas	Millan	13977961.8	269996.91
Himalayas	Millan	10405796.31	287496.71
Himalayas	Millan	6388436.329	329996.22
Himalayas	Millan	6673212.119	344996.05
Himalayas	Millan	9728431.022	364995.82
Himalayas	Millan	10528431.62	372495.73
Himalayas	Millan	11113451.78	404995.36
Himalayas	Millan	19523637.4	489994.39
Himalayas	Millan	23542684.37	494994.33
Himalayas	Millan	23941293.09	559993.58

Himalayas	Millan	15293899.49	689992.09
Himalayas	OGGM	19793.4744	9999.8854
Himalayas	OGGM	19860.6123	9999.8854
Himalayas	OGGM	24777.5482	9999.8854
Himalayas	OGGM	27564.3815	9999.8854
Himalayas	OGGM	28038.0088	9999.8854
Himalayas	OGGM	31828.2486	9999.8854
Himalayas	OGGM	32094.3589	9999.8854
Himalayas	OGGM	35254.723	9999.8854
Himalayas	OGGM	51102.9301	9999.8854
Himalayas	OGGM	67417.4405	9999.8854
Himalayas	OGGM	154186.4659	9999.8854
Himalayas	OGGM	180820.6822	9999.8854
Himalayas	OGGM	19863.0537	12499.857
Himalayas	OGGM	38916.7905	12499.857
Himalayas	OGGM	40176.5417	12499.857
Himalayas	OGGM	57394.362	12499.857
Himalayas	OGGM	70504.5633	12499.857
Himalayas	OGGM	91635.913	12499.857
Himalayas	OGGM	38435.8389	14999.828
Himalayas	OGGM	50436.4339	14999.828
Himalayas	OGGM	55148.2939	14999.828
Himalayas	OGGM	58059.6375	14999.828
Himalayas	OGGM	59636.7679	14999.828
Himalayas	OGGM	74728.1477	14999.828
Himalayas	OGGM	75039.4235	14999.828
Himalayas	OGGM	76695.8986	14999.828
Himalayas	OGGM	85304.1985	14999.828
Himalayas	OGGM	98781.2169	14999.828
Himalayas	OGGM	64585.4417	17499.8
Himalayas	OGGM	66139.379	17499.8
Himalayas	OGGM	72485.7418	17499.8
Himalayas	OGGM	74382.6927	17499.8
Himalayas	OGGM	81454.1449	17499.8
Himalayas	OGGM	83886.9784	17499.8
Himalayas	OGGM	90136.9068	17499.8
Himalayas	OGGM	93243.5606	17499.8
Himalayas	OGGM	107163.0789	17499.8
Himalayas	OGGM	129443.0971	17499.8
Himalayas	OGGM	152735.0665	17499.8
Himalayas	OGGM	247804.7781	17499.8
Himalayas	OGGM	262001.3928	17499.8
Himalayas	OGGM	96187.8628	19999.771
Himalayas	OGGM	125533.2297	19999.771
Himalayas	OGGM	174647.6573	19999.771
Himalayas	OGGM	199878.0811	19999.771

Himalayas	OGGM	485576.7121	19999.771
Himalayas	OGGM	74830.6856	22499.742
Himalayas	OGGM	100141.6749	22499.742
Himalayas	OGGM	114007.4829	22499.742
Himalayas	OGGM	165463.1922	22499.742
Himalayas	OGGM	226606.2905	22499.742
Himalayas	OGGM	86662.8255	24999.714
Himalayas	OGGM	193751.4423	24999.714
Himalayas	OGGM	221133.9411	24999.714
Himalayas	OGGM	253179.4724	24999.714
Himalayas	OGGM	274966.3321	24999.714
Himalayas	OGGM	417152.2031	24999.714
Himalayas	OGGM	101938.5294	27499.685
Himalayas	OGGM	104448.2662	27499.685
Himalayas	OGGM	115782.3649	27499.685
Himalayas	OGGM	120965.411	27499.685
Himalayas	OGGM	166777.8744	27499.685
Himalayas	OGGM	252345.7417	27499.685
Himalayas	OGGM	289817.2362	27499.685
Himalayas	OGGM	336550.0992	27499.685
Himalayas	OGGM	403169.209	27499.685
Himalayas	OGGM	273551.5534	29999.656
Himalayas	OGGM	319885.2511	29999.656
Himalayas	OGGM	359243.931	29999.656
Himalayas	OGGM	405761.9528	29999.656
Himalayas	OGGM	1462594.327	29999.656
Himalayas	OGGM	155204.5207	32499.628
Himalayas	OGGM	203818.4656	32499.628
Himalayas	OGGM	211394.0624	32499.628
Himalayas	OGGM	201014.5427	34999.599
Himalayas	OGGM	202629.5144	34999.599
Himalayas	OGGM	244125.621	34999.599
Himalayas	OGGM	293789.3587	34999.599
Himalayas	OGGM	344017.0547	34999.599
Himalayas	OGGM	468339.3608	34999.599
Himalayas	OGGM	665157.1742	34999.599
Himalayas	OGGM	166840.1295	37499.57
Himalayas	OGGM	175395.9397	37499.57
Himalayas	OGGM	278683.3306	39999.542
Himalayas	OGGM	389976.0008	39999.542
Himalayas	OGGM	408637.8964	39999.542
Himalayas	OGGM	406590.8007	42499.513
Himalayas	OGGM	561216.7147	42499.513
Himalayas	OGGM	760158.5272	42499.513
Himalayas	OGGM	959316.4017	42499.513
Himalayas	OGGM	391754.5449	44999.484

Himalayas	OGGM	655373.3508	44999.484
Himalayas	OGGM	708583.1904	44999.484
Himalayas	OGGM	1156830.008	47499.456
Himalayas	OGGM	566979.5881	49999.427
Himalayas	OGGM	754683.7364	49999.427
Himalayas	OGGM	791858.6035	49999.427
Himalayas	OGGM	1646117.615	49999.427
Himalayas	OGGM	434356.5959	52499.399
Himalayas	OGGM	599331.5124	52499.399
Himalayas	OGGM	1274320.117	52499.399
Himalayas	OGGM	737928.5573	54999.37
Himalayas	OGGM	914941.9101	59999.313
Himalayas	OGGM	1471653.061	59999.313
Himalayas	OGGM	548229.8029	62499.284
Himalayas	OGGM	695440.0304	64999.255
Himalayas	OGGM	1250489.824	67499.227
Himalayas	OGGM	804703.9153	69999.198
Himalayas	OGGM	815975.7588	72499.169
Himalayas	OGGM	2234571.567	72499.169
Himalayas	OGGM	1169354.279	74999.141
Himalayas	OGGM	1282215.534	74999.141
Himalayas	OGGM	1925407.628	74999.141
Himalayas	OGGM	657477.8189	77499.112
Himalayas	OGGM	1573827.184	79999.084
Himalayas	OGGM	1098045.281	82499.055
Himalayas	OGGM	1820914.196	82499.055
Himalayas	OGGM	581376.3958	89998.969
Himalayas	OGGM	935614.2807	89998.969
Himalayas	OGGM	2727909.42	92498.94
Himalayas	OGGM	1196543.908	94998.912
Himalayas	OGGM	1261451.612	97498.883
Himalayas	OGGM	3114441.857	97498.883
Himalayas	OGGM	1615850.628	107498.77
Himalayas	OGGM	1869710.024	109998.74
Himalayas	OGGM	5215252.749	117498.65
Himalayas	OGGM	2479297.767	119998.63
Himalayas	OGGM	2839819.759	124998.57
Himalayas	OGGM	2279781.01	134998.45
Himalayas	OGGM	2439389.777	134998.45
Himalayas	OGGM	3965226.787	144998.34
Himalayas	OGGM	3159514.583	152498.25
Himalayas	OGGM	1878978.717	154998.22
Himalayas	OGGM	4232212.254	169998.05
Himalayas	OGGM	5976910.282	172498.02
Himalayas	OGGM	7223241.218	172498.02
Himalayas	OGGM	4426650.944	177497.97

Himalayas	OGGM	6436826.888	182497.91
Himalayas	OGGM	7315102.959	184997.88
Himalayas	OGGM	10062626.41	189997.82
Himalayas	OGGM	4420089.74	202497.68
Himalayas	OGGM	7863397.458	219997.48
Himalayas	OGGM	4238346.217	224997.42
Himalayas	OGGM	12444342.29	227497.39
Himalayas	OGGM	5253064.816	237497.28
Himalayas	OGGM	6946364.507	242497.22
Himalayas	OGGM	3157007.287	244997.19
Himalayas	OGGM	8116541.53	244997.19
Himalayas	OGGM	12921746.49	244997.19
Himalayas	OGGM	11688060.67	254997.08
Himalayas	OGGM	11068798.97	269996.91
Himalayas	OGGM	8052808.13	274996.85
Himalayas	OGGM	5083982.28	294996.62
Himalayas	OGGM	15265203.52	297496.59
Himalayas	OGGM	5590597.57	299996.56
Himalayas	OGGM	14174293.17	329996.22
Himalayas	OGGM	6396874.953	362495.85
Himalayas	OGGM	11675579.12	364995.82
Himalayas	OGGM	11327847.51	394995.47
Himalayas	OGGM	11777358.96	467494.64
Himalayas	OGGM	29851141.15	502494.24
Himalayas	OGGM	25830116.66	534993.87
Himalayas	OGGM	14996323.55	547493.73
Himalayas	OGGM	22155871.65	577493.38
Himalayas	OGGM	33899496.87	762491.26
Himalayas	OGGM	73921246.59	897489.72
Himalayas	OGGM	94019289.64	1732480.2
Peruvian Andes	Farinotti’s Ensemble	17590.7626	9996.7761
Peruvian Andes	Farinotti’s Ensemble	24356.1589	9996.7761
Peruvian Andes	Farinotti’s Ensemble	26599.0879	9996.7761
Peruvian Andes	Farinotti’s Ensemble	28835.9154	9996.7761
Peruvian Andes	Farinotti’s Ensemble	34798.348	9996.7761
Peruvian Andes	Farinotti’s Ensemble	36730.0981	9996.7761
Peruvian Andes	Farinotti’s Ensemble	37005.888	9996.7761
Peruvian Andes	Farinotti’s Ensemble	39916.3264	9996.7761

Peruvian Andes	Farinotti's Ensemble	44261.8488	9996.7761
Peruvian Andes	Farinotti's Ensemble	44926.9175	9996.7761
Peruvian Andes	Farinotti's Ensemble	50177.9097	9996.7761
Peruvian Andes	Farinotti's Ensemble	50362.1764	9996.7761
Peruvian Andes	Farinotti's Ensemble	51293.2726	9996.7761
Peruvian Andes	Farinotti's Ensemble	56846.9015	9996.7761
Peruvian Andes	Farinotti's Ensemble	62135.7232	9996.7761
Peruvian Andes	Farinotti's Ensemble	73268.6076	9996.7761
Peruvian Andes	Farinotti's Ensemble	94637.4486	9996.7761
Peruvian Andes	Farinotti's Ensemble	180123.7957	9996.7761
Peruvian Andes	Farinotti's Ensemble	35057.0536	12495.97
Peruvian Andes	Farinotti's Ensemble	37690.4817	12495.97
Peruvian Andes	Farinotti's Ensemble	40369.0612	12495.97
Peruvian Andes	Farinotti's Ensemble	48326.7	12495.97
Peruvian Andes	Farinotti's Ensemble	56599.1787	12495.97
Peruvian Andes	Farinotti's Ensemble	66702.1217	12495.97
Peruvian Andes	Farinotti's Ensemble	70482.6408	12495.97
Peruvian Andes	Farinotti's Ensemble	143950.1588	12495.97
Peruvian Andes	Farinotti's Ensemble	443405.5878	12495.97
Peruvian Andes	Farinotti's Ensemble	49287.0837	14995.164
Peruvian Andes	Farinotti's Ensemble	57865.86	14995.164
Peruvian Andes	Farinotti's Ensemble	61353.5048	14995.164
Peruvian Andes	Farinotti's Ensemble	65595.3009	14995.164

Peruvian Andes	Farinotti's Ensemble	66472.7035	14995.164
Peruvian Andes	Farinotti's Ensemble	83043.2873	14995.164
Peruvian Andes	Farinotti's Ensemble	132341.3537	14995.164
Peruvian Andes	Farinotti's Ensemble	328766.0448	14995.164
Peruvian Andes	Farinotti's Ensemble	49997.3038	17494.358
Peruvian Andes	Farinotti's Ensemble	92327.4026	17494.358
Peruvian Andes	Farinotti's Ensemble	117213.1759	17494.358
Peruvian Andes	Farinotti's Ensemble	118211.3891	17494.358
Peruvian Andes	Farinotti's Ensemble	80893.1018	19993.552
Peruvian Andes	Farinotti's Ensemble	82613.7383	19993.552
Peruvian Andes	Farinotti's Ensemble	111251.9636	19993.552
Peruvian Andes	Farinotti's Ensemble	108642.9417	22492.746
Peruvian Andes	Farinotti's Ensemble	118429.8245	22492.746
Peruvian Andes	Farinotti's Ensemble	120869.2234	22492.746
Peruvian Andes	Farinotti's Ensemble	148481.1683	22492.746
Peruvian Andes	Farinotti's Ensemble	100959.8726	24991.94
Peruvian Andes	Farinotti's Ensemble	155192.871	24991.94
Peruvian Andes	Farinotti's Ensemble	488738.8684	24991.94
Peruvian Andes	Farinotti's Ensemble	152763.2346	27491.134
Peruvian Andes	Farinotti's Ensemble	187893.5068	27491.134
Peruvian Andes	Farinotti's Ensemble	373912.6181	27491.134
Peruvian Andes	Farinotti's Ensemble	207309.8525	32489.522
Peruvian Andes	Farinotti's Ensemble	315376.8081	34988.716

Peruvian Andes	Farinotti's Ensemble	443353.1145	37487.91
Peruvian Andes	Farinotti's Ensemble	441088.2199	42486.298
Peruvian Andes	Farinotti's Ensemble	215102.7495	44985.492
Peruvian Andes	Farinotti's Ensemble	254992.2291	47484.686
Peruvian Andes	Farinotti's Ensemble	556459.9486	47484.686
Peruvian Andes	Farinotti's Ensemble	171459.5977	49983.88
Peruvian Andes	Farinotti's Ensemble	1144416.088	49983.88
Peruvian Andes	Farinotti's Ensemble	511347.544	54982.269
Peruvian Andes	Farinotti's Ensemble	643392.3625	59980.657
Peruvian Andes	Farinotti's Ensemble	628040.868	69977.433
Peruvian Andes	Farinotti's Ensemble	633923.9805	69977.433
Peruvian Andes	Farinotti's Ensemble	1071908.953	69977.433
Peruvian Andes	Farinotti's Ensemble	651033.9411	79974.209
Peruvian Andes	Farinotti's Ensemble	885544.4942	79974.209
Peruvian Andes	Farinotti's Ensemble	542993.8324	84972.597
Peruvian Andes	Farinotti's Ensemble	747771.5426	84972.597
Peruvian Andes	Farinotti's Ensemble	983066.7547	84972.597
Peruvian Andes	Farinotti's Ensemble	3023152.245	87471.791
Peruvian Andes	Farinotti's Ensemble	1280868.664	92470.179
Peruvian Andes	Farinotti's Ensemble	862181.6673	97468.567
Peruvian Andes	Farinotti's Ensemble	2684703.044	99967.761
Peruvian Andes	Farinotti's Ensemble	1499664.071	107465.34
Peruvian Andes	Farinotti's Ensemble	2805743.11	187439.55

Peruvian Andes	Farinotti's Ensemble	3046729.847	189938.75
Peruvian Andes	Farinotti's Ensemble	2132794.85	207433.1
Peruvian Andes	GlabTop2	26027.9831	9996.7761
Peruvian Andes	GlabTop2	28823.7123	9996.7761
Peruvian Andes	GlabTop2	31200.8754	9996.7761
Peruvian Andes	GlabTop2	37138.9018	9996.7761
Peruvian Andes	GlabTop2	37984.5763	9996.7761
Peruvian Andes	GlabTop2	40508.1765	9996.7761
Peruvian Andes	GlabTop2	47500.5504	9996.7761
Peruvian Andes	GlabTop2	49514.0612	9996.7761
Peruvian Andes	GlabTop2	54732.105	9996.7761
Peruvian Andes	GlabTop2	74783.0117	9996.7761
Peruvian Andes	GlabTop2	84050.0427	9996.7761
Peruvian Andes	GlabTop2	105522.6101	9996.7761
Peruvian Andes	GlabTop2	114385.7186	9996.7761
Peruvian Andes	GlabTop2	124186.0248	9996.7761
Peruvian Andes	GlabTop2	36343.2599	12495.97
Peruvian Andes	GlabTop2	40051.7808	12495.97
Peruvian Andes	GlabTop2	45821.4045	12495.97
Peruvian Andes	GlabTop2	52393.9919	12495.97
Peruvian Andes	GlabTop2	56604.0599	12495.97
Peruvian Andes	GlabTop2	67416.0028	12495.97
Peruvian Andes	GlabTop2	88427.2932	12495.97

Peruvian Andes	GlabTop2	53776.6026	14995.164
Peruvian Andes	GlabTop2	71450.3463	14995.164
Peruvian Andes	GlabTop2	77291.9682	14995.164
Peruvian Andes	GlabTop2	80507.484	14995.164
Peruvian Andes	GlabTop2	98315.4617	14995.164
Peruvian Andes	GlabTop2	125812.6975	14995.164
Peruvian Andes	GlabTop2	132863.6462	14995.164
Peruvian Andes	GlabTop2	152265.3483	14995.164
Peruvian Andes	GlabTop2	227346.1156	14995.164
Peruvian Andes	GlabTop2	65273.1392	17494.358
Peruvian Andes	GlabTop2	95213.4347	17494.358
Peruvian Andes	GlabTop2	181353.8678	17494.358
Peruvian Andes	GlabTop2	90520.1241	19993.552
Peruvian Andes	GlabTop2	131847.1284	19993.552
Peruvian Andes	GlabTop2	255333.9158	19993.552
Peruvian Andes	GlabTop2	128602.3252	22492.746
Peruvian Andes	GlabTop2	225522.973	22492.746
Peruvian Andes	GlabTop2	165342.1857	27491.134
Peruvian Andes	GlabTop2	222406.3024	32489.522
Peruvian Andes	GlabTop2	337359.4649	32489.522
Peruvian Andes	GlabTop2	267711.5159	34988.716
Peruvian Andes	GlabTop2	486879.1166	37487.91
Peruvian Andes	GlabTop2	448925.048	39987.104

Peruvian Andes	GlabTop2	226362.546	44985.492
Peruvian Andes	GlabTop2	574752.3892	44985.492
Peruvian Andes	GlabTop2	789656.2283	44985.492
Peruvian Andes	GlabTop2	459957.867	47484.686
Peruvian Andes	GlabTop2	992158.0611	49983.88
Peruvian Andes	GlabTop2	354080.1468	57481.463
Peruvian Andes	GlabTop2	1366696.698	72476.627
Peruvian Andes	GlabTop2	1457962.431	74975.821
Peruvian Andes	GlabTop2	3315290.698	74975.821
Peruvian Andes	GlabTop2	2055236.854	87471.791
Peruvian Andes	GlabTop2	1489395.165	99967.761
Peruvian Andes	GlabTop2	714569.3595	102466.95
Peruvian Andes	GlabTop2	1434245.715	117462.12
Peruvian Andes	GlabTop2	2224508.437	132457.28
Peruvian Andes	GlabTop2	2297264.514	134956.48
Peruvian Andes	GlabTop2	4119992.123	149951.64
Peruvian Andes	GlabTop2	11900308.94	319896.83
Peruvian Andes	HF	25209.1553	9996.7761
Peruvian Andes	HF	30458.9271	9996.7761
Peruvian Andes	HF	39686.9082	9996.7761
Peruvian Andes	HF	43949.4496	9996.7761
Peruvian Andes	HF	45563.9191	9996.7761
Peruvian Andes	HF	52442.8042	9996.7761

Peruvian Andes	HF	56832.2578	9996.7761
Peruvian Andes	HF	57284.9927	9996.7761
Peruvian Andes	HF	59313.1472	9996.7761
Peruvian Andes	HF	64722.7796	9996.7761
Peruvian Andes	HF	68506.9596	9996.7761
Peruvian Andes	HF	69669.9146	9996.7761
Peruvian Andes	HF	71194.0813	9996.7761
Peruvian Andes	HF	78742.9163	9996.7761
Peruvian Andes	HF	82694.2788	9996.7761
Peruvian Andes	HF	18713.4474	12495.97
Peruvian Andes	HF	31685.3383	12495.97
Peruvian Andes	HF	40987.7582	12495.97
Peruvian Andes	HF	42969.541	12495.97
Peruvian Andes	HF	43263.6356	12495.97
Peruvian Andes	HF	44819.5303	12495.97
Peruvian Andes	HF	59768.3227	12495.97
Peruvian Andes	HF	62542.0863	12495.97
Peruvian Andes	HF	63157.1224	12495.97
Peruvian Andes	HF	81807.1137	12495.97
Peruvian Andes	HF	109990.1635	12495.97
Peruvian Andes	HF	76262.027	14995.164
Peruvian Andes	HF	80572.1604	14995.164
Peruvian Andes	HF	87662.1591	14995.164

Peruvian Andes	HF	92423.807	14995.164
Peruvian Andes	HF	96190.9027	14995.164
Peruvian Andes	HF	118039.3255	14995.164
Peruvian Andes	HF	118479.8572	14995.164
Peruvian Andes	HF	66087.0857	17494.358
Peruvian Andes	HF	72591.3357	17494.358
Peruvian Andes	HF	102769.5917	17494.358
Peruvian Andes	HF	116111.2363	17494.358
Peruvian Andes	HF	113038.4968	19993.552
Peruvian Andes	HF	116958.1312	19993.552
Peruvian Andes	HF	143170.381	19993.552
Peruvian Andes	HF	149166.9822	19993.552
Peruvian Andes	HF	159861.7754	19993.552
Peruvian Andes	HF	204955.8754	19993.552
Peruvian Andes	HF	282815.2876	19993.552
Peruvian Andes	HF	72643.809	22492.746
Peruvian Andes	HF	85682.8169	22492.746
Peruvian Andes	HF	96172.5981	22492.746
Peruvian Andes	HF	106453.7063	22492.746
Peruvian Andes	HF	119580.5765	22492.746
Peruvian Andes	HF	196028.0905	22492.746
Peruvian Andes	HF	203814.8859	22492.746
Peruvian Andes	HF	240581.5933	22492.746

Peruvian Andes	HF	266774.3181	22492.746
Peruvian Andes	HF	451344.9219	22492.746
Peruvian Andes	HF	86789.6377	24991.94
Peruvian Andes	HF	157253.9738	24991.94
Peruvian Andes	HF	181990.8694	24991.94
Peruvian Andes	HF	276928.5141	24991.94
Peruvian Andes	HF	148389.645	27491.134
Peruvian Andes	HF	190608.6956	27491.134
Peruvian Andes	HF	243966.732	27491.134
Peruvian Andes	HF	466447.4733	27491.134
Peruvian Andes	HF	149841.8134	29990.328
Peruvian Andes	HF	194651.5813	29990.328
Peruvian Andes	HF	279915.832	29990.328
Peruvian Andes	HF	378350.884	29990.328
Peruvian Andes	HF	442323.1732	32489.522
Peruvian Andes	HF	450307.6588	32489.522
Peruvian Andes	HF	164779.623	34988.716
Peruvian Andes	HF	224288.0197	34988.716
Peruvian Andes	HF	362245.2382	34988.716
Peruvian Andes	HF	270979.5049	37487.91
Peruvian Andes	HF	296911.0835	37487.91
Peruvian Andes	HF	315378.0284	39987.104
Peruvian Andes	HF	303077.3078	47484.686

Peruvian Andes	HF	425767.2331	47484.686
Peruvian Andes	HF	456050.4357	49983.88
Peruvian Andes	HF	510564.1053	49983.88
Peruvian Andes	HF	410253.4374	52483.075
Peruvian Andes	HF	574254.5029	52483.075
Peruvian Andes	HF	926121.0081	64979.045
Peruvian Andes	HF	1109904.512	72476.627
Peruvian Andes	HF	1118275.836	102466.95
Peruvian Andes	HF	2384476.379	117462.12
Peruvian Andes	HF	2382976.619	119961.31
Peruvian Andes	HF	2235928.094	154950.03
Peruvian Andes	HF	3686499.11	232425.04
Peruvian Andes	HF	5266414.399	254917.79
Peruvian Andes	Millan	37701.4645	9996.7761
Peruvian Andes	Millan	37824.7158	9996.7761
Peruvian Andes	Millan	42613.2106	9996.7761
Peruvian Andes	Millan	44070.2602	9996.7761
Peruvian Andes	Millan	45703.0344	9996.7761
Peruvian Andes	Millan	45867.7762	9996.7761
Peruvian Andes	Millan	50663.5929	9996.7761
Peruvian Andes	Millan	62437.1397	9996.7761
Peruvian Andes	Millan	63680.6352	9996.7761
Peruvian Andes	Millan	81102.9951	9996.7761

Peruvian Andes	Millan	85084.8652	9996.7761
Peruvian Andes	Millan	89371.8128	9996.7761
Peruvian Andes	Millan	97115.8974	9996.7761
Peruvian Andes	Millan	107317.6855	9996.7761
Peruvian Andes	Millan	118579.9226	9996.7761
Peruvian Andes	Millan	165915.7312	9996.7761
Peruvian Andes	Millan	228908.1118	9996.7761
Peruvian Andes	Millan	253641.3464	9996.7761
Peruvian Andes	Millan	319771.1429	9996.7761
Peruvian Andes	Millan	47616.4798	12495.97
Peruvian Andes	Millan	53464.2034	12495.97
Peruvian Andes	Millan	55027.4199	12495.97
Peruvian Andes	Millan	87841.5446	12495.97
Peruvian Andes	Millan	93440.3249	12495.97
Peruvian Andes	Millan	102482.8189	12495.97
Peruvian Andes	Millan	136468.4408	12495.97
Peruvian Andes	Millan	152456.9369	12495.97
Peruvian Andes	Millan	156862.2545	12495.97
Peruvian Andes	Millan	193414.1873	12495.97
Peruvian Andes	Millan	215190.6118	12495.97
Peruvian Andes	Millan	93496.4592	14995.164
Peruvian Andes	Millan	102137.4713	14995.164
Peruvian Andes	Millan	144322.3532	14995.164

Peruvian Andes	Millan	148584.8946	14995.164
Peruvian Andes	Millan	189720.3102	14995.164
Peruvian Andes	Millan	198589.5203	14995.164
Peruvian Andes	Millan	212034.8912	14995.164
Peruvian Andes	Millan	219517.8296	14995.164
Peruvian Andes	Millan	222071.9375	14995.164
Peruvian Andes	Millan	294294.7398	14995.164
Peruvian Andes	Millan	359951.0562	14995.164
Peruvian Andes	Millan	641912.127	14995.164
Peruvian Andes	Millan	113504.6551	17494.358
Peruvian Andes	Millan	151279.3381	17494.358
Peruvian Andes	Millan	158802.5467	17494.358
Peruvian Andes	Millan	174428.6109	17494.358
Peruvian Andes	Millan	427944.2654	17494.358
Peruvian Andes	Millan	633462.7035	17494.358
Peruvian Andes	Millan	118997.2685	19993.552
Peruvian Andes	Millan	144906.8815	19993.552
Peruvian Andes	Millan	150035.8427	19993.552
Peruvian Andes	Millan	163027.2585	19993.552
Peruvian Andes	Millan	215236.9836	19993.552
Peruvian Andes	Millan	235686.9315	19993.552
Peruvian Andes	Millan	328007.0123	19993.552
Peruvian Andes	Millan	828931.8922	19993.552

Peruvian Andes	Millan	201506.0602	22492.746
Peruvian Andes	Millan	243928.9025	22492.746
Peruvian Andes	Millan	257596.3698	22492.746
Peruvian Andes	Millan	269451.6773	22492.746
Peruvian Andes	Millan	127893.3253	24991.94
Peruvian Andes	Millan	154302.045	24991.94
Peruvian Andes	Millan	187729.9853	24991.94
Peruvian Andes	Millan	274712.4319	24991.94
Peruvian Andes	Millan	347818.7383	24991.94
Peruvian Andes	Millan	351106.2523	24991.94
Peruvian Andes	Millan	352111.7874	24991.94
Peruvian Andes	Millan	458980.399	24991.94
Peruvian Andes	Millan	509939.3068	24991.94
Peruvian Andes	Millan	158994.1353	27491.134
Peruvian Andes	Millan	576009.3081	27491.134
Peruvian Andes	Millan	971372.528	27491.134
Peruvian Andes	Millan	388119.4622	29990.328
Peruvian Andes	Millan	283867.1944	32489.522
Peruvian Andes	Millan	480193.0404	32489.522
Peruvian Andes	Millan	915919.22	32489.522
Peruvian Andes	Millan	259964.9907	37487.91
Peruvian Andes	Millan	441044.2888	39987.104
Peruvian Andes	Millan	549338.2219	39987.104

Peruvian Andes	Millan	711362.3859	39987.104
Peruvian Andes	Millan	279590.0093	42486.298
Peruvian Andes	Millan	1035316.75	42486.298
Peruvian Andes	Millan	1745859.088	42486.298
Peruvian Andes	Millan	1211503.827	44985.492
Peruvian Andes	Millan	469669.0906	49983.88
Peruvian Andes	Millan	629115.9608	49983.88
Peruvian Andes	Millan	1181985.759	57481.463
Peruvian Andes	Millan	823890.7933	62479.851
Peruvian Andes	Millan	1323722.276	62479.851
Peruvian Andes	Millan	6479987.872	67478.239
Peruvian Andes	Millan	1094667.727	87471.791
Peruvian Andes	Millan	2559460.231	92470.179
Peruvian Andes	Millan	3672256.877	94969.373
Peruvian Andes	Millan	1215588.203	99967.761
Peruvian Andes	Millan	903065.6992	102466.95
Peruvian Andes	Millan	5601141.657	109964.54
Peruvian Andes	Millan	3567263.881	124959.7
Peruvian Andes	Millan	2256120.556	127458.9
Peruvian Andes	Millan	2956851.605	129958.09
Peruvian Andes	Millan	2279867.781	134956.48
Peruvian Andes	Millan	2486220.911	149951.64
Peruvian Andes	Millan	5593736.818	157449.22

Peruvian Andes	Millan	5173353.591	212431.49
Peruvian Andes	Millan	7456338.042	222428.27
Peruvian Andes	Millan	5833073.696	299903.28
Peruvian Andes	Millan	11811480.16	344888.78
Peruvian Andes	OGGM	27923.1238	9996.7761
Peruvian Andes	OGGM	30056.225	9996.7761
Peruvian Andes	OGGM	30083.0718	9996.7761
Peruvian Andes	OGGM	32450.4724	9996.7761
Peruvian Andes	OGGM	39634.4349	9996.7761
Peruvian Andes	OGGM	42516.8061	9996.7761
Peruvian Andes	OGGM	46753.721	9996.7761
Peruvian Andes	OGGM	46802.5334	9996.7761
Peruvian Andes	OGGM	58753.0251	9996.7761
Peruvian Andes	OGGM	61003.276	9996.7761
Peruvian Andes	OGGM	67392.8169	9996.7761
Peruvian Andes	OGGM	69525.9181	9996.7761
Peruvian Andes	OGGM	70325.2208	9996.7761
Peruvian Andes	OGGM	73584.6677	9996.7761
Peruvian Andes	OGGM	402870.5644	9996.7761
Peruvian Andes	OGGM	32653.0438	12495.97
Peruvian Andes	OGGM	40748.5775	12495.97
Peruvian Andes	OGGM	43726.1329	12495.97
Peruvian Andes	OGGM	50432.9544	12495.97

Peruvian Andes	OGGM	54300.1154	12495.97
Peruvian Andes	OGGM	72470.5251	12495.97
Peruvian Andes	OGGM	105073.5362	12495.97
Peruvian Andes	OGGM	107886.3497	12495.97
Peruvian Andes	OGGM	112904.2627	12495.97
Peruvian Andes	OGGM	117240.0227	12495.97
Peruvian Andes	OGGM	170130.6805	12495.97
Peruvian Andes	OGGM	564573.787	12495.97
Peruvian Andes	OGGM	60727.486	14995.164
Peruvian Andes	OGGM	61958.7784	14995.164
Peruvian Andes	OGGM	64333.5008	14995.164
Peruvian Andes	OGGM	78275.5378	14995.164
Peruvian Andes	OGGM	102100.862	14995.164
Peruvian Andes	OGGM	106071.7494	14995.164
Peruvian Andes	OGGM	128064.1687	14995.164
Peruvian Andes	OGGM	136411.0862	14995.164
Peruvian Andes	OGGM	492879.3788	14995.164
Peruvian Andes	OGGM	63214.4769	17494.358
Peruvian Andes	OGGM	102952.6381	17494.358
Peruvian Andes	OGGM	103688.4848	17494.358
Peruvian Andes	OGGM	69392.9043	19993.552
Peruvian Andes	OGGM	83897.504	19993.552
Peruvian Andes	OGGM	144900.78	19993.552

Peruvian Andes	OGGM	180040.8146	19993.552
Peruvian Andes	OGGM	643857.3005	19993.552
Peruvian Andes	OGGM	75659.194	22492.746
Peruvian Andes	OGGM	92172.4233	22492.746
Peruvian Andes	OGGM	150307.9717	22492.746
Peruvian Andes	OGGM	297513.9165	22492.746
Peruvian Andes	OGGM	72791.4665	24991.94
Peruvian Andes	OGGM	111181.1856	24991.94
Peruvian Andes	OGGM	177081.5639	24991.94
Peruvian Andes	OGGM	301959.5043	24991.94
Peruvian Andes	OGGM	447549.7591	24991.94
Peruvian Andes	OGGM	135155.3876	27491.134
Peruvian Andes	OGGM	155458.8984	27491.134
Peruvian Andes	OGGM	201528.0258	27491.134
Peruvian Andes	OGGM	262898.6149	27491.134
Peruvian Andes	OGGM	198312.51	29990.328
Peruvian Andes	OGGM	199338.7904	29990.328
Peruvian Andes	OGGM	229797.7175	29990.328
Peruvian Andes	OGGM	264199.4649	29990.328
Peruvian Andes	OGGM	184448.5729	32489.522
Peruvian Andes	OGGM	186902.6154	32489.522
Peruvian Andes	OGGM	198074.5496	32489.522
Peruvian Andes	OGGM	941268.711	32489.522

Peruvian Andes	OGGM	352765.8734	37487.91
Peruvian Andes	OGGM	270884.3208	39987.104
Peruvian Andes	OGGM	326307.121	39987.104
Peruvian Andes	OGGM	646717.7062	42486.298
Peruvian Andes	OGGM	1726735.617	47484.686
Peruvian Andes	OGGM	260714.2607	49983.88
Peruvian Andes	OGGM	839003.1071	49983.88
Peruvian Andes	OGGM	518266.6993	54982.269
Peruvian Andes	OGGM	1399623.091	54982.269
Peruvian Andes	OGGM	983939.2761	77475.015
Peruvian Andes	OGGM	2434922.757	79974.209
Peruvian Andes	OGGM	568726.5005	87471.791
Peruvian Andes	OGGM	1019838.343	87471.791
Peruvian Andes	OGGM	629522.3238	92470.179
Peruvian Andes	OGGM	1324530.121	102466.95
Peruvian Andes	OGGM	4134547.976	107465.34
Peruvian Andes	OGGM	2077455.031	109964.54
Peruvian Andes	OGGM	2629719.555	127458.9
Peruvian Andes	OGGM	7527018.373	152450.84
Peruvian Andes	OGGM	11053254.23	152450.84
Peruvian Andes	OGGM	3743932.98	159948.42
Peruvian Andes	OGGM	1491018.177	164946.81
Peruvian Andes	OGGM	8314285.235	169945.19

Peruvian Andes	OGGM	9005967.689	192437.94
Peruvian Andes	OGGM	3303426.848	207433.1
Peruvian Andes	OGGM	5247314.114	214930.69
Peruvian Andes	OGGM	12165338.21	237423.43
Peruvian Andes	OGGM	3163716.045	239922.63
Peruvian Andes	OGGM	10977006.84	244921.01
Peruvian Andes	OGGM	23457721.86	562318.65
Peruvian Andes	OGGM	20657523.84	587310.6
Peruvian Andes	OGGM	40940600.56	949693.73
Peruvian Andes	OGGM	132516485.3	1609481
Southern Alps	Farinotti's Ensemble	26431.4328	9970.3595
Southern Alps	Farinotti's Ensemble	70689.204	12462.949
Southern Alps	Farinotti's Ensemble	202145.9357	12462.949
Southern Alps	Farinotti's Ensemble	234748.9018	12462.949
Southern Alps	Farinotti's Ensemble	124256.1532	14955.539
Southern Alps	Farinotti's Ensemble	73343.0576	19940.719
Southern Alps	Farinotti's Ensemble	220582.9464	22433.309
Southern Alps	Farinotti's Ensemble	1533437.217	49851.798
Southern Alps	Farinotti's Ensemble	466728.0227	54836.977
Southern Alps	Farinotti's Ensemble	795624.2229	102196.19
Southern Alps	Farinotti's Ensemble	1138956.572	114659.13
Southern Alps	Farinotti's Ensemble	2851299.793	219347.91
Southern Alps	Farinotti's Ensemble	11151098.77	261721.94

Southern Alps	Farinotti's Ensemble	16604225.92	720358.48
Southern Alps	GlabTop2	44301.8905	9970.3595
Southern Alps	GlabTop2	56122.5233	9970.3595
Southern Alps	GlabTop2	69677.8064	9970.3595
Southern Alps	GlabTop2	142279.0507	9970.3595
Southern Alps	GlabTop2	36088.0887	12462.949
Southern Alps	GlabTop2	101538.3507	12462.949
Southern Alps	GlabTop2	167433.7615	12462.949
Southern Alps	GlabTop2	173071.9073	12462.949
Southern Alps	GlabTop2	41382.408	17448.129
Southern Alps	GlabTop2	60568.8387	17448.129
Southern Alps	GlabTop2	183461.8569	17448.129
Southern Alps	GlabTop2	142577.8451	19940.719
Southern Alps	GlabTop2	178358.0113	24925.899
Southern Alps	GlabTop2	1422319.8	42374.028
Southern Alps	GlabTop2	982266.0184	92225.826
Southern Alps	GlabTop2	1794084.469	124629.49
Southern Alps	GlabTop2	1813122.719	137092.44
Southern Alps	GlabTop2	3164173.07	226825.68
Southern Alps	GlabTop2	69662293.74	1443209.5
Southern Alps	HF	33429.671	9970.3595
Southern Alps	HF	42554.7651	9970.3595
Southern Alps	HF	59830.3725	9970.3595

Southern Alps	HF	75060.9729	9970.3595
Southern Alps	HF	127744.6228	9970.3595
Southern Alps	HF	177524.0039	12462.949
Southern Alps	HF	69253.6523	14955.539
Southern Alps	HF	108783.9614	14955.539
Southern Alps	HF	98072.0929	17448.129
Southern Alps	HF	144317.668	17448.129
Southern Alps	HF	390488.6073	27418.489
Southern Alps	HF	322423.1342	34896.258
Southern Alps	HF	644059.1187	34896.258
Southern Alps	HF	353706.7802	52344.388
Southern Alps	HF	657375.8531	52344.388
Southern Alps	HF	1585321.851	52344.388
Southern Alps	HF	545046.067	59822.157
Southern Alps	HF	592794.894	64807.337
Southern Alps	HF	489091.9578	69792.517
Southern Alps	HF	576031.6794	77270.286
Southern Alps	HF	721264.5952	79762.876
Southern Alps	HF	1017527.098	134599.85
Southern Alps	HF	3223806.427	171988.7
Southern Alps	HF	12179916.31	513473.52
Southern Alps	Millan	61705.596	9970.3595
Southern Alps	Millan	87813.5885	9970.3595

Southern Alps	Millan	97334.5395	9970.3595
Southern Alps	Millan	115863.44	9970.3595
Southern Alps	Millan	127647.256	9970.3595
Southern Alps	Millan	111577.7798	12462.949
Southern Alps	Millan	247749.4985	12462.949
Southern Alps	Millan	44126.9345	14955.539
Southern Alps	Millan	383072.3005	14955.539
Southern Alps	Millan	117422.2215	17448.129
Southern Alps	Millan	198460.6027	17448.129
Southern Alps	Millan	226466.9434	19940.719
Southern Alps	Millan	186999.3141	22433.309
Southern Alps	Millan	241502.0496	22433.309
Southern Alps	Millan	251157.3362	22433.309
Southern Alps	Millan	217018.409	24925.899
Southern Alps	Millan	223950.316	27418.489
Southern Alps	Millan	173532.8782	32403.668
Southern Alps	Millan	522053.964	34896.258
Southern Alps	Millan	542503.4245	34896.258
Southern Alps	Millan	400847.0648	42374.028
Southern Alps	Millan	697076.5541	54836.977
Southern Alps	Millan	1796482.735	62314.747
Southern Alps	Millan	1372974.005	64807.337
Southern Alps	Millan	1469206.17	69792.517

Southern Alps	Millan	2421722.982	72285.107
Southern Alps	Millan	1073883.91	89733.236
Southern Alps	Millan	2399083.073	132107.26
Southern Alps	Millan	6104118.329	256736.76
Southern Alps	Millan	26013926.46	715373.3
Southern Alps	OGGM	37772.5342	9970.3595
Southern Alps	OGGM	40742.5257	12462.949
Southern Alps	OGGM	125241.6877	14955.539
Southern Alps	OGGM	159212.9615	14955.539
Southern Alps	OGGM	116087.6879	22433.309
Southern Alps	OGGM	181216.0309	22433.309
Southern Alps	OGGM	624460.4005	22433.309
Southern Alps	OGGM	245423.0407	24925.899
Southern Alps	OGGM	265447.7386	27418.489
Southern Alps	OGGM	443339.9107	39881.438
Southern Alps	OGGM	1344137.308	72285.107
Southern Alps	OGGM	3030189.974	92225.826
Southern Alps	OGGM	8100118.4	181959.06
Southern Alps	OGGM	6426822.609	224333.09
Southern Alps	OGGM	7708948.834	309081.15
Southern Alps	OGGM	59467533.2	418755.1
Southern Alps	OGGM	20606117.01	446173.59
Southern Alps	OGGM	137190375.3	2103745.9

APPENDIX G

Table for total area and volume for Model_DEM combination of Himalayas

Model_DEM combination	Total_Volume (km^3)	Total_Area (km^2)
OGGM_SRTM	0.670567729	15.25889461
OGGM_Copernicus	0.654524703	15.16643161
OGGM_ASTER	0.608397652	15.43132562
OGGM_ALOS	0.601324991	15.88614364
GlabTop2_ALOS	0.548224712	18.07776672
GlabTop2_Copernicus	0.510565309	19.16483177
GlabTop2_ASTER	0.472580287	18.11025372
GlabTop2_SRTM	0.44862059	20.37434782
Millan_SRTM	0.440641251	14.9515176
Millan_Copernicus	0.432667236	14.28428457
Millan_ALOS	0.401195427	13.82696755
Millan_ASTER	0.38348985	13.75949455
HF_ASTER	0.234557764	12.74240151
HF_Copernicus	0.234557764	12.07266948

HF_SRTM	0.229930942	13.09226152
HF_ALOS	0.195967344	11.96021448
Ensemble_ASTER	0.145437667	7.4870043
Ensemble_Copernicus	0.144676712	7.117152285
Ensemble_ALOS	0.132925872	7.327068293
Ensemble_SRTM	0.123354348	7.651938306

APPENDIX H

Table for pixel distribution in Alaska

	HF_Milan	OGGM_HF	OGGM_Millan	OGGM_GlabTop2	HF_GlabTop2	Millan_GlabTop2	GlabTop_Farinotti	HF_Farinotti	Farinotti_Millan	OGGM_Farinotti
1	21301	54608	18854	79121	85794	20677	48087	56654	21462	68819
2	5578	22326	3018	25035	36587	9471	69536	50354	8901	29645
Total	26879	76934	21872	104156	122381	30148	117623	107008	30363	98464

APPENDIX I

		No of Overdeepenings	Area of Overdeepenings (sq km)	No of Overdeepenings	Area of Overdeepenings (sq km)	No of Overdeepenings	Area of Overdeepenings (sq km)	4 Pixels		20 Pixels	
								No of Overdeepenings	Area of Overdeepenings	No of Overdeepeiningss	Area of Overdeepenin
ALASKA	Farinotti's Ensemble	524	52.05	135	50.75	49	49.13	74.24%	2.50%	90.65%	5.61%
	Millan's	1640	45.72	413	41.44	81	31.43	74.82%	9.36%	95.06%	31.26%
	Huss_Farinotti	750	40.34	220	38.27	66	35.44	70.67%	5.13%	91.20%	12.15%
	GlabTop2	496	52	148	50.88	68	49.21	70.16%	2.15%	86.29%	5.37%
	OGGM	512	22.93	117	21.66	32	19.96	77.15%	5.54%	93.75%	12.95%
EUROPEAN ALPS	Farinotti's Ensemble	38	0.63	14	0.55	4	0.3	63.16%	12.70%	89.47%	52.38%
	Millan's	204	2.3	52	1.77	8	0.98	74.51%	23.04%	96.08%	57.39%
	Huss_Farinotti	79	0.88	22	0.67	4	0.34	72.15%	23.86%	94.94%	61.36%
	GlabTop2	54	1.19	17	1.06	6	0.67	68.52%	10.92%	88.89%	43.70%
	OGGM	56	1.48	21	1.35	9	1.04	62.50%	8.78%	83.93%	29.73%
NEW ZEALAND SOUTHERN ALPS	Farinotti's Ensemble	60	1.79	13	1.63	6	1.52	78.33%	8.94%	90.00%	15.08%
	Millan's	117	2.24	30	1.94	10	1.52	74.36%	13.39%	91.45%	32.14%
	Huss_Farinotti	92	1.83	24	1.55	11	1.33	73.91%	15.30%	88.04%	27.32%
	GlabTop2	51	2.38	15	2.25	5	2.02	70.59%	5.46%	90.20%	15.13%
	OGGM	55	4.2	18	4.06	8	3.85	67.27%	3.33%	85.45%	8.33%
ANDES	Farinotti's Ensemble	354	3.92	79	2.99	20	1.91	77.68%	23.72%	94.35%	51.28%
	Millan's	419	5.62	106	4.47	22	2.84	74.70%	20.46%	94.75%	49.47%
	Huss_Farinotti	375	3.84	88	2.86	12	1.32	76.53%	25.52%	96.80%	65.63%
	GlabTop2	216	2.94	61	2.38	13	1.47	71.76%	19.05%	93.98%	50.00%
	OGGM	360	9.18	98	8.3	28	6.93	72.78%	9.59%	92.22%	24.51%
HIMALAYAS	Farinotti's Ensemble	329	8.1	104	7.33	30	5.86	68.39%	9.51%	90.88%	27.65%
	Millan's	996	16.33	277	13.83	62	9.38	72.19%	15.31%	93.78%	42.56%
	Huss_Farinotti	636	13.46	200	11.96	57	8.93	68.55%	11.14%	91.04%	33.66%
	GlabTop2	416	16.94	144	15.89	55	14.13	65.38%	6.20%	86.78%	16.59%
	OGGM	330	18.67	167	18.08	73	15.86	49.39%	3.16%	77.88%	15.05%